Aus dem Zentrum für klinische Tiermedizin
Tierärztliche Fakultät der Ludwig – Maximilians - Universität München

Arbeit angefertigt unter Leitung von Prof. Dr. R. Korbel

IMAGING OF PHYSIOLOGICAL RETINAL STRUCTURES IN VARIOUS RAPTOR SPECIES USING OPTICAL COHERENCE TOMOGRAPHY (OCT)

Inaugural - Dissertation zur Erlangung der tiermedizinischen Doktorwürde der
Tierärztlichen Fakultät der Ludwig – Maximilians - Universität München

vorgelegt von
María Luisa Velasco Gallego
aus Valladolid

München 2015

Aus dem Zentrum für klinische Tiermedizin der Tierärztlichen Fakultät
der Ludwig-Maximilians-Universität München

Lehrstuhl für aviäre Medizin und Chirurgie

Arbeit angefertigt unter der Leitung von Prof. Dr. R. Korbel

Mitbetreuung durch: Priv.-Doz. Dr. Monika Rinder

Gedruckt mit Genehmigung der Tierärztlichen Fakultät
der Ludwig-Maximilians-Universität München

Dekan:	Univ.-Prof. Dr. Joachim Braun
Berichterstatter:	Univ.-Prof. Dr. Rüdiger T. Korbel
Korreferent/en:	Priv.-Doz. Dr. Sven Reese

Tag der Promotion: 31. Januar 2015

A mi querida familia y a Edu

INDEX

LIST OF ABBREVIATIONS

2D	-	two dimensions
3D	-	three dimensions
A-scan	-	axial scan, intensity profile
AMD	-	age-related macular degeneration
AS-OCT	-	anterior segment OCT
B-scan	-	cross-sectional image
BW	-	body weight.
C-scan	-	or “C-mode”, “coronal scan”, “3D scan”, 3D OCT visualization
CCD camera	-	charge-couple device camera
cSLO	-	confocal scanning laser pophthalmoscopy
CSR	-	central serous retinopathy
E	-	equator
EDI SD-OCT	-	enhanced depth imaging SD-OCT
ELM	-	external limiting membrane
OPL	-	outer plexiform layer
ONL	-	outer nuclear layer
Er	-	reference field
ERM	-	epiretinal membranes
Es	-	sample field
Es´	-	modified sample field
FA	-	fluorescein angiography
Fig.	-	Figure
GCL	-	ganglion cell layer
Gl.	-	Glandula
H	-	horizontal
h	-	hour
HR-SD-OCT	-	high resolution-spectral domain optical coherence tomography
H&E	-	hematoxylin & eosin
ICG dye	-	indocyanine-green dye
ILM	-	internal limiting membrane
i.n.	-	identification number
INL	-	inner nuclear layer
IOP	-	intra-ocular pressure

IPL	-	inner plexiform layer
ipRGCs	-	intrinsically photosensitive retinal ganglion cells
IS/OS	-	junction between the inner segment and the outer segment of the photoreceptors
Ir	-	mean intensity reference arm
IRC	-	inner retinal complex
Is	-	mean intensity sample arm
l_c	-	correlation length
Δλ	-	full-width of the coherence function at half maximum measured in wavelength units
Λo	-	central wavelength of the light source
LASIK	-	laser-assisted in situ keratomileusis
M.	-	Musculus (muscle)
min	-	minutes
MR	-	magnetic resonance
µm	-	micrometer
mm	-	millimeter
n	-	refractive index of the sample under examination.
N	-	nasal
nm	-	nanometer
OCDR	-	optical coherence-domain reflectometry
OCT	-	optical coherence tomography
OD	-	Oculus dexter (right eye)
ON	-	optic nerve
ONH	-	optic nerve head
ONL	-	outer nuclear layer
OPL	-	outer plexiform layer
PED	-	pigment epithelial detachment
Ps	-	pecten superior
OS	-	Oculus sinister (left eye)
RNFL	-	retinal nerve fiber layer
RPE	-	retinal pigment epithelium
S	-	superior
SD-OCT	-	spectral domain-optical coherence tomography
SLD	-	super luminiscent diode
SLO	-	scanning laser ophthalmoscopy
SS-OCT	-	swept-source optical coherence tomography

T	-	temporal
τ	-	optical time delay
TD-OCT	-	time domain-optical coherence tomography
UBM	-	ultrasound biomicroscopy
UHR-OCT	-	ultra-high-resolution optical coherence tomography
UV	-	ultraviolet
V	-	vertical

1 INTRODUCTION

In bird species, especially in wild birds and raptor species, vision is considered as the most important of the five main senses. The large size of the avian eye in comparison with the body size is a good indicator to understand its importance. A healthy and unimpaired vision is necessary to develop normal behaviours in raptor species, like independent feeding and flying. Total or partial impairments of visual acuity will have a major influence on their ability to orient themselves in the space, to respond to external stimuli or to a change of the environment, especially while hunting. Even a slight deficit of vision and visual acuity may prevent rehabilitation of wild birds with a consequential indication for euthanasia because of animal welfare reasons. For all this reasons, the important role of ocular lesions in avian medicine is obvious.

Regarding wild birds, and among them the raptor species, ocular lesion are commonly present occurring in more than 35 % of all patients suffering from collision trauma. About 80 % of the posttraumatic lesions are located at the posterior segment of the eye, whereby only about 20 % are located in the anterior segment (KORBEL et al. 2001). Therefore, in birds with a history of trauma it is vital to carry out a thorough ophthalmological examination to come to an exact diagnosis, prognosis and treatment of the patient (KORBEL 1994; 1999; KORBEL et al. 2001; KORBEL et al. 1997).

The technique of Optical Coherence Tomography (OCT) was reported for the first time in 1991 (HUANG et al. 1991). Although OCT was used for various applications, it was soon shown to be especially valuable in ophthalmology, in particular for in-vivo imaging of the healthy and pathological retina and optic nerve head, showing results that revolutionised the ophthalmologic diagnostic (VAN VELTHOVEN et al. 2007).
Right now, OCT is a well-established technique to examine the retinal sublaminae in human medicine. Using OCT, cross-sectional retinal images are obtained. These images allow to measure and quantify the total retinal thickness and sublaminae in vivo, and to identify the different retinal layers. With regards to clinical aspects, OCT has shown a high potential as a diagnostic tool and has successfully used for post-therapeutical objective evaluation and monitoring of the patients.

Up to now, OCT, especially high resolution-spectral domain-OCT (HR-SD-OCT), has only occasionally been used for the examination of the avian eye, and only a few bird species and individuals have been included. In a first pilot investigation including birds

of prey, the limited number of only four hawk and owl individuals were used and first information about the potential of OCT for visualisation of the raptor retina was obtained. In a single bird patient a traumatic lesion was also imaged (RUGGERI et al. 2010). However, this investigation was limited with regard to interspecific and intraspecific variations of retinal structures and to variations depending on the retinal area which have not been considered, but which are fundamental for the decision for or against the suitability of OCT for clinical avian ophthalmological use. Rauscher et al. in 2013 examined a broad range of avian species using OCT, focusing on the visualization of retinal alterations. Among the patients under study there were various raptor species.

However, a scientifically based use of OCT for diagnosing ocular disorders is depending on a profound knowledge of the physiological anatomic structures of the retina in a variety of bird species and on knowledge of their intraspecific variation, and even of intra-individual variation depending on the location in the eye and specially regarding the retinal layers in various eye regions and in various species of birds of prey.
Therefore, the aim of the present study is to scientifically evaluate the retinal anatomy of the raptor eye visualized using OCT, considering intra- and interspecific variations, and to validate the OCT technique comparing OCT images with histological sections.
.

2 LITERATURE

2.1 Optical Coherence Tomography (OCT)

Optical coherence tomography (OCT) is a technique based on low coherence interferometry. It can be characterized as a non-invasive medical imaging technique, which allows non-contact, high resolution and cross-sectional imaging of the anatomical structure of biological tissue. Huang et al. in 1991 applied this technique for the first time for human research. Since then, OCT has experienced different improvements as a diagnostic tool resulting in a great success in the retinal cross-sectional imaging (GABRIELE et al. 2011, HUANG et al. 1991, RUGGERI et al. 2007). Thanks to the low coherence interferometry, it images the tissue morphology in situ and in real time using the echo time delay and magnitude of the backscattered light. The tissue is scanned by an optical beam, which backscattering produces a two-dimensional data set, from which cross sectional images are built (DREXLER & FUJIMOTO 2008, SRINVASAN et al. 2006).

One of the most important functions of the optical imaging technique is the depth penetration, which depends on the interaction between the light and the tissue chromophores and other optical properties of the tissue. Therefore, the tissue itself determines the penetration of the OCT light (DREXLER & FUJIMOTO 2008).

Through the short temporal coherence of a broadband light source, OCT possesses an optical sectioning ability to reach tissue structures at greater depths than those obtained with conventional bright-field and confocal microscopes. In transparent tissues like a frog embryo, OCT reaches a depth of 2 cm. Non-transparent tissues have a high scattering, but even in those OCT is able to penetrate the tissue surface between 1 and 2 mm. With this method the skin was imaged, showing small blood vessels and other structures (SCHMITT 1999).

2.1.1 Physical and technical baselines of OCT

According to Van Velthoven et al. (2007), "*OCT is the optical analogue of ultrasound imaging"*. Light permits tissue imaging at higher resolution in comparison with sound due to shorter wavelengths. OCT is performed without tissue contact, as the difference in optical impedance, the refractive index between air and tissue, is not as large as the difference in acoustic impedance between air and tissue. The speed of light is 150.000 times faster than that of sound. Due to this fact, and by contrast to sound, light cannot be measured directly. This is the reason why the OCT systems are based on the low coherence interferometry. In the low coherence interferometry light is divided into two light beams, one impinges with the retina and the other travels a known path length. The sample beam signal interferes with the reference beam signal (VAN VELTHOVEN et al. 2007). This physical procedure is performed in a Michelson interferometer (Figure 1).

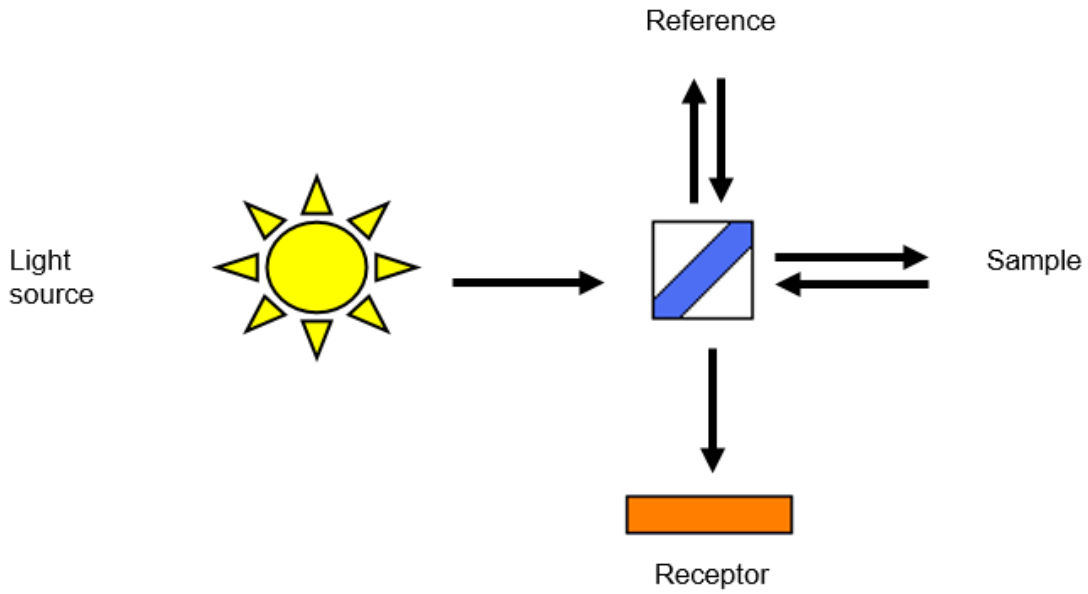

Figure 1: Scheme of Michelson´s interferometer.

When the first OCT applications in medicine were reported more than ten years ago, they were based on white light interferometry which continuously developed to optical coherence-domain reflectometry (OCDR). The OCDR is a one-dimensional optical technique which at first was not aimed for biomedical diagnostic. However, its potential to study the eye and other biological tissues was soon recognized (SCHMITT 1999).

2.1.1.1 Theoretical fundaments of OCT

2.1.1.1.1 Low coherence interferometry

Schmitt in 1999 gave a detailed explanation of the low coherence interferometry which represents the basic OCT physical method. Figure 2 shows the basic components of an OCT system. The centre of the system is an interferometer illuminated by a broadband light source. At the beginning of the following section the principle functions of interferometer are described, and more details related to complications by scattering in a tissue sample are introduced later in the section.

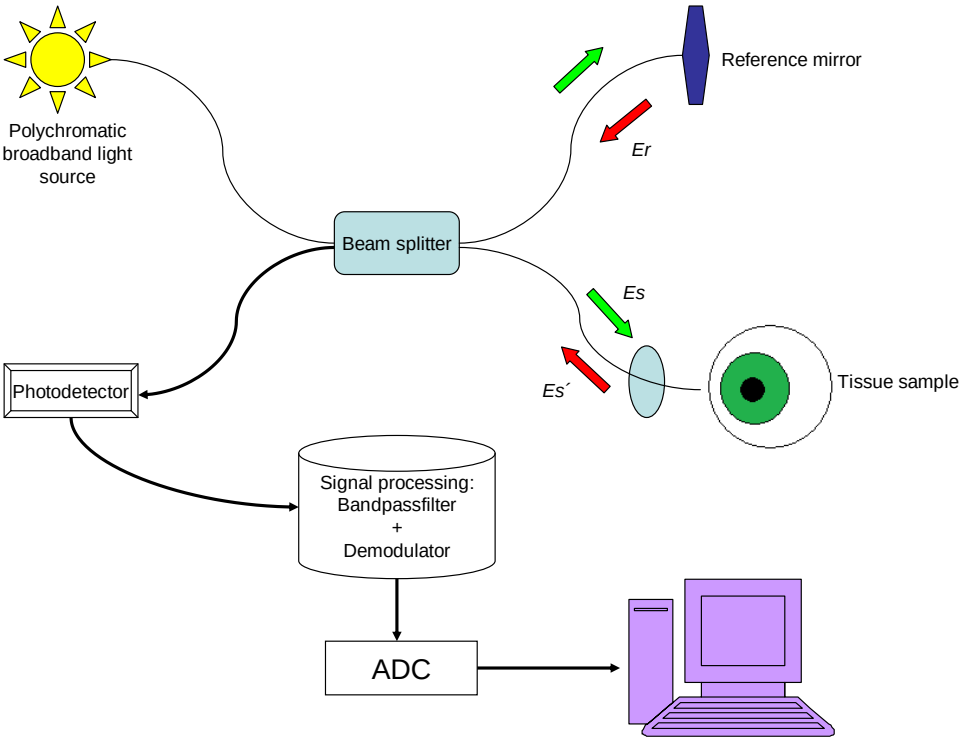

Figure 2: Components of an OCT system

The interferometer in an OCT device divides the light source beam into a reference beam *Er* and a sample beam *Es*. The scanning optics and the objective lens focus the sample beam to a point below the tissue surface. The light scatters back from the tissue before the modified sample beam *Es´* mixes with *Er* on the surface of the photo-detector. The photo-detector captures all the light from the reference and sample beams. The intensity that comes into contact with the photo-detector is calculated by equation 1:

(1)

$$I_d = < \mid E_d^2 \mid > = 0.5(I_r + I_S^{`}) + \mathrm{Re}\{ < E_S^*(t+\tau)E_r^{`}(t) > \}$$

The first term of the aforementioned equation is the mean of the intensities returning from the reference (*Ir)* and sample (*Is)* arms of the interferometer. The position of the reference mirror determines the optical time delay *τ*, represented by the second term of the equation. This second term refers to the information about the amplitude of the interference. The interference carries the information about the structure of the tissue. The interference is created from the encounter of *Es´* and *Er*, and therefore it depends on the spatial and temporal characteristics or "delay" in relation to each other. The interferometer produces a cross-correlation between both. The measure of the amplitude of the cross-correlated value is obtained once the interference signal integrates on the surface of the detector

Various techniques have been devised to modulate *τ* to facilitate the separation of the cross-correlation signal from the mean component of the intensity. On the supposition that the tissue works as an ideal mirror that does not modify the sample beam, the correlation amplitude depends on the temporal-coherence characteristics of the source.

The Fourier transform explains how *G(τ)* is related to the power spectral density of the source, *S(v)*. Sources with broad spectra are favourable because they produce interference patterns of short temporal and spatial range. Within the Wiener–Khinchin theorem the Fourier transform is used.

In the formula 2 the correlation length can be seen. The correlation length l_c is the corresponding measure of the correlation width, derived from the formulas comprised in the Fourier transform,

(2)

$$l_c = \left(\frac{2\ln 2}{\pi}\right) \cdot \frac{\lambda_0^2}{n\Delta\lambda}$$

where *Δλ* is the full-width, or spectral bandwidth, of the coherence function at half maximum. The spectral bandwidth is inversely proportional to the coherence length (SCHMITT 1999, VAN VELTHOVEN et al. 2007).

To resume, this physical explanation goes from the TD-OCT to the SD-OCT. In the TD-OCT, the light source, emits a beam, which is split in two directions. One beam goes to the reference mirror and the other to the sample. The reflected beams recombine at the beam splitter. They are conducted to a detector. While the sample remains fixed, the reference mirror moves and produces a different interference pattern, which is measured by the detector. In the SD-OCT, the reference mirror remains fixed, and the difference is made by the detection system and a broader bandwidth light source. The most important fact is that the interference will only be detected when the difference in the path length of the light from both arms is less than the coherence length of the light source (VAN VELTHOVEN et al. 2007).

That is the reason why a low coherent light is used, which means, that it has a broad spectral bandwidth. This broad spectral band consists of a high number of wavelengths and produces a small coherence length. If the terminology of ultrasound is used, with different and adjacent A-scans (reflectivity versus depth image) a final and longitudinal image is built (B-scan). This image is shown in a greyscale or a false colours scale (VAN VELTHOVEN et al. 2007).

2.1.1.1.2 Resolution

Van Velthoven et al. (2007) mentioned, "*the axial (depth) resolution in an OCT image is solely determined by the coherence length l_c of the light source"*. Equation 2 shows that the l_c is inversely proportional to the full bandwidth $\Delta\lambda$. l_c can be calculated with the equation 2, where λo is the central wavelength of the light source. *n* represents the refractive index of the sample under examination. Van Velthoven et al. (2007) also said, "*the axial resolution inside a medium or tissue with refractive index n is improved by a factor n because the wavelength is n times smaller in the medium or tissue".*
In the visualization of the OCT scan, the size of the spot and the focusing optics of the sample arm are the two elements determining the lateral or transverse resolution. It is similar to confocal microscopy (confocal gating), and can be considered as an extension of this technique. The examination of the retinal tissue with an OCT system leads to a transversal resolution of ~20 µm (VAN VELTHOVEN et al. 2007).

2.1.2 OCT systems

2.1.2.1 Time Domain OCT

This was the first OCT used in clinical systems, which provided information about the microarchitecture of the retina in quantitative form (SRINVASAN et al. 2006). Despite its undeniable ability to demonstrate the microstructure of biological tissues, its scanning speed was limited to 400 axial scans (A-scans) per second. The reason is the need to move the reference mirror, which means a physical constraint. The light beam sent from the light source is split into two and both are sent to the reference arm, which contains the reference mirror, and to the tissue sample. After scattering back from the tissue and from the reference mirror, the modified beam from the sample recombines with the reference beam, producing interference. Its interference profile is detected by the photoreceptor. From the interference profile a reflectivity profile referred to the tissue depth is represented. In order to detect different depths of the tissue sample, the location of the reference mirror has to be changed. (GABRIELLE et al. 2011, SCHMITT 1999).

These OCT systems had a 10 to 15 µm axial resolution, and this resolution power was enough to visualize diseases like macular hole, glaucoma, macular degeneration and oedema, as well as diabetic retinopathy (SRINVASAN et al. 2006). Any OCT system allows in vivo, in situ, in real time and non-contact retinal imaging (HUANG et al. 1991, VAN VELTHOVEN et al. 2007).

2.1.2.2 Spectral Domain OCT

The most powerful feature of the spectral domain OCT (SD-OCT) is its high improvement in imaging speed. It achieves a 25 to 50 times increase in speed in comparison with the standard resolution OCT devices and 100 times over conventional UHR-OCT devices. It is also called Fourier domain OCT because a Fourier transformation is used to measure the echo time delay of light, obtaining the interference spectrum of the light signal (SRINVASAN et al. 2006).

As explained before, the TD-OCT devices vary the location of the coherence point as a function of time by the movement of the reference mirror. Hence, the signal is collected in the domain of the time (VAN VELTHOVEN et al. 2007). According to Van Velthoven et al. (2007), "*the time-domain signal for a given position of the reference arm can be calculated by summing the interference contributions from all wavelengths in the spectrum of the light source*".

On the contrary, in the SD-OCT the reference mirror is always fixed in the same position. The OCT signal is obtained as a function of the wave number or frequency. A spectrometer works as a detector, which receives the different low coherent wavelengths of the light source. In this case, the signal for the SD is calculated by summing the interference contributions from all the differences in path lengths. Then the device performs the Fourier transformation of the data, turning it into data depending on the time (VAN VELTHOVEN et al. 2007).

Tissue penetration is also an important factor in diagnostic imaging devices. Independient of the optical tissue features, long wavelengths allow deeper tissue penetration than short wavelengths. Commercial SD-OCT devices for retinal examination are usually centered at ~800 nm, allowing the differentiation of the majority of retinal sublaminae, with a limited tissue penetration beyond the retinal pigment epithelium. On the contrary, in the examination of the anterior segment longer wavelengths are needed, and therefore they are based on TD-OCT since it provides a deeper tissue penetration than SD-OCT (DREXLER & FUJIMOTO 2008, VAN VELTHOVEN et al. 2007).

The significant acquisition of speed is so powerful that it provides important advantages to the system. These are reduction in the eye motion artefacts in B-scans, which allows the preservation of the fundus contour, higher axial resolution which leads to a better

delineation of retinal and subretinal layers, lower speckle size, which improves the image quality, and an increase in the transverse pixel number, which contributes to the improved A-scan resolution (DREXLER & FUJIMOTO 2008).

2.1.2.3 OCT systems development

The important new developments in the OCT devices recently enabled in-vivo cellular resolution of retinal imaging, especially when 3D-UHR-OCT was combined with adaptive optics. Among them non-invasive depth-resolved functional imaging of the retina was possible, such as blood flow observation, spectroscopic, polarization-sensitive and physiological information (DREXLER & FUJIMOTO 2008).

2.1.2.3.1 Resolution improvement

Improvements of the image quality and axial resolution of the OCT devices were obtained by the use of broader bandwidth light sources, because the axial OCT resolution is inversely proportional to the spectral bandwidth of the light source. Drexler et al. in 2001 used a broadband Ti:Sapphire as the light source which is a short pulse femtosecond laser, with a bandwidth of 125 nm centred at 815 nm, reaching an axial resolution of 3 µm (DREXLER et al. 2001, GABRIELE et al. 2011, VAN VELTHOVEN et al. 2007). In the case of the frequency domain OCT systems, these devices offer a higher detection sensitivity, which means that they show higher signal in detriment of noise, and so it serves as a perfect reflector (GABRIELE et al. 2011).

Compared with the standard resolution OCT devices used before, it provided additional information about subtle structural changes, occurring in glaucoma and macular disease. Due to the layered structure of the retina, the axial image resolution has been an important parameter. Thanks to the development of systems providing improved axial image resolution it was possible to visualize the detailed architectural morphology of the retina on the level of single retinal layers (DREXLER & FUJIMOTO 2008, SRINVASAN et al. 2006).

The UHR-OCT is able to show a very good delineation of all intraretinal layers, identifying even really small cystic changes between layers. This improvement in resolution, however, brought limitation such as lower scanning speed, and high costs of light sources. Then the research focused on a more affordable light source resulting in an inexpensive compact, broadband SLD (VAN VELTHOVEN et al. 2007).

This broadband SLD light source is now utilized in commercial systems. The main advantage of OCT over standard or confocal microscopy is its high axial resolution reaching 3 µm, which in ophthalmoscopy, despite the small pupil aperture and the long

focus depth, allows non-invasive optical biopsy of the retina, and the visualization of intraretinal morphology with a quality level comparable to histopathology (DREXLER & FUJIMOTO 2008).

2.1.2.3.2 Imaging speed improvement

The main limitation of Ultra-High-Resolution OCT (UHR-OCT) described before was a slow acquisition speed (VAN VELTHOVEN et al. 2007). This acquisition speed was caused by the necessity of the reference mirror to move in order to detect the delay of the backscattered signals. When the backscattering was detected by the frequency of the signal, in the so called frequency domain, without the need to move the reference mirror, significant speed improvements were possible. The information of the frequency domain is in principle obtained with two methods; it can be obtained with a broad-bandwidth light source, a charge-couple device camera (CCD camera) and a spectrometer in a system called spectral domain OCT (SD-OCT), or with a narrow-bandwidth light source through a broad range of frequencies detected with a photo detector in a system called swept-source OCT (SS-OCT) (GABRIELE et al. 2011, VAN VELTHOVEN et al. 2007).

The main principle of the two systems is the same. The frequencies are detected by the respective detector, from which an intensity profile (A-scan) is obtained through a Fourier transform, and so the echo time delays of light are obtained by the Fourier transforming of the interference spectrum of the light signal. This method improves the speed of the A-scan collection.

The speed improvement is substantial because it results in a 25 to 50 fold increase over OCT standard resolution systems, and 100 times over conventional UHR-OCT systems. Three dimensional (3D) images were possible to be collected thanks to the high acquisition speed together with the improvement in sensitivity of the system. Thus, broadband volumetric retinal imaging with SD-OCT at speeds up to 312,500 A-scans/s and SS-OCT at 249,000 A-scans/s were performed (GABRIELE et al. 2011, SRINVASAN et al. 2006).

This improvement allowed the obtaining of intraretinal information which was not possible with any other non-invasive diagnostic techniques before. Drexler and Fujimoto in 2008 said, that "*This kind of OCT device works as an optical biopsy in situ and in real time of the retina, with resolutions comparable with those of excisional biopsy and*

histopathology". The improved acquisition speed became so important to the clinicians because it allowed the 3D visualization, which gives more comprehensive information than a limited set of scans taken at supposed pathologic retinal locations. It provides important structural information necessary for a precise registration of fundus features, allowing a mapping of retinal layers thicknesses, and serially production of volumetric views of retinal structures in the same way as those obtained with a magnetic resonance (MR). These factors admit the detection of early stages of retinal disease. The scanning speed improvement allowed to create the en-face systems, responsible systems of the 3D-OCT imaging (DREXLER & FUJIMOTO 2008, VAN VELTHOVEN et al. 2005).

2.1.2.3.3 Speckle reduction

Speckle noise produces a degradation of the image quality by creating a grainy appearance. The features characterized by a low intensity appearance are darkened (SCHMITT et al. 1999). For instance, the accuracy to measure retinal thickness or RNFL thickness decreases when speckle noise increases (ADLER et al. 2004).

A speckle reduction leads to an improvement of the OCT image quality and a better capacity to distinguish the different retinal layers and intraretinal details. The noise varies randomly in the OCT scans, therefore a possible solution is to average multiple scans made on the same retinal position and the same incident angle. The average is calculated with an algorithm and is obtained after the imaging. Another method is the use of wavelet-filtering techniques, which is based on an algorithm that estimates which pixel is degrading or carrying the signal, and is therefore able to distinguish between speckle noise and the real edge features (ADLER et al. 2004, SCHMITT et al. 1999, VAN VELTHOVEN et al. 2007).

2.1.2.3.4 Eye-Tracking system

During ophthalmological examinations performed through OCT, eye motion artefacts which could not be corrected with image processing were a frequent problem. Especially involuntary eye movements are common in the ophthalmological examination of the living patient. The resulting artefacts restricted the number of A-scans that could be obtained in a cross-sectional image (B-scan). The problem could partly be solved in the Fourier domain OCT due to its improved image acquisition speed (DREXLER & FUJIMOTO 2008). However, eye movements were still impairing the quality of imaging, even in high speed SD-OCT devices and were especially relevant while acquiring 3D

OCT images. Each pixel is related to a concrete retinal location, which is translated into a retinal reference point. In order to correct artefacts related to eye movements and to obtain an undistorted OCT image, the relationship between pixel-retinal must be known. The problem was solved using a secondary beam as a sensor, which finds identifiable fundus structures, detects the transverse eye movement through the changes in the reflectance patterns and, after eye movements, relocates the OCT main beam in the adequate acquiring retinal position. This method is called active retinal tracking, and provides reproducible measurements, and, in addition, is allowing repeated image acquisition at the exact same retinal location over time, therefore allowing the monitoring of disease progression along the time (FERGUSON et al. 2004, VAN VELTHOVEN et al. 2007). However, comparative data confirming that this new built-in eye-tracking system in fact increases reproducibility and thus sensitivity and specificity, are still lacking (GABRIELLE et al. 2011).

2.1.2.3.5 En-Face OCT systems

The en-face OCT system is the combination of the OCT diagnostic method and the confocal scanning laser ophthalmoscopy (cSLO). The first approaches were performed by Podoleanu et al. in 1997, who for the first time, combined the scanning of the fundus surface using SLO and the high resolution tomographic images produced by OCT (DREXLER & FUJIMOTO 2008, VAN VELTHOVEN et al. 2007).

The development of ultrabroad-bandwidth and tuneable light sources, as well as high-speed Fourier detection techniques, has led to a significant improvement in ophthalmic OCT imaging performance facilitating the acquisition of three-dimensional data sets (3D-OCT) in combination with cSLO data, thus enabling volumetric rendering and the generation of OCT fundus images that precisely and reproducibly relate OCT images to fundus features.

The imaging in an en-face system is carried out in a different way. The system is based on the Michelson interferometer like other OCT systems, but includes an additional scanning laser ophthalmoscope (SLO) with a central wavelength of 820 nm and a spectral bandwidth of 20 nm. The en-face scans, also called coronal scans or C-scans (3D scans) are obtained by fast scanning of the XY plane instead fast scanning of the Z plane. A scheme is shown in Figure 3. Conventional OCT system have their fast scanning focused on the acquisition of A-scans, which means that the fastest acquisition speed is focused on the depth scanning on the XZ plane (Figure.3.a). In the en-face or

C-scan, the fastest scan is performed on the XY plane, and the slowest on the Z plane (Fig 3.b). Hence, a coronal scan is constructed by first fast scanning the XY plane (B-scan), followed by a slow scanning in depth or Z plane (A-scan). These two processes are made simultaneously thanks to the production of a confocal signal, which provides a high quality fundus image, and produces a reliable positioning of the OCT-B-scan and eye movement correction (VAN VELTHOVEN et al. 2007).

a

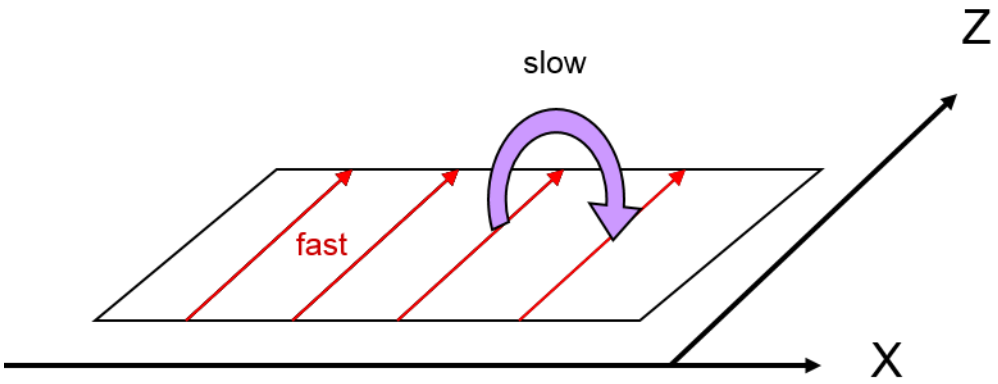

b

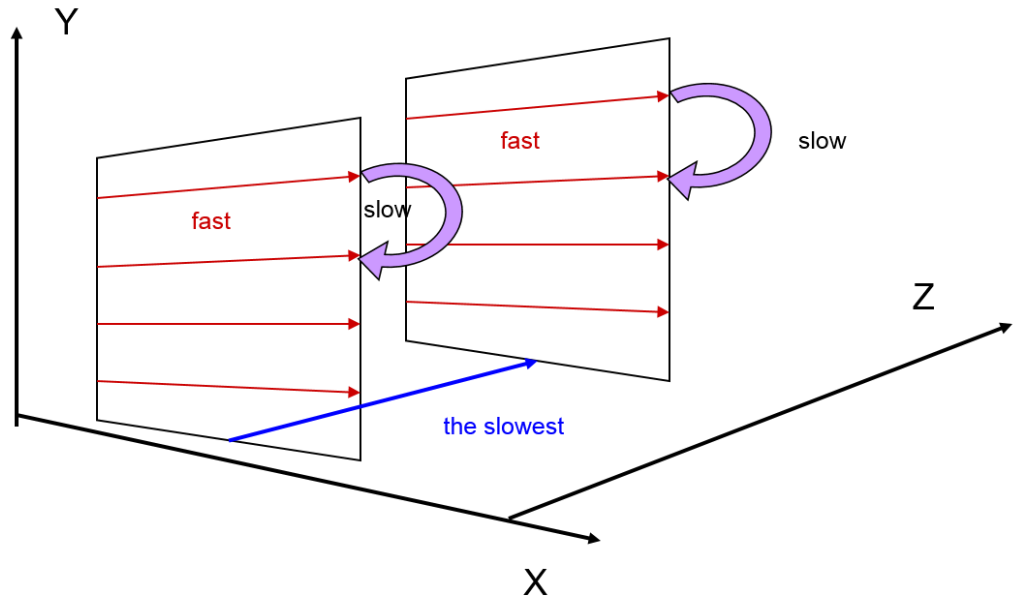

c

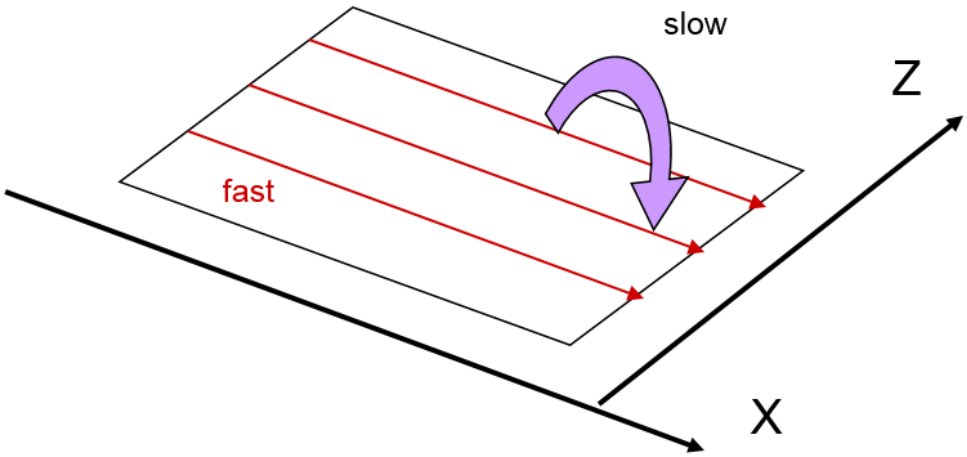

Figure.3: OCT scanning methods. A) TD-OCT. B) En face-OCT, coronal scan (C-scan). C) En face-OCT, B-scan (According to VAN VELTHOVEN et al. 2007, modified)

2.1.2.3.5.1 Indocyanine-Green-Angiography in combination with UHR-OCT/SLO

Blood flow in the retinal and choroidal blood vessels can be visualized with angiography using the fluorescent dye indocyanine-green (ICG dye). A disadvantage of this technique is that it is difficult to exactly localize the pathologic process in the angiogram. When using the laser of the confocal scanning laser ophthalmoscope to produce the angiogram, the ICG dye is excited to emit fluorescent light which can be detected in real time. The combination of this system with OCT then allows an exact localisation of pathological processes, for example vascular constrictions. The developed software allows the comparison of the SLO, OCT C-scan, the ICG frame and an overlay of the ICG and OCT frame (DOBRE et al. 2005, YANNUZI et al. 2004).

2.1.2.3.5.2 Full-field OCT

A full-field OCT consists on a system able to visualize en-face tomograms without the need of scanning. Dubois et al. in 2002 reported the development of an interference Linnik microscope able to produce this tomograms, and they called the system UHR full-field OCT. The Linnik interference microscope is similar to a bulk Michelson interferometer. The difference lays on the presence of microscopic objectives in both arms (DUBOIS et al. 2002). In this case the reference mirror oscillates, and its oscillation modulates the interference signal. It uses an incoherent light source, which is a diode emitting in infrared and is centred at 840 nm, or a quartz-tungsten halogen lamp centred at 770 nm. The images are recorded with a charge-coupled device (CCD) camera synchronized with the oscillation of the reference mirror. The camera takes two images in the opposition phase of the oscillation period, and the difference between them produces the en-face image. A group of these images is utilized to build the 3D images set. Although the reference mirror moves, the system is considered as a static system. Limitation of the axial resolution is caused by the CCD detection camera, but the axial resolution is nevertheless extremely high (about 0.8 µm) due to the broad spectrum of the light source (VAN VELTHOVEN et al. 2007).

2.2 Anatomy of the avian eye

Even if the anatomy of the avian eye is comparable to the mammalian eye, it possesses a considerable number of particularities and differences (REESE et al. 2008). Vision is of high importance in birds. In case of a loss in visual acuity, birds in comparison with mammals can almost not compensate this with other sensory organs (KORBEL 1991).

A brief description of the avian eye anatomy is necessary to understand its complexity and specialization.

2.2.1 Adnexal structures

The lids (Palpebrae) of the bird are mobile. In the majority of species the lower lid (Palpebra ventralis) is more mobile than the upper lid (Palpebra dorsalis), and often contains a fibroelastic tarsal plate (Tarsus). Feathers can be present or not. The nictitating membrane (Palpebra tertia) is present dorsonasal to the conjunctival sac, is well developed, and moves over the cornea thanks to the pyramidal muscle and the quadratus muscle. There is no presence of Meibomian glands. A lacrimal gland (Gl. lacrimalis), which varies in size depending on the species is located inferior and lateral to the eye globe. The nictitating membrane gland (Gl. lacrimalis membranae nictitantis), before known as Harderian gland, is located at the base of the nictitating membrane. The nasolacrimal punctum (Ostium canaliculum lacrimalis) drains lacrimal secretions into the nasal cavity through the nasolacrimal duct (Ductus nasolacrimalis) (EVANS & MARTIN 1993, KERN & COLITZ 2013, REESE et al. 2008, WILLIAMS 1994, WOOD 1915).

2.2.2 Orbit

The orbit (Orbita) has an osseous structure formed by the Ossa frontale, praefrontale, sphenoidale, ethmoidale, palatinum, quadratum, and a portion of the zigomatic arc. The Septum interorbitale separates both eyes, is thin and in some species even membranaceous (MURPHY 1984, REESE et al. 2008).

The majority of species, raptors among them, have an open orbit. Due to its size, the rectus and oblique muscles are not well developed, which limits the torsional movements of the eye. The orbit is tightly packed with the infraorbital diverticulum of the infraorbital sinus (WILLIAM, 1994). The Margo supraorbitalis bone closes the orbit superiorly and caudally. The ligamentum suborbitale closes the ventral orbita in the majority of bird species. In diurnal species the orbit surrounds almost the whole bulbus thus providing protection against trauma. In diurnal raptors, the Processus supraorbitalis, an extension from the Os lacrimale, ensures additional protection. On the contrary, in nocturnal species, the orbit is flat, and protection of the eye bulbus is given by the scleral ring. (REESE et al. 2008, SEIDEL 1998, TIEDEMANN 1810).

The Sinus infraorbitalis of birds is analogous to the fat protection structure which protects the mammalian eye, working as a pillow and separates the bulbus from the caudal part of the nasal cavity (FREWEIN & SINOWATZ 2004).

2.2.3 Extraocular muscles

Six very thin muscles allow eye movements of small amplitude (Musculi bulbi):

- M. rectus nasalis and M. rectus temporalis
- M. rectus dorsalis and M. rectus ventralis
- M. obliquus dorsalis and M. obliquus ventralis

The Figure 4 represents the extraocular muscles in the avian eye.

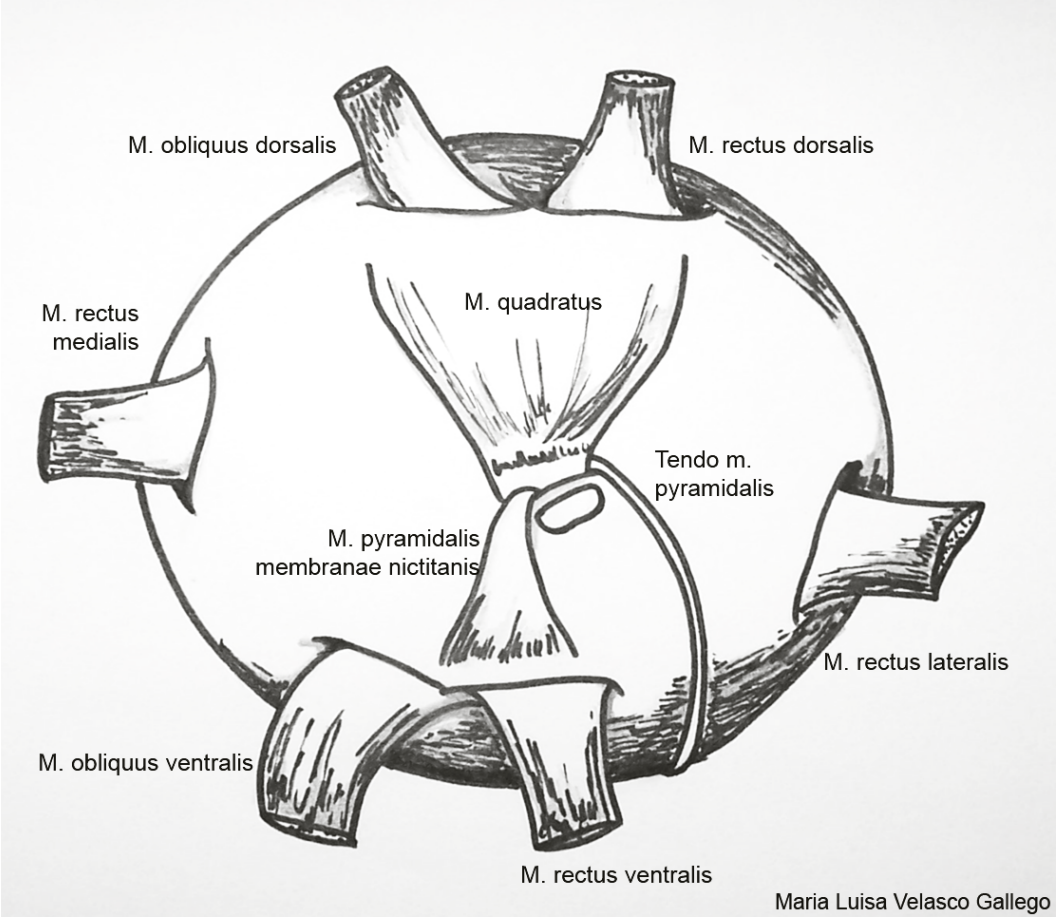

Figure 4. Musculi bulbi

2.2.4 Globe

In the majority of bird species, especially in raptor species, the eye globe (Bulbus oculi) itself is very large relative to body size, and the posterior segment is bigger than the anterior segment (KERN & COLITZ 2013). Its shape varies from near spherical (for example in chickens) to tubular (in Strigiformes) and has been classified in three types, tubular (Figure 5. a), spherical (globose) (Figure 5. b), and flat (planus) (Figure 5. c) (DUKE-ELDER 1958, EVANS & MARTIN 1993). The flat shape is the most prevalent type occurring in most avian species. The globose shape is typical of diurnal birds needing high resolution distance vision, like diurnal raptors. The tubular globe shape is typical of owls (KERN & COLITZ 2013).

a

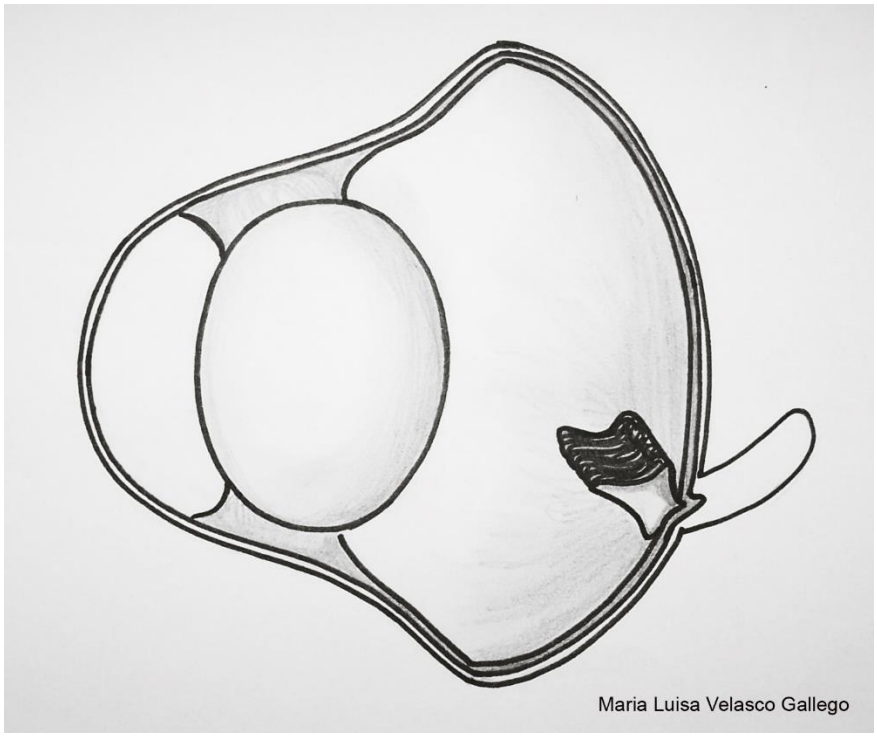

b

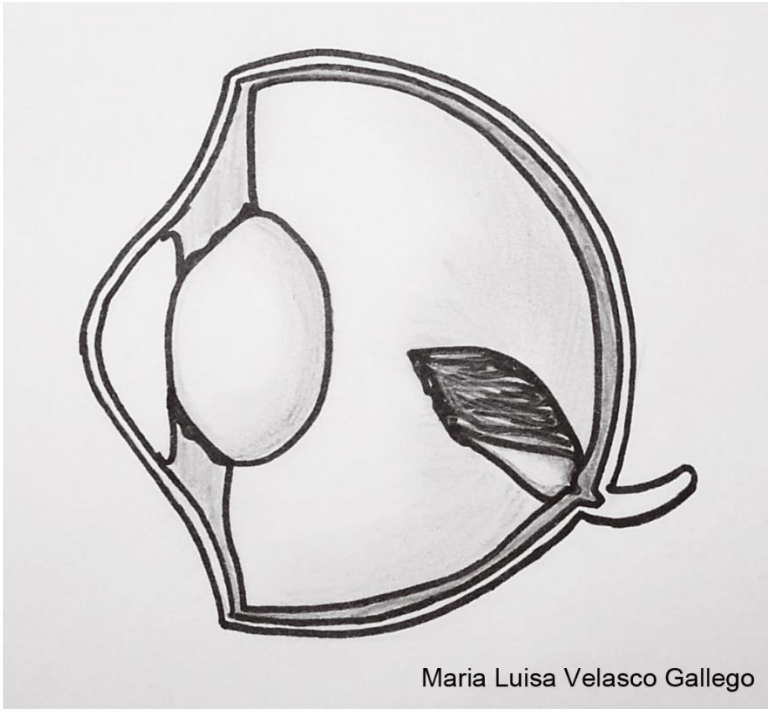

c

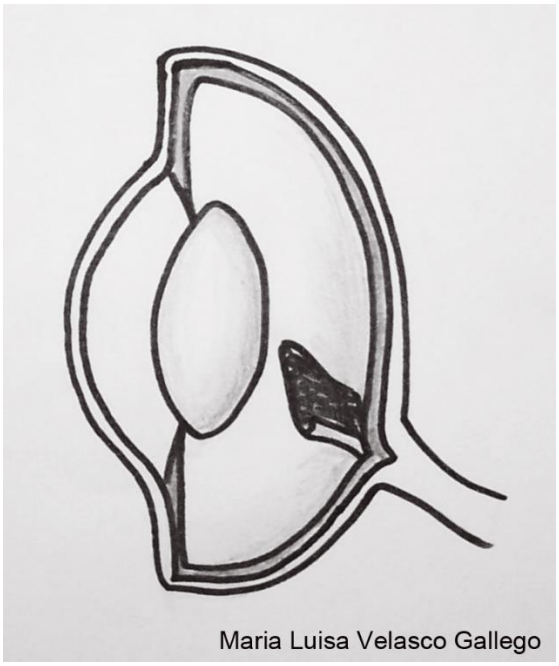

Figure 5: Shapes of the globe in birds. Vertical section, naso-temporal view. a) Tubular. b) Spherical. c) Flat.

Fibrous tunic

The fibrous tunic (Tunica fibrosa bulbi), which represents the outer fibrous case of the eyeball, is formed by the sclera and the cornea. It does not possess direct vascular supply (EVANS & MARTIN 1993).

Sclera and scleral ring

The sclera is located immediately posterior to the cornea and is composed of hyaline cartilage. The sclera contains the scleral ring (Annulus ossicularis sclerae), consisting of 10 to 18 bony ossicles, sometimes these are pneumatic. Rather than the intraocular pressure, the scleral ring together with the hyaline cartilage of the sclera is responsible for maintaining the globe shape (EVANS & MARTIN 1993, KERN & COLITZ 2013, WILLIAMS 1994). The Ossicula posteriora sclerae are ossifications of the sclera posterior to the equator and distinct from the scleral ring. It changes its name to Os nervi optici (Gemmingers osscile or Os opticus) when it surrounds the optic nerve (EVANS & MARTIN 1993).

Cornea

The bird cornea is similar to the mammals' cornea. It possesses five layers:

1. Anterior epithelium (Epithelium corneae externum)
2. Anterior limiting membrane (Lamina limitans superficialis) also known as Bowman´s membrane.
3. Substantia propria (Substantia propria corneae).
4. Posterior limiting membrane (Lamina limitans profunda) or Descemet´s membrane.
5. Posterior epithelium (Epithelium corneae internum).

The cornea in birds is thinner than in mammals, but its thickness varies among birds. By changing its shape it contributes to the eye accommodation. The transition area between the opaque sclera and the transparent cornea is delimited by a pigmented ring called corneoscleral junction (Junctura corneoscleralis or Annulus corneae) (EVANS & MARTIN 1993, KERN & COLITZ 2013, WILLIAMS 1994).

Anterior and posterior chamber

The anterior chamber of the eye (Camera anterior bulbi) is composed of the cornea, lens, iris, and the iridocorneal angle. It is filled with the aqueous humour (Humor aquosus), which possesses a refractive index higher than water. The posterior chamber (Camera posterior bulbi) is smaller and is located between the iris and the anterior surface of the lens (EVANS & MARTIN 1993).

Uvea

Also known as Tunica vasculosa bulbi, the uvea is the vascular layer of the eyeball, and is located internal to the sclera. It is composed of the Choroidea, the Corpus ciliare and the Iris.

a. Choroidea

In some species the choroid can be examined through the fundus (KERN & COLITZ 2013). The choroid contains blood vessels bound in connective tissue to supply nutrients to the retina. It reaches its maximal thickness in the fundus with a powerful capillary bed. It divides into five layers (EVANS & MARTIN 1993):

1.- Lamina suprachoroidea, highly pigmented and thin, attached to the sclera
2.- Spatium perichoroideale.
3.- Lamina vasculosa, mostly arterial tissue.
4.- Lamina choriocapillaris.
5.- Lamina basalis, attached to the retina.

b. Ciliary body

The ciliary body (Corpus ciliare) in birds consists of striated muscle fibers dedicated to accommodative mechanisms. The ciliary processes (Processus ciliares), of non-sensory retinal tissue, go from the ciliary body to the lens capsule. They are very numerous in avian species, heavily pigmented and may converge to another.

The ciliary muscle (Musculus ciliaris) is the main muscle of the ciliary body. It begins posteriorly on the inner surface of the sclera, extends from the optic cup across the scleral ring up to the corneoscleral junction, and attaches on the corneal limbus. One up to four different muscles can occur, but usually two are found: the Crampton´s muscle and the Brucke´s muscle, and their sizes vary among the species (EVANS & MARTIN 1993).

c. Iris and Pupil

The iris is composed of dilator muscles, striated sphincter, smooth muscles and myoepithelium. Within its stroma several pigments occur which are responsible for the iris coloration (KERN & COLITZ 2013). Differences and variations in iris colours were noted in some species according to age and gender. They are created by varying chromatophores (WILLIAMS 1994). The aperture of the pupil is formed by the iris, determining the amount of incidental light and brightness and thus the quality of the retinal image. The circular movement of the pupil is regulated by the retina (pupillary light reflex) and, in addition, by voluntary control. The muscles responsible are the M. sphincter pupillae and M. dilator pupillare which are both striated. In some avian species a secondary non-striated dilator system exists. The ciliary artery (Circulus arteriosus ciliaris) provides the iris blood supply; it surrounds the iris and changes its name to Circulus arteriosus iridis. The drainage is performed through two annular channels (Sinus venosus sclerae or Canal of Schlemm) in the iridocorneal angel (Angulus iridocornealis);

they are relative large and well developed (Sinus ciliosclerales) (EVANS & MARTIN 1993, KERN & COLITZ 2013).

Lens

The lens (Lens crystallina) is soft, pliable and its shape is variable depending on the species. A pad (Pulvinus annularis lentis) of modified lens fibres surrounds the equator of the lens (Corpus centrale lentis). It has an important role in the accommodation and is not present in mammals (EVANS & MARTIN 1993). It is bigger in species with larger accommodation range like birds of prey. The lens refraction power changes by contraction and relaxation of the ciliary muscles. Brucke's muscle and Crampton's muscle exert pressure on the annular pad, compressing the lens and moving the ciliary body axially. A lenticular space filled with fluid is located between the lenticular central body and the annular pad. Depending on the bird species, the ciliary muscle fibre groups (corneal accommodation) or the internal and posterior muscle fibre groups (lenticular accommodation) predominate in the accommodation process (KERN & COLITZ 2013).

Vitreous chamber

The vitreous chamber (Camera vitrea bulbi) is filled by the vitreous humour (Humor vitreus), which has a higher refractive index than water. This space is enclosed by the retinal surface and the posterior surface of the lens (EVANS & MARTIN 1993).

Fundus

The internal surface of the eyeball (Fundus oculi) is delimited by the Ora serrata (EVANS & MARTIN 1993). Its colour varies among species, but is usually grey or red in vivo, flecked with other pigmentations (KERN & COLITZ 2013, WILLIAMS 1994). Other features of the fundus are explained in detail later.

Equator and eye meridians

According to Evans and Martin (1993), "*the equator is the greatest circumference of the eyeball and is usually located approximately perpendicular to the Axis bulbi"*. All avian eyes studied to date show complex asymmetry with respect to the axis bulbi. The equator always lies posterior to the scleral ossicles, typically near, or coincident with, the Ora serrata which limits the nervous retina. The eye meridians (Meridiani bulbi) are

theoretical lines passing through both the anterior and posterior poles and thus surrounding the surface of the eyeball.

Eye axis

Axis bulbi (A. opticus) is the line which goes through the central point of the cornea and the centre of the lens. Axis visualis (A. visus) is the line which goes through the centre of the fovea and the centre of the lens. The Axis visualis thus indicates the area of highest spatial resolution in the visual field. In cases two foveae, a central and a temporal one, are present, an Axis visualis centralis and an Axis visualis temporalis can be differentiated (EVANS & MARTIN 1993).

2.2.5 Retina

2.2.5.1 Anatomy and physiology of the avian retina

Birds are remarkable due to their unique retinal structures. In comparison with the mammalian retina, the avian retina differs in the general morphology as well as in the areas with higher visual acuity and in vascularization. The retina, also called Tunica interna bulbi or Tunica nervosa bulbi is the innermost layer of the eyeball (EVANS & MARTIN 1993).

The avian retina is avascular and atapetal. The absence of blood vessels inside the retina allows the light to cross the retinal surface and reach the photoreceptors with a low scattering, a feature which ensures sharp vision. The choroid, responsible for the retinal oxygenation and the pecten are well developed (KERN & COLITZ 2013 RUGGERI et al. 2010).

2.2.5.1.1 Pecten

The pecten (Pecten oculi) is a highly vascularized and pigmented structure with high interspecific shape variations. It protrudes into the vitreous and darkens the optic nerve head. It is larger and more developed in diurnal species than in nocturnal species. It is compound by neuroectodermal cells covered by a vascular mesodermal core (choroidal tissue). The same structure appears in reptiles. The main function of the pecten is supposed to be nutritive, but it has been considered as a structure with more than 30 possible functions. It disperses a serum filtrate that extends to the retina providing

nutrition and oxygen to the inner retinal portion (KERN & COLITZ 2013, RUGGERI et al. 2010, WILLIAMS 1994). In addition, it has been assumed that the pecten functions as a glare shield of some retinal areas, that it reduces the scattered radiation, or that it even works as an orientation sensor. More likely are pressure-regulatory and thermo-regulatory functions, together with the aforementioned nutritive function (REESE et al. 2008).

Three types of pecten exist (EVANS & MARTIN 1993, REESE et al. 2008):

- Pecten oculi conicus: only found in kiwis (Apterygidae) (Figure 6. a).
- Pecten oculi vanellus: found in the remaining species of Struthioniformes and in Tinamiformes (Figure 6. b).
- Pecten oculi plicatus: in all other species (Figure 6. c)

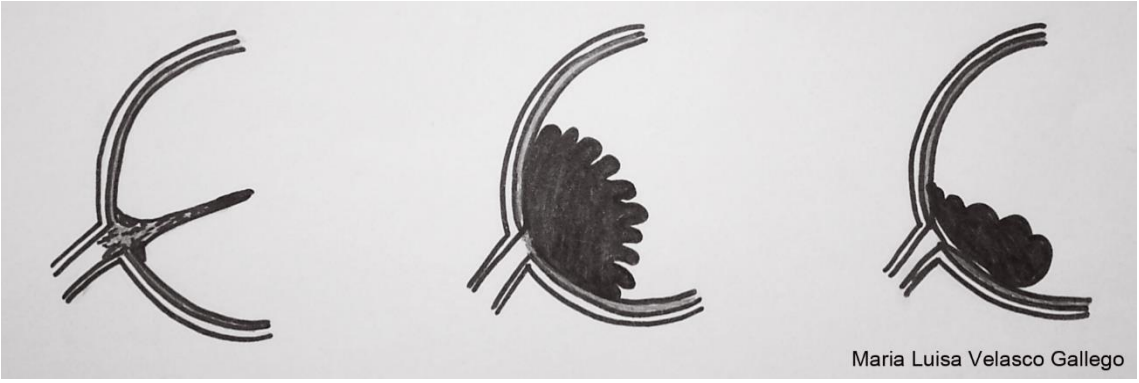

Figure 6. Shapes of the Pecten oculi in birds. From left to right: A) Pecten oculi conicus. B) Pecten oculi vanellus. C) Pecten oculi plicatus.

2.2.5.1.2 Areae and Foveae

The bird retina has definite portions called areas, where cells with special features such as increased density, specific size or a regular disposition occur (EVANS & MARTIN 1993). In these areas, the density of functional photoreceptors is higher and cones predominate over the rods (OFRI 2008). These photoreceptors are longer and thinner in comparison with those found in other retinal regions. There are even areas which contain a specific type of ganglion cells, called giant ganglion cells (COHIMBRA et al. 2012, HAYES et al. 1991). These regions are associated with higher spatial resolution, improved visual acuity and movement detection (EVANS & MARTIN 1993).

In many bird species a circular depression called fovea occurs in these areas, resulting from a radial displacement of several internal retinal layers (EVANS & MARTIN 1993).

Monofoveate, bifoveate and afoveate species exist. Diurnal raptors are bifoveate. In this case, one fovea (deep fovea) is located on the naso-central region of the retina, and another fovea (shallow fovea) occurs in the temporal region. The central fovea has a higher density of photoreceptors than the temporal fovea, and is therefore related with a higher visual acuity. It has been suggested that in bifoveate birds the fovea temporalis serves for near vision and the fovea centralis for long-range vision (TUCKER 2000). In nocturnal avian species such as owls, only one fovea placed on the temporal retinal area occurs, with a high density of photoreceptors (KERN & COLITZ 2013, RUGGERI et al. 2010, WILLIAMS 1994).

2.2.5.1.3 Retinal layers

The retina is divided into two main layers:

- Stratum pigmentosum retinae: an outer pigmented layer adjacent to the choroid.
- Stratum nervosum retinae: this neural retina is the inner nervous layer.

The pigmented retina lengthens outside of the fundus and interior to the Ora serrata as a layer of pigmented non-nervous tissue, and forms the ciliary processes. It also extends to the interior surface of the iris and to the pecten (EVANS & MARTIN 1993).

The neural retina extends up to the Ora serrata, indicating the transition from the choroid to the cilliar body (REESE et al. 2008). It has four main divisions:
Stratum neuroepitheliale: the neuroepithelial layer lies between the retinal pigmented epithelium (RPE) and the external limiting membrane (ELM), which consists of the outer segment and nuclei of the photoreceptor cells.
Stratum bipolare: the bipolar layer in turn is subdivided into the outer plexiform layer (OPL), an inner nuclear layer (INL), and the inner plexiform layer (IPL)

- OPL: contains the photorreceptor cells synaptic terminals.
- INL: compound by nuclei of the horizontal, bipolar, amacrine and Müller cells.
- IPL: like the OPL, contains visual synaptic terminals.

Stratum ganglionaris: is the ganglion cell layer, formed by the ganglion cells (GCL)
Stratum neurofibrarum: the optic fiber layer, which forms the optic nerve when it exits from the bulbus. Unlike in mammals, these fibers exit the bulbus at an elongated instead of circular area.
The Müller cells, are glia cells surrounding the neurons of the retina and are the only cells of the retina extending through all the retinal layers. The terminal bars of processes of adjacent Müller cells form the external and internal limiting membranes (ELM; ILM). A

special feature of the bird retina is that it has the greatest regularity of differentiated layers (EVANS & MARTIN 1993, MARTIN 1985).

There is a remarkable variation in photoreceptor type and density between avian species. In all species cones and rods exist, even double cones with oil droplets, whose proportions vary depending on the visual ecology of each species. Pigment granules are present inside pigment epithelial processes which respond to incoming light by elongating between the rods. Some avian species possess UV vision (KERN & COLITZ 2013). The visual acuity of birds is improved due to a high density of functional photoreceptors in the retina and is remarkably higher than in humans. Diurnal species generally possess more cones than rods, and therefore they have higher visual acuity compared to nocturnal species which have more rods than cones, providing higher visual sensitivity (RUGGERI et al. 2010).

Ora serrata

The anterior retinal border, which separates the sensory retina and the ciliary body, has been named Ora serrata or Ora terminalis, marking the transition from the sensory to non-sensory retina (EVANS & MARTIN 1993).

2.3 Ultrahigh Resolution Spectral-Domain OCT (UHR-SD-OCT)

2.3.1 Indications and applications

The OCT technique has been used in diverse medical research areas including cardiology (BEZERRA et al. 2010, KOBAYASHI et al. 2014), orthopaedics (PILGE et al. 2014), dermatology (GARCÍA HERNÁNDEZ et al. 2013) and ophthalmology (JIAO et al. 2005) among others, demonstrating high potential in the field of diagnostics. However, the most successful application relates to ophthalmology, in particular retinal sectional imaging and 3D retinal imaging (JIAO et al. 2005). In order to determine the value of this technique as a diagnostic tool, it had to be verified that OCT provides an accurate Figure of the retinal anatomy. Thus OCT retinal scans have been compared with light microscopy histology of the retina (HUANG et al. 1998).

OCT has rapidly developed as a non-invasive, optical medical diagnostic imaging modality that enables in vivo cross-sectional visualization of the internal microstructure in biological systems (FERCHER 1996, FUJIMOTO et al. 1995). OCT provides images of retinal structure that cannot be obtained by any other non-invasive diagnostic technique, like the identification or quantification of the overall retinal thickness or the identification of retinal sublaminae in vivo, due to its cross-sectional retinal imaging. Ocular media are essentially transparent; transmitting light with only minimal optical attenuation and scattering providing easy optical access to the retina. For these reasons, ophthalmic diagnosis is one of the most developed clinical OCT applications (DREXLER & FUJIMOTO 2008, FUJIMOTO et al. 1995).
For instance, the development of broadband light sources emitting new wavelengths, e.g., 1050 nm, has enabled not only 3D-OCT imaging with enhanced choroidal visualization, but also reduced scattering losses and improved OCT performance in cataract patients (DREXLER & FUJIMOTO 2008).

2.3.1.1 OCT in human medicine and research

In the past, use of OCT in human medicine and research has mainly focussed on the following topics (VAL VELTHOVEN et al. 2007):

- Improvement of knowledge about the pathophysiology of retinal diseases.
- Detection of early stages of retinal pathology.
- Fast and high quality imaging diagnosis of retinal diseases.
- Mapping of single retinal layers.
- Macular topographic analysis.
- 3D retinal layer reconstruction.
- Accurate follow-up of the patient.
- Avoiding discomfort of the patient.

OCT was already utilized by Schmidt-Erfurth et al. (2005) to visualize eyes of patients with vitreoretinal diseases and patients with lesions in the area between the outer retina and the RPE. Diseases like macular hole, glaucoma, age-related macular degeneration, macular oedema and diabetic retinopathy have been studied through cross-sectional OCT standard imaging systems (RUGGERI et al. 2007, SRINVASAN et al. 2006).

OCT is of particular importance regarding the potential of allowing longitudinal tracking of disease progression. Especially patients with subtle retinal changes which might not be detected during a conventional ophthalmologic examination and which require an accurate longitudinal imaging benefit from this option (DREXLER & FUJIMOTO 2008, GABRIELE et al. 2011).

The 3D OCT visualization, also known as C-mode, provides an improvement in the subjective analyses. The viewing perspective given by the C-mode helps in the diagnosis of many retinal diseases and improves the visualization of lesions such as vitreoretinal traction, age-related macular degeneration, cystoid macular oedema or central serous retinopathyMeasurements performed with an OCT/SLO or en-face system provide more detailed surface structures because the data points are obtained throughout the scanned area (GABRIELE et al. 2011, ISHIKAWA et al. 2009). The 3D OCT has another important advantage over the conventional OCT devices. It permits a quick overview of the retinal area involved in the disease (VAN VELTHOVEN et al. 2006).

Although evaluation of 3D images obtained by OCT requires a certain degree of experience due to the unfamiliar type of the scans, it was reported that many clinicians will get used to the 3D imaging and will thus be able to recognize the different retinal lesion patterns like neurosensory and pigment epithelial detachment (PED) (VAN VELTHOVEN et al. 2007). According to Van Velthoven et al. (2005), a neurosensory detachment visualized using OCT is characterized by a border composed of concentric rings of the compressed retinal layers with a hyporeflective centre, while a PED is recognized by its hyperreflective ring of RPE surrounding an optically empty area casting a shadow in the deeper frames. C-scans allow an easy identification of the extent of alterations. Using OCT a diffuse RPE involvement was detected in central serous retinopathy (CSR) (VAN VELTHOVEN et al. 2005).

The main clinical applications of OCT are retinal thickness measurement, glaucoma, diabetic retinopathy, objective assessment of macular hole, vitreo-retinal evaluation, intraoperative OCT, anterior segment OCT (AS-OCT) and progress monitoring of retinal vasculopathies (DREXLER & FUJIMOTO 2008, GABRIELE et al. 2011, SRINVASAN et al. 2006, VAN VELTHOVEN et al. 2007).

2.3.1.1.1 Retinal thickness measurement

The ability of the last SD-OCT en face systems to visualize and reproduce retinal thickness measurements is clearly higher than in TD-OCT, allowing a quantification of the retinal thickness even in the early stages of disease (GABRIELE et al. 2011).

Traditionally, in order to assess various retinal parameters such as total retinal thickness and inner retinal complex (IRC) using TD-OCT, six radial macular scans were performed. Nowadays with 3D high resolution of retina imaging of SD-OCT, it is possible to visualize subtle structural changes, like those pathological processes appearing in the IS/OS junction posterior to macular hole surgery (GABRIELE et al. 2011). The modern commercial systems produce not only B-scan lines built up from 512 adjacent A-scans in 1.3 seconds, but also six radial scan lines built up from 768 A-scans in 1.9 seconds. All those lines are commonly used to obtain a retinal thickness map to determine the distance between the RPE and ILM. This is especially relevant at a 6 mm area around the macula, and it has been shown that the measurements are reliable and reproducible (VAL VELTHOVEN et al. 2007).

The measurement and determination of the retinal thickness is important to assess retinal disease. For instance, a thickening of the epiretinal membranes (ERM) causes a thickening of the whole retina and consequently loss of the foveal depression (VAL VELTHOVEN et al. 2007).

OCT has also been shown to be indispensable to differentiate between secondary ERM pseudo-holes and idiopathic full-thickness macular holes. It is also useful to objectively evaluate the retinal decrease after surgical approaches (VAL VELTHOVEN et al. 2007).

2.3.1.1.2 Glaucoma

The OCT technique is useful to quantify in vivo the retinal nerve fiber layer (RNFL) thickness and the features of the optic disc. Differences present in these areas in healthy and glaucomatous eyes can be detected by OCT and the structural damage inflicted by glaucoma can be evaluated (GABRIELE et al. 2011, VIZZERI et al. 2009).

With the 3D scanning or en-face method, already available in the latest SD-OCT commercial systems, it is now possible to precisely locate the retinal lesions and to create an RNFL thickness map, which is compound by all thickness measurements outside of the optical nerve head (ONH). However, until now, a quantitative valuation using the available RNFL information is not yet possible (ISHIKAWA et al. 2005, GABRIELE et al. 2011, KIM et al. 2010).

2.3.1.1.3 Diabetic retinopathy

OCT is very useful in the diagnoses of diabetic retinopathy. Through the retinal thickness map, the more affected areas can be accurately determined. It has been demonstrated that the correlation between retinal thickness and visual acuity in diabetic macular oedema and epiretinal membrane (ERM) is very high.

OCT is a powerful tool to detect even early stages of diabetic retinopathy thanks to its Doppler modality. No other blood flow imaging modality allows imaging of the retinal microvasculature occlusion, with the exception of fluorescein angiography, which is only qualitative. OCT-Doppler visualize the retinal blood flow and movement. The venous blood flow is distinguished from the arterial due to the flow direction towards the nerve head. It is also possible to measure the volumetric flow rate.

The location of the damages and the thinning areas found on the patient retina correlates with the areas with a low venous flow (GABRIELE et al. 2011, WANG et al. 2009).

2.3.1.1.4 Objective assessment of macular hole

OCT allows a very objective assessment of the macular hole in retinal disease, because it clearly demonstrates the hole configuration. For standardization purposes several parameters have been already established such as macular hole index and hole form factor. The diameter of the macular hole has been shown to be the best prognostic index and a useful indicator for surgical intervention (JOHNSON et al. 2001, ULRICH et al. 2002, VAN VELTHOVEN et al. 2007).

2.3.1.1.5 Vitreo-retinal evaluation

OCT technique is also very helpful to assess pathological processes at the vitreoretinal interface and it can be used to decide on a surgical intervention. OCT was successfully used in identifying the stage 0 macular hole revealing already localized perifoveal vitreous detachment which leads to this first macular hole stage even in idiopathic macular holes. Then, progressing disorders including development of a foveal pseudocyst, further outer retinal disruption and a full thickness macular hole were visualized (JOHNSON et al. 2001, ULRICH et al. 2002, VAN VELTHOVEN et al. 2007).

2.3.1.1.6 Intraoperative OCT

First tests exist to use OCT as an intraoperative tool in surgery of the anterior eye segment. Visualization in patients with macular disease was improved under vitrectomy when either the epiretinal membrane or the internal limiting membrane (ILM) was removed. Currently, the use of the OCT devices in this area is still under development (GABRIELE et al. 2011).

2.3.1.1.7 Anterior Segment OCT (AS-OCT)

The aim of AS-OCT is to provide information about the anatomy and pathology of structures of the cornea and the anterior chamber of the eye. It is a non-contact technique like conventional retinal OCT, and its resolution is higher than ultrasound biomicroscopy (UBM). Structures like sclera and iris are visualized in high resolution with AS-OCT. It can image structures such as the trabecular meshwork and Schlemm´s canal or the iridocorneal angle which can easily be measured. AS-OCT is mainly used for diagnosis and follow-up of patients with ceratoconus and LASIK (Laser-Assisted in Situ Keratomileusis), measurement of the lens thickness in phakic eyes and assessment in intracorneal ring replacement surgery (GABRIELE et al. 2011, KAGEMANN et al. 2010, RADHAKRISHNAN et al. 2001).

2.3.1.1.8 Progress monitoring of retinal vasculopathies

OCT is a useful tool to monitor progress over time not only in processes like retinal thickness changes or size changes in cystoid structures and serous retinal detachments, but also in retinal vasculopathies. However, fluorescein angiography (FA) is still the gold standard to evaluate retinal vasculopathies. OCT is also used to prove the efficiency of antiangiogenic drugs, and the age-related macular degeneration (AMD) patient management (VAN VELTHOVEN et al. 2006, VAN VELTHOVEN et al. 2007).

2.3.1.2 OCT in veterinary medicine and research

OCT has become a powerful tool regarding the investigation of the animal eye, not only as a model of human diseases but also as a way to achieve knowledge about the anatomy, physiology and pathology of the retina among different animal species.

In the last years, an increasing number of studies performed in veterinary medicine and research was possible certainly due to an increasing commercial availability of OCT devices as a technique characterized by a non-invasive nature of image acquisition
3D retinal views allow an accurate comparison of the location, spatial registration and degree of retinal lesions and of other ocular diseases over time. Quantitative evaluation of the structure and morphology of the different retinal layers were also achieved (SRINVASAN et al. 2006, RUGGERI et al. 2007). Especially in research, this lead to a considerable reduction of the number of animals needed.

Small animal models preferred in developmental biology, such as *Xenopus laevis* larvae and zebrafish embryos, have already been studied by OCT. In *Xenopus laevis* OCT was successfully used for imaging developing structures, and the structural morphology could be identified in vivo and at greater imaging depths than with confocal and light microscopy. Using OCT in the zebrafish embryo resulted in three-dimensional data sets, which allowed the construction of C-mode slabs of the embryo. SD-OCT provided ultra-high resolution visualization of the eye, brain, heart, ear, and spine of the developing embryo (BOPPART et al. 1996, GABRIELLE et al. 2011, KAGEMANN et al. 2008).
Rodents are popular models for human disease, due to their low cost and easy access to transgenic specimens. Using OCT, eye growth, physiological eye features, myopia, and retinal degeneration were characterized with high image quality, and a high correlation between OCT images and histology was found (RUGGERI et al. 2007, HUBER et al. 2009). This non-contact, non-invasive and in vivo imaging of the rodent retina proved to be appropriate for longitudinal studies and repeated examinations of the same individuals allowing a reduction in experimental animal numbers. Other rodents such as the tree shrew were also successfully imagined through OCT (ABBOTT et al. 2009).

Due to their larger eyes, rats were used to study structural retina changes in experimental longitudinal studies, and OCT was shown to be appropriate to observe the development of pathological changes produced by retinal vein occlusion, retinal ganglion cell degeneration, post nerve-crush injury and increased intraocular pressure (ABBOTT et al. 2009, BAI et al. 2010, GABRIELLE et al. 2011, GLOESMANN et al. 2003, NAGATA et al. 2009, SRINVASAN et al. 2006).

Other animals like pigs, cats, and rabbits, and also avian specimens like chickens serving as animal models have been imaged with OCT. Especially nonhuman primates were used due to their eye size and structural features most similar to human eyes rendering large modifications of the OCT system unnecessary (CONG et al. 2008, GABRIELLE et al. 2011, GLOESMANN et al. 2003, HUANG et al. 1998, KIM et al. 2009, RUGGERI et al. 2010, STROUTHIDIS et al. 2009 a). Recent investigations very often aimed at the characterization of the retinal pathological changes in the areas of the RNFL and ONH caused by increased intra-ocular pressure (IOP), which is commonly present in glaucoma, as well as in measurement of the RNFL. Using OCT, eye structures like the end of the Bruch´s membrane, the border tissue and the anterior opening of the scleral canal were visualized and the images and the results compared with histological specimens (STROUTHIDIS et al. 2009).

OCT using animal models has gained special relevance in research on glaucoma using conventional and enhanced depth imaging SD-OCT (EDI SD-OCT) in nonhuman primates. With the EDI SD-OCT it was possible to obtain reliable images from the choroid and sclera, which was not possible with a conventional SD-OCT (YANG et al. 2012).

Because of the ability of the OCT devices to be used in longitudinal studies, OCT has increasingly been applied for controlling disease treatment protocols, for example the evaluation of the efficacy of pharmacologic drugs and stem cell therapy, and at the same time reducing the number of animals needed for each investigation. Consequently, expectations for the potential of using OCT in this field are huge (GABRIELE et al. 2011). However, interpretation of the retinal structural changes over time, for example before and after pharmacological treatment, is complicated by species-specific differences in retinal structures and possible species-specific interpretation of the OCT signal patterns (ABBOTT et al. 2009).

2.3.1.2.1 OCT in avian ophthalmology

Until now, reports about OCT applications in birds are rare. Several investigations were performed using domestic chicken as animal models for human eye diseases, in breeds such as White Leghorn and Rhode Island Red. In 1998 already, Huang et al. used OCT to scan retinas from normal chicken and chickens with retinal degeneration (rd), and OCT results were validated by correlating with retinal histology using unfixed stained cryosections from the same retinal regions.

Chicken were also used in a longitudinal OCT investigation to observe the effect of topical instillation of a 0.4 % nicotine solution in iridectomised and non-iridectomised eyes (OSTRIN et al. 2011). In 2012 the first report of in vivo volumetric retinal imaging of the chicken with UHR-OCT has been published (MOAYED et al. 2011). In addition, pupil and iris of the chicken were studied through UHR-OCT, resulting in the first measurements of visually evoked pupillary dynamics and quantification of pupillary constriction depending on a visual stimulus in animals (MOAYED et al. 2012).

OCT examinations in avian ophthalmology were not only performed in birds used as animal models. Korbel et al. (2012) carried out OCT eye examination in psittacines such as African grey parrot. In 2013, Korbel et al. (2013 a) examined with the same technique chickens and pet birds. Ruggeri et al., (2010) visualized the retinas in four individuals belonging to four different raptor species. In this report, several retinal features such as

the morphology of foveae and the area of the pecten oculi, as well as the absence of retinal blood vessels and the general retina topography were described. Important differences were found between the individuals. However, from the data presented in this study it was not possible to conclude whether these differences between the single individuals of every species detected in this preliminary study represented true interspecific variations or whether they were individual characters and variations indicating the need for more research in this field. Azmanis et al. (2012), Korbel et al. (2013 b), and Velasco Gallego et al. (2014) presented OCT eye examinations in several avian individuals.

Later, a second study in birds was published including 45 individuals of 25 species including 12 raptor species. However, physiological retinal features were presented only rudimentarily as a brief description of the anatomical structures observed in the posterior chamber and fundus, or peculiarities like physiologic pigmentations. Descriptions were focussing on the visualization of pathological findings in raptors, and on a comparison of the results obtained with OCT and direct ophthalmoscopy. (Rauscher et al. 2013). Rauscher et al. (2013) said that "*OCT diagnostics provide more detailed and accurate information about the pathologies of the posterior eye, with a higher incidence of detecting pathologic changes in comparison with direct ophthalmoscopy. Futhermore, we conclude that SD-OCT is an excellent tool for the in vivo evaluation of evelopmental or pathologic alterations of avian retinas, as well as for studies on structural differences between species in living birds*".

2.4 SD-OCT Reflectance patterns

Each OCT-acquired image is displayed by the software in a greyscale. When the B-scan is represented in a so-called positive setting, low backscattered areas are represented with a darker grey, and the high backscattered are shown in a brighter grey. It has been shown for humans and rodents, that all the retinal layers known from histology can be distinguished thanks to this colours differences (RUGGERI et al. 2007).

An appropriate understanding of the OCT reflectance patterns is vital for the clinician to be able to come to accurate diagnoses. With the OCT device, changes in tissue optical scattering properties of refractive index discontinuities can be observed, but it is not possible to differentiate between tissues or structures with similar optical backscattering properties (ABBOTT et al. 2009, SRINVASAN et al. 2006).

In humans and mouse, layers consisting of nerve fibers or plexiform layers produced a higher backscattering than nuclear layers, which generated a poor backscattering (RUGGERI et al. 2007).

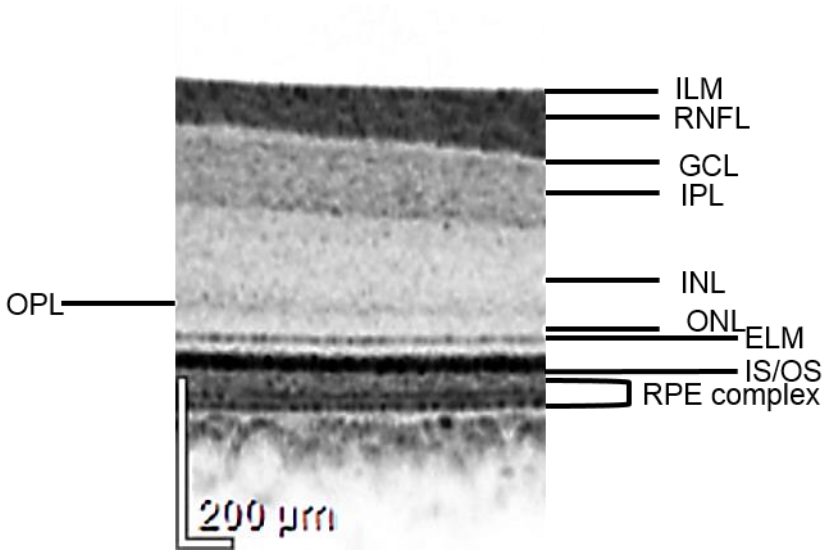

Figure 7. OCT-section. Equator area, *Buteo buteo*. All the retinal layers can be distinguished with high quality. Internal limiting membrane (ILM), retinal nerve fiber layer (RNFL), ganglion cell layer (GCL), inner plexiform layer (IPL), inner nuclear layer (INL), outer plexiform layer (OPL), outer nuclear layer (ONL), junction between the inner segment and the outer segment of the photoreceptors (IS/OS), retinal pigment epithelium (RPE) complex.

As shown in the OCT image of Figure 7, the most internal retinal layer, the internal limiting membrane (ILM) is the first structure which produces backscattering, and which can be well distinguished from the non-backscattering vitreous. It represents the borderline between the retinal nerve fiber layer (RNFL) and the vitreous. The RNFL is the first layer with high light backscattering with the ganglion cell layer (GCL) immediately beneath (RUGGERI et al. 2007). According to Ruggeri et al. (2007) this GCL can be identified in the mouse retina. The next four layers have lower backscattering than the RNFL and GCL. These layers are the inner plexiform layer (IPL), the inner nuclear layer (INL), the outer plexiform layer (OPL), and the outer nuclear layer (ONL). The INL and ONL present in a darker grey than IPL and OPL confirming the view that nuclear layers produce a lower backscattering than plexiform layers.

The next layer observed in OCT images is the external limiting membrane (ELM), which is formed by numerous occluding junctions and can be visualized as a thin line with relative high backscattering. Next to it, the junction between the inner segment (IS) and the outer segment (OS) of the photoreceptors can be seen, representing the change in grey of a layer with a high backscattering and a layer with a low backscattering (RUGGERI et al. 2007). The high reflectance in the region between IS and OS occurs at the abrupt transition from the IS ellipsoid to the OS (GLOESMANN et al. 2003,

SRINVASAN et al. 2006). According to Srinvasan et al. (2006), "*the reflective band posterior to the photoreceptor IS/OS junction may be due to scattering from the OS tips in the region of interdigitation between the photoreceptor OS and the melanin-containing RPE cell processes that extend into the OS layer*" (GLOESMANN et al. 2003, SRINVASAN et al. 2006). This distinct, highly reflective band observed in the OS of the human and rodent retina is consistent with directional reflectance components in the OS detected in earlier fundus reflectometry studies, and confirms results of previous OCT studies of the porcine retina. This three layer complex was first described by Sander et al. (2005). Depending on the OCT device used, it is possible to visualize a further layer in this region, usually seen as a unique high backscattering layer. It was hypothesized that the first high backscattering layer represents the OS of the photoreceptors weaved together with the end of the RPE cells containing melanin, and that the second layer arises at the transition area of the RPE cell bodies, the choroid and the choroid complex (VAN VELTHOVEN et al. 2007).

Beneath this low backscattering layer the retinal pigment epithelium complex (RPE complex) can be seen as a high backscattering layer delimitating the retina from the choroid. It is composed of multiple layers. In the murine retina three layers are observed in this complex, but the layers number varies among species. Retinal pathologies such as serous fluid accumulation and macular holes produce an elevation of the two innermost RPE complex layers (RUGGERI et al. 2007, SRINVASAN et al. 2006).

Blood vessels can be clearly observed in the retina of mammals. They are very low backscattering structures which produce absorption of the OCT beam due to the choroid melanin, and therefore produce a shadow in the tissue located immediately below the blood vessels (SRINVASAN et al. 2006). The choroid can be well recognized due to its high reflectivity, and also its vessels can be identified because they typically cast a shadow over the neighbouring tissue caudal to the choroidal blood vessels. The melanin content of the choroidea plays an important role in the absorption of the light beam, it varies among species. High melanin content will interrupt the light beam way through the tissue (SRINVASAN et al. 2006).

The internal retinal layers identified by OCT have already been confirmed by histology. However, structures below the RPE, which include Bruch´s membrane, choriocapillaris and the choroid complex have to be verified. In addition, the RPE as shown in OCT images seems to be thicker compared to histological retinal samples, where the RPE represents as a mono-cellular layer (DREXLER & FUJIMOTO 2008). Further reflectance

patterns influencing or disturbing the OCT image can include opacities in intraocular media, found in the vitreous, in corneal haze, or in cataract patients (DREXLER & FUJIMOTO 2008).

2.4.1 Bird-eye-specific reflectance patterns and OCT imaging

Anatomical peculiarities of the avian eye might have to be taken into consideration in order to carry out accurate interpretations of the OCT reflectance patterns. At the moment, however, it is not known whether ultraviolet (UV)-sensitive cones detected in chicken as a fourth type of photoreceptors, are influencing the light scattering pattern of the retina. Furthermore, an influence of intrinsically photosensitive retinal ganglion cells (ipRGCs) which have been detected in chicken (MOAYED et al. 2012), but also in mammals or amphibians (MARKWELL et al. 2010), is still unknown. Rauscher et al. (2013) remarked that the exact correlation of the retinal sublaminae with the layers observed in an OCT-scan is controversial. Furthermore, they specified that an ultrastructural investigation of these features should be performed in order to determine the relationship between the layers observed with OCT and the retinal tissue (RAUSCHER et al. 2013).

As mentioned before, eyes of four specimens of birds of prey were imaged in vivo with OCT for the first time by Ruggeri et al. in 2010, providing 3-D images with 2.8 µm axial resolutions. In this preliminary study backscattering patterns correlated well with the expected high or low backscattering of each retinal layer. Plexiform layers were highly backscattering and nuclear layers were low backscattering, as observed in mammals and chickens (RUGGERI et. al. 2010). Absence of blood vessels (avascularity) in the raptor retina was confirmed by OCT in this investigation. Deep fovea and shallow fovea were visualized and measured, and a good correlation of measurements in OCT and in histology was found. A further peculiarity was described for the broad-winged hawk retina using OCT. Contrary to what has been previously described in raptors the “shallow fovea” in this bird seemed not to be a depression but a modest retinal thickening. Whether this represented a characteristic of an individual bird or of the entire species is unknown. The outer segments of photoreceptors in this region appeared thickened, suggesting a higher photoreceptor density. In this study a low backscattering layer was recognized in the deep foveal region immediately external to the RNFL. Whether this line corresponded to the GCL or the extended axons of the photoreceptors is, however, still unknown, and cannot be distinguished in the OCT image. The same layer was also detected in the shallow foveal area (RUGGERI et al. 2010).

The base of pecten and the optic nerve head (ONH) have also been visualized in these four raptor individuals with OCT. The pecten protrusion into the vitreous could be visualized, but it created a shadow to the retinal tissue inferior to this structure (RUGGERI et al. 2010).

In mammals, the retinal blood vessels are generally taken as a reference and landmark to calculate the spatial relationship between the retinal structures in order to create a retinal map. In birds, however, the retina is avascular, and therefore, differing methods to create a retinal mapping for use in OCT were needed to determine the spatial location of structures with high importance in the avian ophthalmology such as foveas, pecten or OHN. It has been suggested to use the retinal thickness as a reference for the retinal mapping in absence of other landmarks (RUGGERI et al. 2010). However, its usefulness has still to be proven.

Ruggeri et al. (2010) imaged a blind eye of the broad-winged hawk using OCT revealing retinal lesions with retinal detachment, subretinal appearance of proteinaceous fluid and cysts (RUGGERI et al. 2010).

2.5 Alignment and comparison of histology and UHR-SD-OCT of retinal layers

Correct interpretations of OCT data, which are reflectance patterns, and their correlation with anatomical structures require evaluation by histology. Since anatomical differences in retinal structures exist, transfer of evaluation results and of interpretations of OCT reflectance patterns between mammals and birds and even between species within these classes is problematic. OCT data collected from humans, until now, are generally not based on a thorough evaluation by histology of human retina but rely on transfer of evaluation data from related species, for example the tree shrew (ABBOTT et al. 2009). This is because availability of retinal tissue of human origin for histology is highly limited due to the low donor rate (ABBOTT et al. 2009).

First OCT-histology comparisons were performed by Huang et al. (1991) and Huang et al. (1998) in human and avian ophthalmology. Huang et al. (1991) evaluated the results of OCT retinal examination with histology of human retina using Stevenol's blue-stained and Toluidin blue-stained plastic sections. In 1998 Huang et al. provided objectivity to the comparison of the OCT results from chicken eyes with normal and degenerated retinas. They validated the OCT results using unfixed, stained cryosections from the same retinal locations, and using tissues embedded into resin for electron microscopy. The eyes were not fixated to avoid shrinkage. In order to obtain high objectivity computer programs such as MATLAB were used for the post-acquisition image processing of OCT scans and histologic sections. A high correlation of retinal reflectance patterns obtained by OCT and retinal layers detected by histology was obtained (Huang et al. 1998).

Abbott et al. in 2009 remarked that the reflectivity patterns observed with OCT in vitro were different than in vivo due to fixation procedures. The use of different OCT devices with different axial resolutions and consequently differing number of bands of reflectivity in the OCT signal in recent studies revealed another complication, the variation in retinal reflectivity patterns among studies. Therefore, a complete understanding of the signal production in the OCT technique is needed (ABBOTT et al. 2009). In the investigation of Abbott et al. (2009) on tree shrews some of the OCT results could not be explained due to the lack of histological sections of choroid and sclera.

With regard to comparisons of OCT signals and retinal histology, there is a general concurrence in the scientific literature that the nerve fiber and plexiform layers are highly

reflective, and the nuclear layers less reflective. Other layers like the ganglion cell layer (GCL) differed in reflectivity among species (ABBOTT et al. 2009).

2.5.1 Histologic preparation of the eye

First of all, it is important to remark that tissue processing using fixation or dehydration for histological purposes is always associated with tissue shrinkage. According to Werther et al (2013), retinal detachment is a typical artefact observed in avian eyes after formalin fixation, and clearly influenced by the shrinkage. However, it seems that comparisons between OCT images and histology are generally performed without correcting for shrinkage or for other parameters interfering processing (ABBOTT et al. 2009). When shrinking is taken into account, the extent is often calculated after performing the B-scans based on a comparison of the OCT scan with the histological sample (ABBOTT et. al. 2009). In order to assess shrinkage in retinal tissues of mammals, Abbott et al. (2009) dissected the retina from the sclera and choroid. They cut the retina into quadrants through the optic disc and embedded the tissues using epoxy resin. Abbott et al. (2009) measured the lateral shrinkage using structures such as retinal blood vessels and pigment epithelium defects. However, this method developed for mammals cannot easily be transferred to eyes of birds, especially raptors. In raptors, the sclera canot be easily removed from the retinal tissue without producing a number of artefacts. Using retinal blood vessels as landmarks are only useful in mammals due to their vascular retinas, and with retinal alterations, but cannot be considered in avian patients with healthy eyes and avascular retina.

Tissue processing without fixation or dehydration, however, cannot solve these problems because then, in such tissues, mechanical artefacts would appear during the cutting process (ABBOTT et al. 2009). Therefore, quantitative investigations on the correlation between OCT and histology are almost completely lacking. In addition, it is important to note, that in histology, contrast in the tissue slides is obtained through exogenous tissue staining, while in OCT, contrast comes from the differences in the optical properties of the retinal tissue. Because of this fundamental difference, a perfect correlation of OCT images with histology cannot be expected (ABBOTT et al. 2009, DREXLER & FUJIMOTO 2008).

Regarding retinal histologic processing, the axial shrinkage has been found to be nonlinear in mammalian retina. In cryo-processing, for instance, the RNFL and the GCL sustained less shrinkage than the IPL, the INL, and the OPL. In addition, post mortem

artefacts arising especially during eye extraction, such as retinal detachment, are commonly found and can complicate the measurement of retina structures, especially of features of the photoreceptors (ABBOTT et al. 2009, SRINVASAN et al. 2006).

3 MATERIALS AND METHODS

3.1 Avian patients

The study was conducted from February 2012 to July 2013 at the Clinic for Birds, Reptiles, Amphibians and Ornamental Fish of the University Ludwig Maximilian (Munich). The eyes of 56 raptors belonging to 12 species from 3 orders were included in this investigation (Table 1). All participants of the study were wild birds hospitalized in the clinic due to history of trauma and were therefore ophthalmoscopically examined. An ophthalmoscopic examination and a posterior OCT examination were indicated because of this history of trauma in order to evaluate the status of the eye. In all cases both eyes were examined.

The species *Buteo buteo* was the most common patient species and therefore most frequently studied. Several raptor species show no unequivocal sexual dimorphism and therefore the gender was not determined in the majority of the patients of those species. In case of patients that had to be euthanized due to humanitarian reasons, a necropsy was also performed and the gender could be specified. All patients were adults, but their exact age was not known.

Table 1: Species and gender distribution of the birds included in this investigation:

Order	Species	Total	Male	Female	Gender unknown
Accipitriformes	Common buzzard (*Buteo buteo*, LINNAEUS 1758)	15	x	1	14
	European honey buzzard (*Pernis apivorus*, LINNAEUS 1758)	5	x	x	5
	Sparrow hawk (*Accipiter nisus*, LINNAEUS 1758)	4	x	x	4
	Northern goshawk (*Accipiter gentilis*, LINNAEUS 1758)	2	x	x	2
Falconiformes	Common kestrel (*Falco tinnunculus*, LINNAEUS 1758)	7	3	4	x
	Peregrine falcon (*Falco peregrinus*, TUNSTALL, 1771)	5	x	1	4
	Western Marsh-harrier (*Circus aeruginosus*, LINNAEUS 1758)	1	x	x	1
Strigiformes	Tawny owl (*Strix aluco*, LINNAEUS 1758)	5	x	x	5
	Eagle owl (*Bubo bubo*, LINNAEUS 1758)	2	x	x	2
	Long-eared owl (*Asio otus*, LINNAEUS 1758)	7	x	x	7
	Barn owl (*Tyto alba*, SCOPOLI 1769)	1	x	x	1
	Boreal owl (*Aegolius funereus*, LINNAEUS 1758)	1	x	x	1
	Little owl (*Athene noctua*, SCOPOLI 1769)	1	x	x	1

This study focused on the variation of retinal thickness in different physiologic retinal areas outside the foveal areas. The OCT analysis of foveae of different raptor species is included in the study and doctoral thesis of SCHULZE (in preparation) in a parallel investigation.

3.2 Clinical examination of the patients

3.2.1 General clinical examination

Wild raptors brought to the clinic with a history of trauma underwent a general clinical examination. Most of them were examined immediately after hospitalization and in a few cases not later than during the day of entrance. This clinical examination was divided into the following steps:

3.2.1.1 Anamnesis

Personal identification

Parameters such as breed, gender and age (if possible) as well as identification marks (ring) were recorded.

History

As much information as possible about the birds was collected given the fact that they were brought to the clinic by random people who found them. The finder was asked about location, time, state of health and behaviour during the first contact till the handover to the clinic. In case trauma occurred under the observation of the finder, data on the exact cause could be acquired. In general, information on clinical history was restricted to the general condition and behaviour from the point on that the birds were found while information concerning the beginning of the patient sickness was lacking.

3.2.1.2 Adspection

- General condition
- Behaviour
- Feathering condition
- Posture
- Vision capacity
- Skin surface and skin adnexa
- Body orifices
- Respiratory activity
- Body secretions

3.2.1.3 Physical examination

- Nutritional status
- Plumage
- Skin surface and skin adnexa
- Hydration status
- Eyes
- Ears
- Nose and sinuses
- Crop
- Beak and beak opening
- Breathing
- Abdomen palpation
- Cloaca

The examination of the crop was performed as a routine test in all patients included in this study. A crop swab was taken and was microscopically examined. Scent and colour of the crop swab were also considered. Faeces were examined by inspection and microscopic examination.
The procedure of eye examination was mandatory for all trauma patients and is described in detail below.

Depending on the health problems of the individual patient further diagnostic tests were performed:

- X-ray
- Differential blood cell count
- Packed cell volume (PCV); haematocrit
- Biochemistry
- Heavy metal poisoning test: zinc, lead
- Endoscopy
- Ultrasound
- Biopsy and cytology
- Bacteriological, mycological, parasitological and virological investigations

Every examination was performed fast and accurately to minimize the stress of the patients. Some investigations such as x-rays or endoscopy were performed using general anaesthesia or light sedation.

3.2.1.4 Ophthalmological examination

3.2.1.4.1 Instrumentation

The ophthalmological examination was performed with a slit lamp (SL 15 Slit lamp, Kowa, Tokio, Japan), a Finnoff transilluminator (Ladegriff beta NT 3.5 V, Heine, Herrsching, Germany), a headband indirect ophthalmoscope (Omega 100, Heine, Herrsching, Germany) completed by different ophthalmoscopic magnifiers (Double Aspheric" lenses, with 30, 78 and 90 diopter refraction power and specifically coated, light saving version "Clear View®", Volk Optical Inc. Mentor, USA), and with an applanation tonometer (Tono-Vet®, Acrivet, Heningsdorf, Germany). If a corneal injury was assumed, a fluorescein test (SE Thilo®, Alcon Pharma GmbH, Vienna, Austria) was also performed. The injured corneal areas were identified by visualizing adhering remains of the fluorescein with the means of blue-light filter of the slit lamp, enabling the accurate localization and evaluation of the lesion.

3.2.1.4.2 Examination procedure

The ophthalmological examination was performed as described by KORBEL et al. (2001).

The examination was performed in a darkened room that allowed the optimal identification and evaluation of the physiological or pathological ocular conditions. The darkness minimized the stress of the patient since it works as an optical immobilization. In addition, noises were also minimized, and a person experienced in handling raptors held the patient during the examination.

Firstly, adspection of individual eyes and a comparison of both eyes and a visual investigation of eye adnexa were performed in order to detect possible injuries and lesions such as wounds, asymmetries, loss of feathers in the periorbital area, changes in the shape or alteration of the ocular globes, and ocular and periocular discharges. Of special importance in the trauma patients, the ears were also inspected because a part of the caudal fundus periphery can be visualized by viewing through the ear opening. This was especially important in owl species, where even parts of the lateral and posterior areas of the bulb could thus be investigated. Bleeding in the ear was regarded as an indication for a fundus lesion. Visus was tested by triggering the menace reflex.

As a second step tonometry was performed. It was carried out bilaterally by every patient immediately before and after the OCT examination in order to detect pathological conditions and to detect a possible increase in intraocular pressure induced by stress (due to eye investigation). Due to the shortage of information about reference values of intraocular pressure in bird patients, it was important to perform the tonometry in both eyes, especially in case only one eye was injured or altered. In this way, at least the healthy eye could be considered as a reference measurement of intraocular pressure. The tonometry was performed three times in each eye. The average rate was calculated and accepted as result of the tonometry.

Third, the anterior eye segment was examined with the help of a Finnoff transilluminator used as a diascleral cone, which emits a rounded light beam. The transparent structures of the anterior eye segment were examined in order to follow the way of the frontal light towards the retinal surface in order to detect ocular alterations such as corneal and lens opacities and lesions, and iris alterations like cysts or colobomas. Traumatic alterations like hyphema or hypopion could be recognized and evaluated as well. In order to identify

and evaluate all the eye structures separately, different kinds of direct lateral oscillatory light were utilized. By the means of the slit lamp, structures in the anterior part of the eye were visualized with a 10 to 16-fold magnification. The slit lamp was also used to visualize the three Purkinje reflexes to discard lesions such as lens absence, lens luxation, opacities present in the lens, structures anterior to the lens or foreign bodies.

The fourth step was the examination of the fundus oculi. Two different techniques were performed, a direct monocular ophthalmoscopy and an indirect binocular ophthalmoscopy. For the direct ophthalmoscopy, a Finnoff transilluminator was used as a diascleral cone, and the examiner had a direct view in bird`s eye. Only a small area of the fundus could be observed due to the limited 5 to 7-fold magnification produced by the bird eye lens itself. Consequently, observation of the fundus was restricted to the area of the pecten and the immediate surroundings.

The indirect binocular ophthalmoscopic examination was performed with the help of a headband ophthalmoscope and a Volk lens. The bird was hold by an experienced person, while the clinician placed the lens in the light way between his eye and the eye of the bird under examination. The complete fundus of the eye could be visualized and investigated by gently tilting the head of the bird and re-locating the lens. The image seen is a mirror image of the fundus itself. This is a very important factor to locate fundus lesions, and to control their evolution with time. The indirect ophthalmoscopy enabled the examination and evaluation of the periphery of the fundus in addition to the area of the pecten and surroundings.

With both techniques, ocular alteration such as bleeding, fibrin deposits, opacities of the vitreous, retinopathies and morphological alterations of the retina and pecten could be detected.

Unlike mammals, birds use striated iris muscles to dilate the pupil. Therefore, conventional mydriatic agents used in mammals to produce mydriasis cannot be applied in birds because their mode of action is based on influencing the smooth muscles of the mammalian iris. In avian patients, mydriasis was achieved by a 3 % tubocurarine injection into the anterior eye chamber, through the Limbus cornealis as a paracentesis. This was used in cases where ophthalmological examinations were expected to require longer time. The injection was applied under general anaesthesia. However, in most cases only a short mydriasis period was needed, and injection of mydriatic agents into the eyes was not necessary.

Ophthalmological examinations were performed immediately after general anaesthesia, taking advantage of mydriasis which is produced under this condition. An advantage of OCT device is that it does not require complete mydriasis. The light beam, after entering the pupil opening, broadens making a bigger area of the fundus visible and thus avoiding the need of mydriatic drugs.

A special case appeared when the eyes of owls had to be ophthalmoscopically examined. These bird species show a physiological mydriasis in case of fear, and this natural reaction was used as an opportunity to perform the ophthalmological examination.

If there was a need to discard a corneal injury, a fluorescein test was performed. A drop of fluorescein was applied into each patient eye. After 20 to 30 seconds, the eye was rinsed with sterile physiological NaCl solution to remove the colorant rests. The examination of the corneal surface with the blue filter of the slit lamp was performed immediately afterwards.

3.3 OCT device and examination

3.3.1 OCT device

In the present study a Spectralis® HRA+OCT Plus (Heidelberg Engineering, Heidelberg, Germany) was used to examine and image the patients (Figures 8 and 9). The pictures were processed with the software Spectralis Software Heidelberg Eye Explorer® (HEYEX) version 5.4 (October 2011, Heidelberg Engineering, Heidelberg, Germany).

Figure 8: Picture of the Spectralis® HRA+OCT Plus device

Figure 9: Detail of the camera of the Spectralis® HRA+OCT Plus device

The Spectralis® HRA+OCT Plus device is composed of two different units. A laser confocal camera is used to produce digital images of the surface of the eye fundus. In addition, spectral domain optical coherence tomography technology (SD-OCT) is used to receive vertical section images of the retina to visualize the cellular layers comparable to a histological section.

To acquire confocal fundus images, the laser beam needs to be focused on the retina. Oscillating mirrors deflect the laser beam to scan a two dimensional (2D) area of the retina. A light sensitive detector measures the intensity of the reflected light, or backscattering, at each retinal point. The backscattering which does not belong to the chosen scanning plane is supressed, obtaining high contrast 2D images. Because of the small diameter of the laser beam, this technique can be applied with very small pupil diameters. This characteristic was especially important in this study, since mydriasis requirements in our patient's pupil could be reduced to a minimum. In addition, it requires low retinal light exposure reducing blinding and stress for the patient.

Three different laser light wavelengths were used. A blue all solid state laser with wavelength 488 ± 2 nm with a barrier filter at 500 nm, a diode laser at 786 nm with a filter at 830 nm and a diode laser at 815 nm to produce infra-red reflectance (IR).

The acquisition of OCT images is based on the spectral domain optical coherence tomography technology (SD-OCT, Heidelberg Engineering) using the beam of a super luminescence diode (SLD) with a central wavelength of 870 nm to scan across the retina surface to produce B-scan images. The spatial resolution obtained in B-scans is up to 11 µm.

When 3D volume OCT scans were produced, a technology of Spectralis® HRA+OCT Plus device called TruTrack Active Eye Tracking was used. It involves two beams of light to take two images at the same time. One beam constantly tracks and images the retina surface, acting as a reference and guiding the beam which obtains the OCT image. This technology was of advantage for avoiding artefacts due to eye motion often present in bird patients.

3.3.2 OCT examination

The OCT examination included several activities such as preparation of the patient, OCT-examination, post-examination observation of the patient, and processing of the OCT data and images.

3.3.2.1 Preparation and restraint of the patient under examination

Based on the results of the clinical examination of the birds described before, the OCT examination took place after a first treatment and stabilization. The patients which tolerated the examination with no signs of stress were examined awake. Bird species expected to show stress related reactions underwent a sedation protocol, as described below.

They were investigated by OCT using sedatives or, in a few cases, applying general anaesthesia, either to avoid pain in the patients with traumatic lesions (for instance fractures), or to decrease the stress during the examination to a minimum.

When inhalation anaesthesia was necessary a conventional half open system with intubation was used. Isofluran (IsoFlo®, Albrecht, Aulendorf, Germany) was used as

anaesthetic gas. Sedation to decrease the stress level of the patient, was performed with Midazolam (Midazolam-ratiopharm, Ratiopharm, 2 mg/kg BW) administered intramuscularly or intranasally (AJADI et al. 2009; MANS et al. 2012; PAUL-MURPHY & FIALKOWSKI 2001; VESAL & ESKANDRANI 2006). The patient was monitored by an experienced veterinarian during the whole OCT examination.

OCT examination was performed in a dark room to minimize the stress of the patient. In addition to the optical immobilization effect darkness has, low light intensities lead to an adaptive relative large pupil diameter which was beneficial for the investigation. Noises were minimized to the lowest level.

Before the beginning of the OCT investigation, the body of the patient was wrapped up in a towel to preserve the plumage intact and to protect the animal against hurting himself by occasional movements such as wings beat. With this gentle fixation, the wings stayed in close contact with the patient body during the whole OCT examination. The head of the bird was always kept free from the towel. Since the light beam of the OCT device must be directed to the pupil of the patient, the head of the patient was gently fixed by the so-called “cap grip” in the proper angle, in order to allow the light beam go through the pupil. This technique of head fixation did not lead to an increase in stress during the examination, and a physiological head position was always respected.

3.3.2.2 OCT-examination

During the OCT examination first the right eye and then the left eye were completely examined. At the beginning, the fundus was imaged with the cSLO modality of the OCT device in order to locate some structures such as pecten and foveae, for an accurate positioning of the OCT scans. If fundus abnormalities or lesions which had not been detected during the previous eye examination were visualized, they were now recorded.

During this stage of the examination the optimal distance between camera and patient eye was determined to reach the highest quality of fundus pictures, which depends on a uniformly high illumination of the fundus image including also the periphery. Since the retinal surface is not flat, dark areas present in the periphery of the picture could not completely be avoided but were minimized. This problem arose especially when the eyes were very small. The image quality determined by the dark periphery was improved by the correction of the dioptres of the system using a regulation button at the left side of the camera head.

Once the cSLO resulted in satisfactory images, OCT cross sectional retinal scans (B-scans) and 3D retinal scans (C-mode) were produced. During this stage of the OCT-examination it was of great importance to avoid even small movements of the eye of the patient which could lead to an unsatisfactory examination.

As shown in Figure 10, OCT investigations were performed at five areas of the avian fundus:

- Superior portion of the pecten, including a part of the optical nerve head (ONH)
- Most sagittal area of the retinal equator
- Most sagittally superiorly visualized fundus area
- Most equatorially temporally visualized fundus area
- Most equatorially nasally visualized fundus area

It was not possible to visualize the area posterior to the pecten, since the pecten obstructs the trajectory of the light beam.

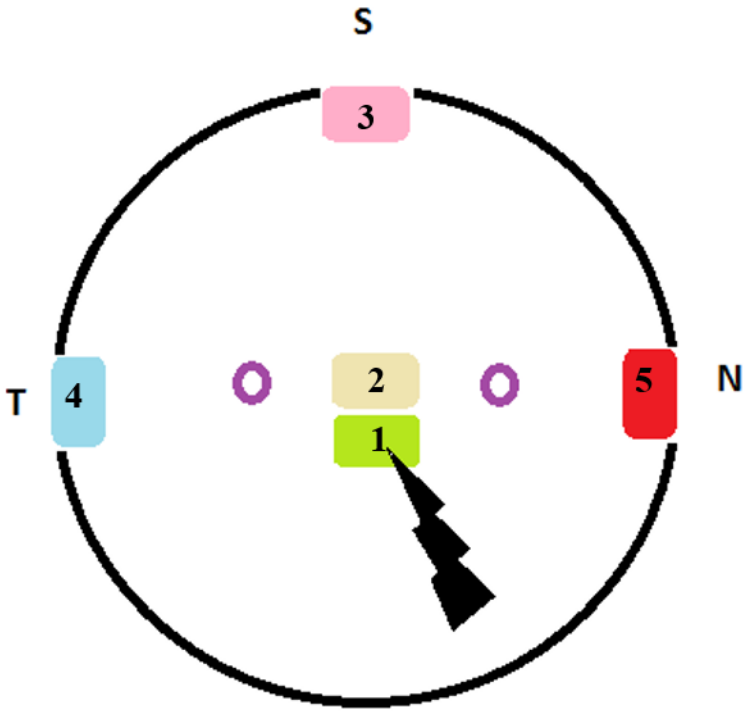

Figure 10: Investigated fundus areas. Diagram representing the avian fundus. Temporal (T), superior (S) and nasal (N) are the spatial references. The numbers represent the areas investigated: superior portion of the pecten including a part of the optical nerve head (ONH) (number 1), most sagittal area of the retinal equator (number 2), most sagittally superiorly visualized fundus area (number 3), most equatorially temporally visualized fundus area (number 4) and most equatorially nasally visualized fundus area (number 5).

In each aforementioned area, at least a sagittal and an axial B-scan were obtained. In the patients with a good tolerance for the investigation procedure, a higher number of B-scans in each area and 3D scans were taken (Figure 11).

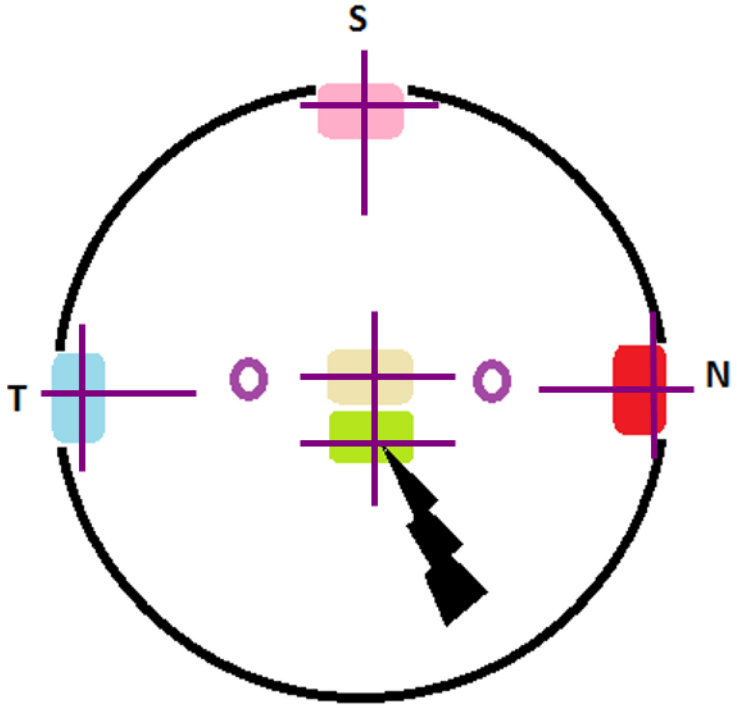

Figure 11: Localisation of the B-scans. Diagram representing the avian fundus. Temporal (T), superior (S) and nasal (N) are the spatial references. The purple perpendicular lines represent the B-scans performed in each aforementioned area.

The camera head is mobile, allowing directing the laser beam to the desired fundus area. It could be moved up, down, left and right. Since the imaging of the B-scan is a very sensible process, the fine movements of the camera were sometimes accompanied by subtle correcting of positioning of the patient head.

While working with the EYEX software in order to perform an OCT modality examination, the software displayed two fields in the screen. In one field of the screen the fundus could be seen, and a mobile green line represented the proper location where the B-scans were to be obtained. This method ensured the accurate positioning of the B-scan in the fundus, and since the fundus pictures were always linked to the B-scan in the software, a posterior observation and comparison of the image were permitted with accuracy. When the desired location of the B-scan was obtained, the B-scan appeared in the second field of the screen. The quality of the B-scan was indicated by a bar, allowing conclusions with accuracy if the B-scan was adequately obtained.

In case the patient could be imagined easily, 3D volume scan were obtained in the aforementioned areas. The velocity of obtaining the 3D varied depending on the quality chosen for the scanning. A fast scan with a low amount of B-scans per second resulted in a lower image quality than B-scan with more scans per second requiring longer recording times.

The EYEX® software was adapted to the eye size of birds by choosing only the sizes S for birds of the size of *Falco tinnunculus*, *Accipiter gentilis* or *Asio otus* and M for birds of the size of *Buteo buteo* and *Strix aluco,* among four different eye sizes included in the OCT system, S, M, L and XL.

During the whole OCT-examination process, the humidity of the patient eyes was preserved by the application of physiologic saline solution in drops. When the bird was showing signs of discomfort, it was always allowed to blink and to move the head for a few seconds before the examination was continued.

After each OCT-examination the device was cleaned and disinfected to avoid the spreading of any infectious disease between birds.

3.3.2.3 Patient status and care post OCT-examination

After each OCT-examination the patient was observed in order to obtain information about the acceptance of the process. When OCT investigation resulted in diagnosis of lesions with poor prognosis for visus and without therapy options, euthanasia was performed immediately due to humanitarian reasons.
In these cases, the eyes of the patients were then immediately taken out and used for histological investigations.

3.3.2.4 OCT data and images processing

Data obtained during the eye examination with Spectralis® HRA+OCT Plus (Heidelberg Engineering) were saved using the EYEX software included in the software program.

The OCT images were processed with the EYEX software. In this study, for each fundus area, B-scans with the best location and with the best quality of perpendicular image pairs were selected. For these scans, the following distances between different retinal layers corresponding to layer thicknesses were measured.

- Total retinal thickness from the RPE up to the ILM (TRT).
- RNFL and GCL (RNFL+GCL).
- Outer retina including layers from the RPE up to the inner border of the ONL (OR).
- Distance between RPE and ELM (RPE-ELM).

Based on the different thickness values, comparisons between different areas of the eyes in individual birds were performed as well as intraspecific and interspecific comparisons in order to obtain information on variations of retina morphology. Details are described in the section 3.5 Data processing (below).

3.4 Histological examination

Histological examinations were included in this study in order to evaluate the OCT technique by comparing OCT images and histological sections from individual raptor eyes. The eyes included originated without exception from birds euthanized after OCT examination due to animal welfare reasons as described already above.

After euthanasia of the patient, the eyes were immediately enucleated, fixed, decalcified, dehydrated, embedded in paraffin, cut and stained using standard protocols with modifications described below.

3.4.1 Euthanasia of the patient

The patients suffering from diseases or traumata without possibilities of full recovering to being able to survive in the wild were euthanized due to humanitarian reasons. Euthanasia was competently and professionally performed under general anaesthesia and in accordance with the animal welfare legislation. The method used was an inhalation anaesthesia with isofluran (IsoFlo®, Albrech, Aulendorf, Germany), and an intravenous injection of T61 (MSD Animal Health, Germany) was administered once reached the plane of surgical anaesthesia.

3.4.2 Enucleating of the eyes

Once the raptor was euthanized, the eyes were carefully enucleated paying attention not to damage the posterior parts of the eyeball. Care was taken to preserve regions where alterations had been found during previous OCT investigations in the eye (if present), and to avoid the production of artefacts (SAUNDERS & RUBIN 1975).

The enucleating technique used in this study was developed by KORBEL (1994) as a modification from SAUNDERS & RUBIN (1975). The upper and the lower lid of the eye were hold together with a curved or straight forceps. With blunt scissors a small slit was performed in the periocular area lateral to the lower eyelid, as close as possible to the orbital dermis leaving the conjunctiva beneath intact. Then, a blunt dissection was carried out with the scissors all around the eyeball. Double blunt curved scissors were used to separate the posterior pole of the globe from the eye muscles. Finally, the globe was separated from the optic nerve and vessels. The curved tip of the scissors allowed an

easier and faster enucleating, with minimal or inexistent damage of the posterior pole of the eye, since its shape adapts better to the posterior eye curvature and in this way pressure on the sclera was avoided. All the adnexa tissues, like eye muscles, were carefully removed to help the penetration of the fixation solution and to reduce shrinkage.

The enucleating of the eye was performed immediately after the euthanasia of the animal and as fast as possible, since the retina is a tissue very sensitive to anoxia and autolysis. Care was taken not to put pressure on the sclera during enucleation to avoid artificial retinal detachment (RAVELHOFER 1996).

3.4.3 Fixation

Immediately after enucleating, a small slit was made on the Limbus cornealis directed caudally to allow the fixation solution to penetrate into the posterior chamber of the eye, and therefore to produce a fast and uniform distribution of the fixation solution into the tissue. A paracentesis to facilitate entering of the fixation solution was not made to avoid retinal alterations due to the mechanical pressure (DOROBEK 2013).

Artefacts are a common problem when eyes or other circular and layered tissue are processed. These problems arise due to the different tension shown by each layer of tissue. The tensions increase when the tissue undergo fixation and dehydration processes connected with shrinkage resulting in changes in the tissue morphology increasing the amount of artefacts. In order to reduce artefacts by fixation, in this investigation, instead of standard formalin solution which were up to date commonly used (WERTHER et al. 2011), Davidson's solution described to be the best fixator for the retina was utilised, since it preserves the morphology of the retinal cells and the whole tissue anatomy with very satisfactory results (LATENDRESSE et al. 2002, MUMFORD 2004).

Davidson´s fixative compounds:

95 % Ethanol	600 ml
Glacial acetic acid	200 ml
Formalin 37 %	400 ml
Deionized water	600 ml

Fixation time in Davidson's solution varied depending on the eye sizes. Eyes of *Falco tinnunculus*, *Accipiter gentilis* and *Asio otus*, considered as small, were fixated in Davidson's solution for 12 hours, while eyes of *Buteo buteo* and *Strix aluco*, regarded as large, were fixated in Davidson's solution for 24 hours.

3.4.4 Decalcification

Since the eyes of all the birds included in this histological investigation possess bony scleral rings, decalcification was necessary to avoid rupture artefacts caused by different hardness while cutting the paraffin block.

For decalcification Osteosoft® (Merck, Darmstadt, Germany) was used containing EDTA and resulting in a soft and gentle decalcification of the tissue. After removal from the fixation solution, the eyes were washed in water for an hour and then incubated in Osteosoft® for 24 hours (small eyes) or 36 hours (big eyes).

3.4.5 Dehydration

Prior to dehydration, the eyes were placed in running tap water for an hour to remove any rest of decalcification solution.

The dehydration of the eyes was performed in a dehydration device Tissue Tek VIP E150/300 Tissue Processor (Floor Model, Sakura, Bayer Diagnostics, Orcq Tournai, Belgium). Small eyes were placed into Elisabeth boxes and big eyes were put directly in the metal basket of the device and were then dehydrated for 15 hours, as described in Table 2.

Table 2: Protocol used for dehydration:

Fluid	Time
Running water	1 h
Alcohol 70 %	1 h
Alcohol 70 %	2 h
Alcohol 96 %	1 h
Alcohol 96 %	1 h
Isopropanol 100 %	1 h
Isopropanol 100 %	1 h
Clearant (Xylol-replacement)	1 h
Xylol-replacement	1 h
Xylol-replacement	1 h
Paraffin	50 min
Paraffin	50 min
Paraffin	1 h
Paraffin	1 h 20 min

3.4.6 Paraffin embedding

The dehydrated eyes were included into a paraffin block immediately after the end of the dehydration program. However, large eyes could not be embedded in total in a single paraffin block. They were divided into three pieces by two sagittal cuts using a microtome razor blade (Figure 13). Cutting was performed carefully to avoid the production of artefacts. If the resulting pieces were still too big to be included in the paraffin block, the anterior eye chamber was cut off and casted aside before the sagittal divisions were performed as explained before (Figure 12).

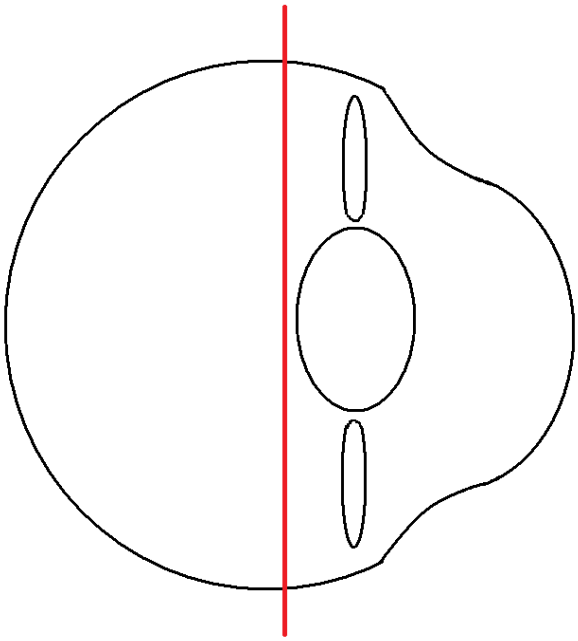

Figure 12: Scheme of the avian eye in a latero-lateral view. The left side of the scheme represents the posterior region of the bulbus, and the right side the anterior. The larger oval structure inside the eye represents the lens, and the two smaller above and under it the ciliary muscles. The red line indicates the cutting line separating the anterior segment of the eye.

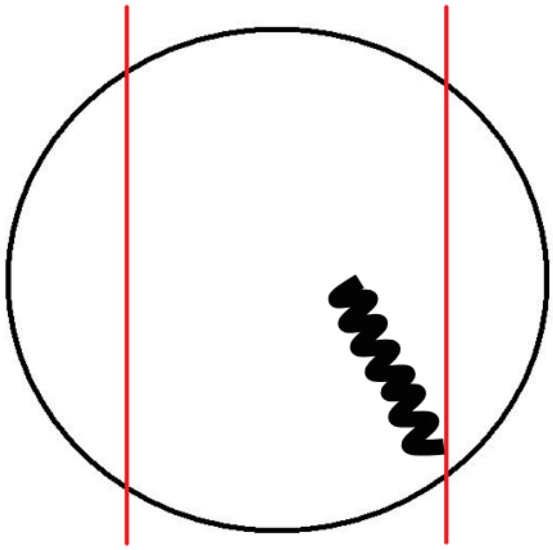

Figure 13: Scheme of the avian eye in an anterior-posterior view. The black folds represent the pecten oculi. The red lines indicate the cutting lines dividing the fundus of the eye.

Eyes of smaller sizes were processed in two different ways. The total eye fundus was embedded after cutting away the anterior eye segment, or the eye was first divided by a single sagittal cut into two parts and then embedded in paraffin blocks with or without the anterior segment (Figure 14). The anterior segment was conserved in some cases to give more stabilization to the tissue and to reduce the presence of artefacts.

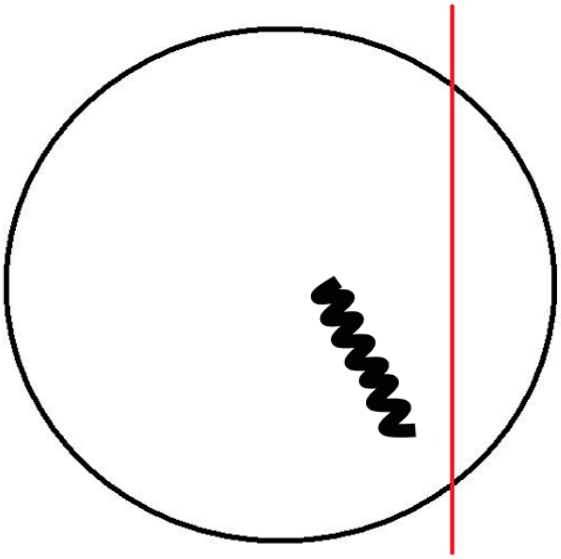

Figure 14: Scheme of the avian eye in an anterior-posterior view. The blak folds represent the pecten. The red line indicates the cutting line dividing the fundus of the eye.

The eyes were first embedded in paraffin (Tissue-Tek III Paraffin, Sakura Finetek Europe BV, Alphen aan den Rijn, Holland). During the investigation, the paraffin originally used proved to be disadvantageous for a good quality of the histological slides. Therefore, this first embedding paraffin was melted during 48 hours in the drying chamber at 60 ºC and the tissue samples were transferred to Paraplast Plus® Embedding Medium, with a melting point of 56 ºC.

3.4.7 Cutting

The cutting of the paraffin blocks was performed with the sliding Microtome Leica SM 2000 R (Leica Microsystems 2000, Nussloch, Germany). The cutting process consisted of a serial cut of the whole block with a thickness of 10 µm and with a distance between cuts of 20 µm.The tissue sections were transferred to Superfrost Plus® microscope slides (Thermo Scientific, Menzel, Braunschweig, Germany), where binding is supported by electrostatic forces.

3.4.8 Staining

The tissue sections were stained using a conventional Hematoxylin & Eosin (H&E) staining method. The staining protocol is described in detail in the next Table (Table 3)

Table 3: H&E staining protocol:

Fluid	Time
Xylol 100 %	10 minutes (two times)
Xylol-Alcohol 50 % each	5 minutes
Alcohol 100 %	3 minutes (two times)
Alcohol 96 %	3 minutes
Alcohol 80 %	3 minutes
Alcohol 70 %	3 minutes
Alcohol 50 %	3 minutes
Aqua destillata	3 minutes (two times)
Hemalaun Mayer	11 minutes
Aqua destillata	Fast wash
Tape water	10 minutes
Aqua destillata	Fast wash
Eosin	6 minutes
Aqua destillata	Fast wash
Alcohol 70 %	Fast wash
Alcohol 80 %	Fast wash
Alcohol 96 %	1 minute
Alcohol 100 %	2 minutes (two times)
Xylol-Alcohol 50 % each	5 minutes
Xylol 100 %	5 minutes (two times)

3.5 Data processing

3.5.1 Processing of the OCT-images

The processing of the OCT pictures was performed with the software Spectralis Software Heidelberg Eye Explorer® (HEYEX) version 5.4 (October 2011, Heidelberg Engineering, Heidelberg, Germany). Two pictures were taken in the investigated areas. Therefore, two B-scans of each area were included in the analysis, perpendicular to each other.

First, the exact location of the B-scan was determined taking the fundus image as a reference using the HEYEX software. The software indicates the exact position of the whole B-section within the fundus area with a green line, and also a concrete point on this line, which can be located on the B-scan. An example can be seen in Figure 15.

Then the retinal layers to be measured were selected. This was made by setting two lines of points at the upper and lower borders of the corresponding retina layers. The line points could then be further set exactly at in the place of interest by moving them up or down thus correcting the lines.

Figure15: Display of OCT and measurements by the software. The fundus picture can be observed on the left upper part. The green line on the fundus picture indicates where the B-scan is obtained. The B-scan is shown in the window on the right upper part. The mark on the line of the fundus image coincides with the position of the vertical green line on the B-scan

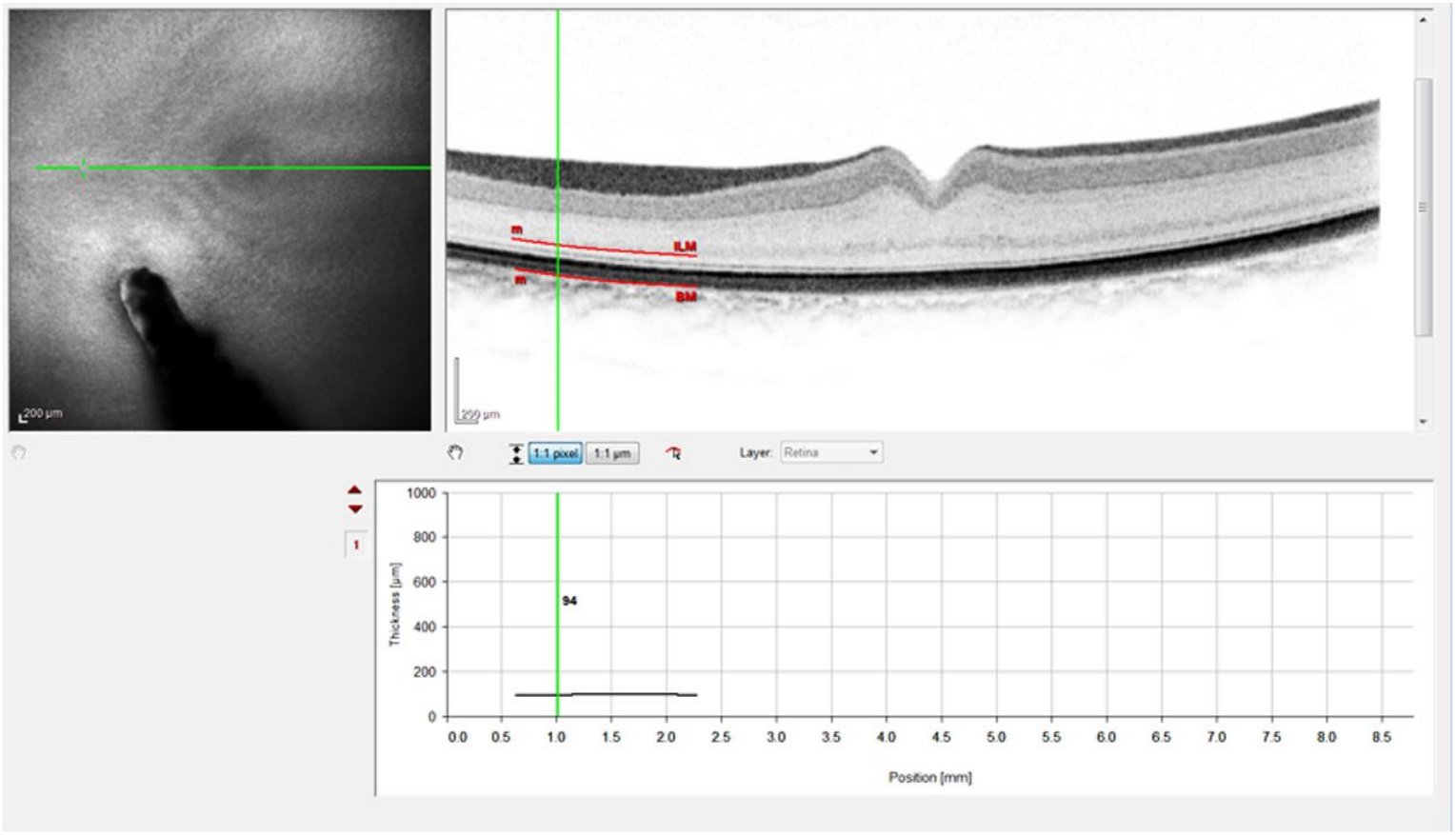

The procedure of thickness determination is illustrated in Figure 15. The two red lines represent the borders of the retina layers analysed. The thickness of these layers was determined as the distance between the two lines. The information contained in this graphic was obtained by creating a program with the software Mathematica 8.0 (Wolfram Research, Hanborough, United Kingdom). The program can be found in appendix 1. Using this software, the mean thickness of the selected area including the standard deviation was calculated. The program creates several graphics where the thicknesses are represented. It creates a graphic of the function of the thickness, with its correction in the form of a graphic with the residual values represented on it. The individual images including the measurements were saved as TIF files.

3.5.2 Processing of the histological sections

For reach bird species included in the histological analysis, one pair of eyes was selected. Serial sections were examined, with an optical/fluorescence microscope (Zeiss Axiophot I, Carl Zeiss, Oberkochen, Germany). This microscope is equipped with an integrated CCD colour camera (Axiocam MRc, Carl Zeiss, Jena, Germany). Areas corresponding to the areas analyzed by OCT were located and selected for photographic documentation and measurement.

They were photographed using the camera and visualized using the AxioVisionTM software which facilitates correct measurements.

On each picture, ten random measurements of each selected distance thickness were made on the section (Figure 16). The data of these measurements were provided as an Excel Table (Microsoft Office Professional Plus 2013), which allows a comfortable data processing.

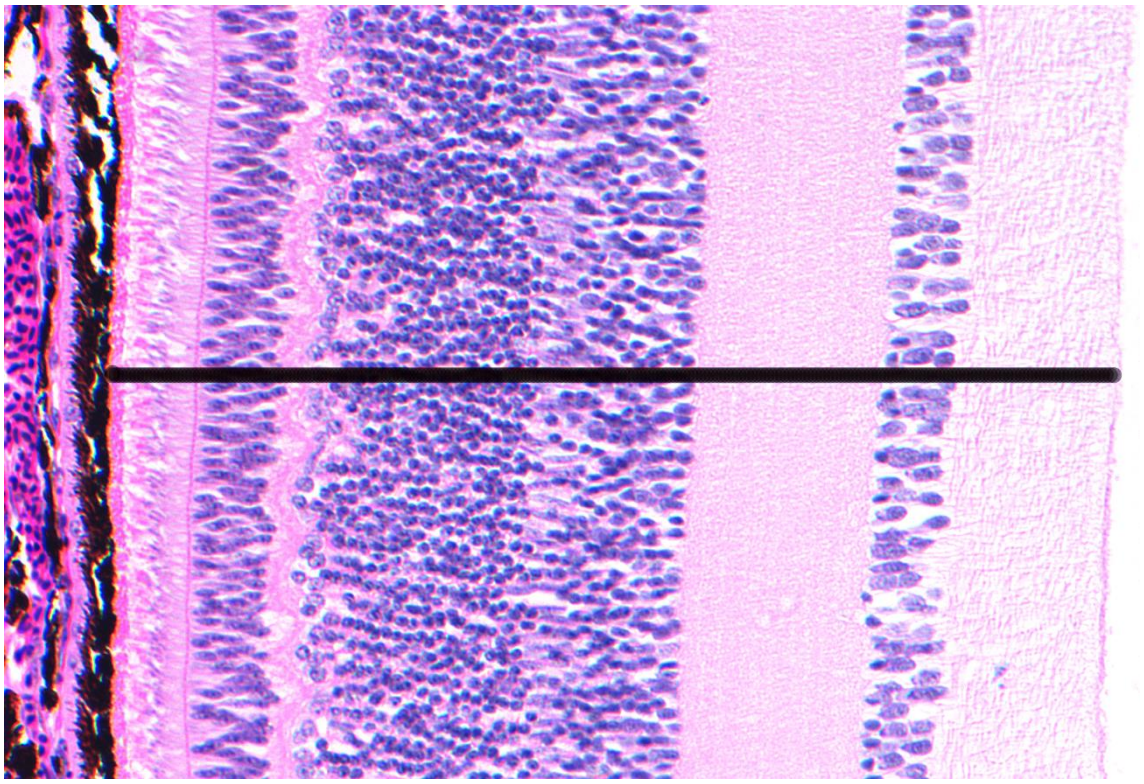

Figure 16. Example of a measurement made on a histologic section of the retina of the *Buteo buteo* 24742, right eye (OD), equator area (E), total retinal thickness (TRT). In black the measurement of the total retinal thickness (TRT) from the retinal pigment epithelium (RPE) (left side) up the internal limiting membrane (ILM) (right side) is shown (316.15 µm). H&E staining.

4 RESULTS

4.1 OCT-examination of the raptor eye

4.1.1 General considerations

In this section, results from the processing of the OCT pictures obtained for each specimen will be presented. Only data of retinal areas classified as healthy were considered in this investigation, while injured eyes or areas where pathological findings were detected using supplementary techniques were not incorporated in the analysis. Therefore, a total of 43 birds and of 70 eyes were included.

In Figure 17 pictures of the fundus produced by confocal scanning laser ophthalmoscope (cSLO) and a picture of the retinal layers obtained by OCT are exemplarily presented as shown by the software HEYEX® (Heidelberg Engineering). The equator of the eye can be located and visualized at the fundus picture. It is characterized by its position within the fundus between the swallow and deep fovea, in the area superior to the pecten, and it is the level where the coroidal blood vessels parting from the optical nerve head region are diverging (not visible in Figure 17). On the left side of fig. 17, the B-scan can be seen with the retinal layers. The distance between the two red lines at the top and the base of the retina was measured to receive the total retinal thickness. Immediately below, a graphic produced by the software is showing only one thickness value determined for the retina at the position of the green line. Using this software, the thickness of only a single position can be seen at the same time. In order to compare thickness values of different retinal points, a program developed with the software Wolfram Mathematica was used (as described in Materials and Methods) to obtain a series of raw measurement data from the graphic, that means, an accurate list of all thickness values of this section. These values were plotted and fitted to a sixth degrees polynomial function as shown in Figures 17, 18, 19 and 20. An example of the coefficients of the aforementioned function calculated by the software is shown in Table 4. The function was adjusted to the next sixth degree polynomial:

$$y=a+b*(x-x0)+c*(x-x0)^2+d*(x-x0)^3+e*(x-x0)^4+f*(x-x0)^5+h*(x-x0)^6$$

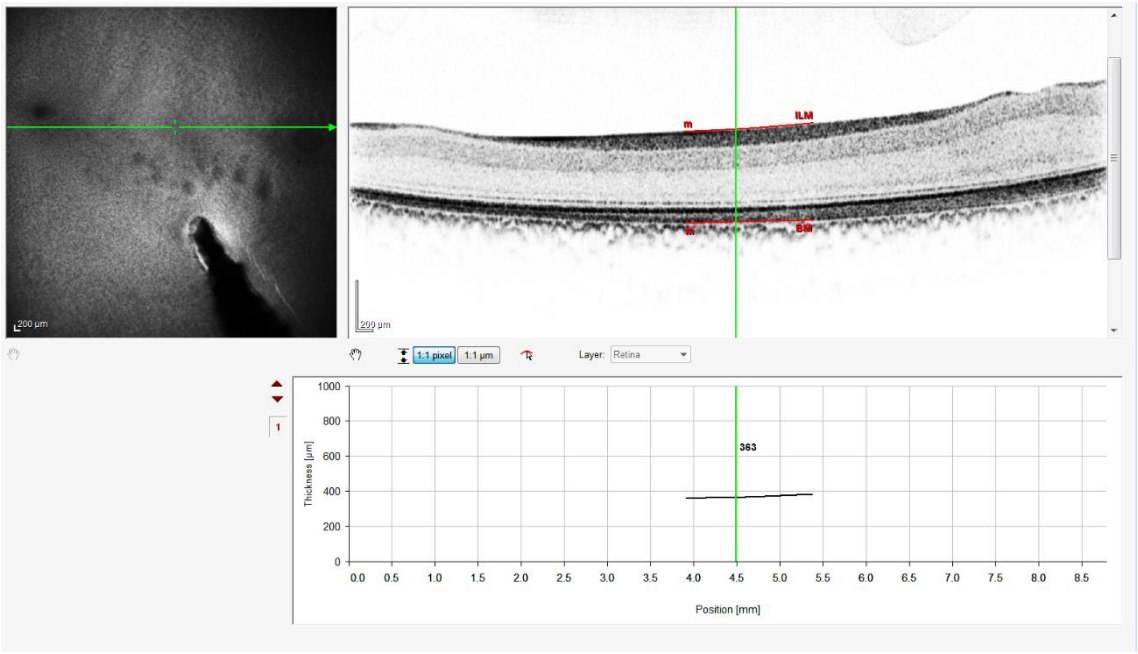

Figure 17. Example of the display shown by the HEYEX® software. Total retinal thickness (TRT) from patient *Buteo buteo* 26235, right eye (OD), equator area (E) horizontal B-scan (H).

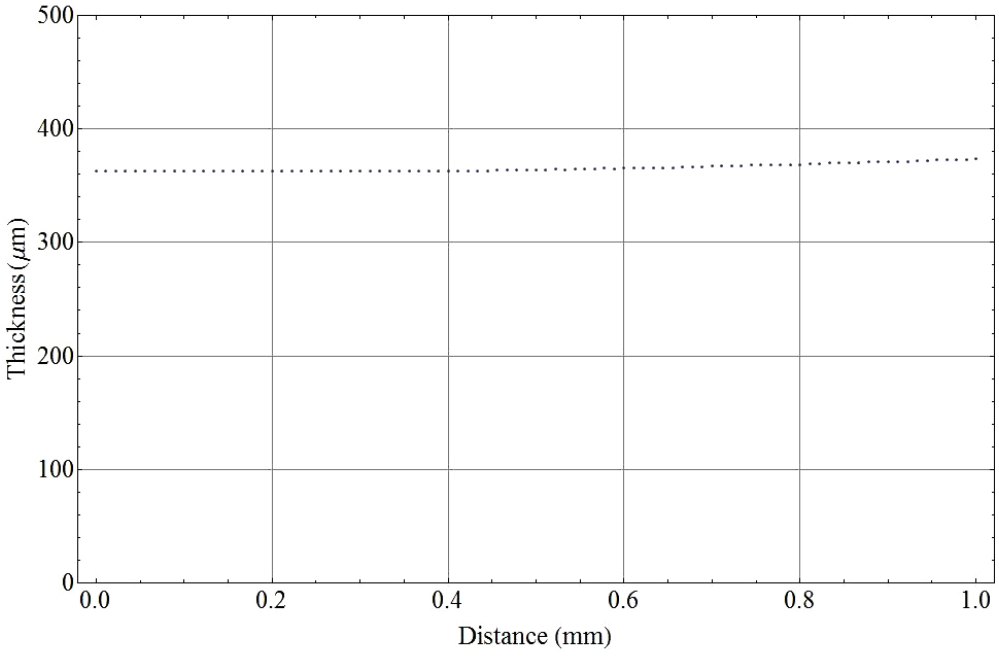

Figure 18. Data plot of the single measured points obtained with the program Wolfram Mathematica. TRT from patient *Buteo buteo* 26235, OD, E, H, B-scan.

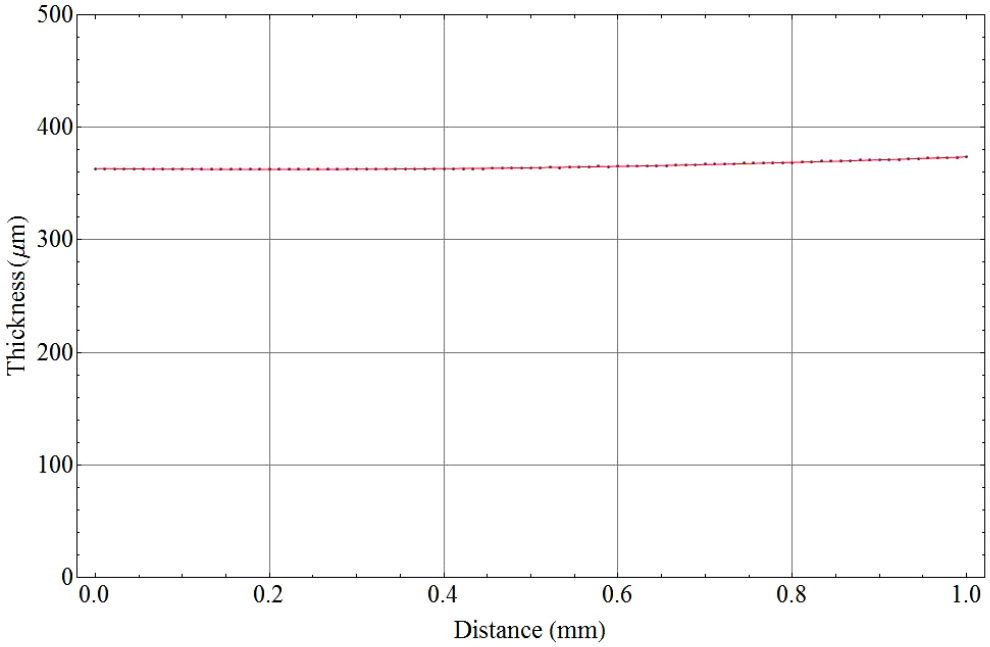

Figure 19. Data plot fit of single measured points obtained with the program Wolfram Mathematica. The plot fit is represented by the line that connects the points, which is the graphic representation of the adjusted function. TRT from patient *Buteo buteo* 26235, OD, E, H, B-scan.

The residual values represent the group of data which are outside of the function adjustment. These show the accuracy of the function adjustment. As shown in Figure 20, these values were randomly distributed, which indicated the high accuracy of the function adjustment.

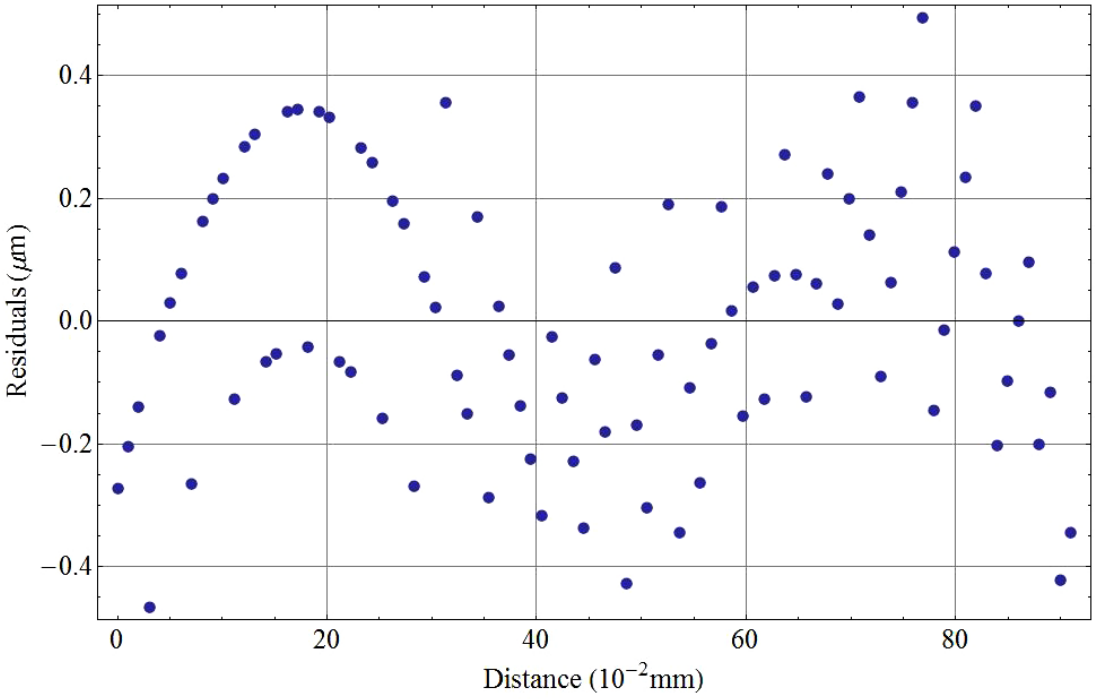

Figure 20. Residuals obtained with the program Wolfram Mathematica. TRT from patient *Buteo buteo* 26235, OD, E, H, B-scan.

Table 4: Example of the coefficients of the function calculated by the software Wolfram Mathematica for each data plot. Data from the TRT from patient *Buteo buteo* 26235, OD, E, H, B-scan

	Estimate	Standard Error	t-Statistic	P-Value
a	364.434	0.195974	1859.61	8.83456×10^{-200}
b	−0.11227	0.0137269	−8.17885	2.29872×10^{-12}
c	0.00195701	0.000275352	7.1073	3.25179×10^{-10}
d	1.03156×10^{-6}	1.6352×10^{-6}	0.630846	0.529814
x0	−9.58844	0.0220535	−434.78	1.64917×10^{-145}

During the analysis of the measured data, complex statistical tests were spared because we are aware of the fact that the number of animals of each species included in this study is not sufficient to be representative and to allow a sound establishment of reference values and to compare mean thickness values. However, this study never aimed at the

establishment of reference values. We wanted to test whether OCT investigations can be performed in a broad species range of raptors and owls and we intended to receive first information on variations of anatomical retinal features among individuals of the same species and of different species and orders. In addition, OCT measurements were posteriorly validated with histology. Means of the measurements belonging to the different retinal layers were simply compared regarding their standard deviation. With the standard deviation an interval is established for each mean. The means were considered equal in cases where their interval of the standard deviation overlapped.

4.1.1.1 Intraspecific variations

4.1.1.1.1 Accipitriformes

- ***Buteo buteo***

Out of the 15 individuals of the species *Buteo buteo* which underwent an OCT-examination, the eyes of 13 individuals were satisfactory imagined. The mean of the thicknesses for each aforementioned area are described in Table 5. Exceptions are the TRT and RNFL+GCL from the area superior to the pecten. For those, the maximal thickness is presented instead of the mean.

Table 5. *Buteo buteo*: Results of thickness measurements of the total retinal thickness (TRT), retinal nerve fiber layer + ganglion cell layer (RNFL+GCL), outer retina (OR), retinal pigment epithelium-external limiting membrane (RPE-ELM) of different ocular areas. Ocular areas: Pecten superior (Ps), equator (E), nasal (N), superior (S), temporal (T). Standard deviation (sd).

Area	Measurement	Maximal thickness (µm)	sd (µm)	Measurements per area
Ps	TRT	431.44	68.61	24
	RNFL+GCL	210.43	101.65	24
		Mean thickness (µm)		
	OR	89.68	16.38	24
	RPE-ELM	74.52	10.99	24
E	TRT	370.25	20.10	26
	RNFL+GCL	85.76	28.89	26
	OR	102.61	8.84	26
	RPE-ELM	83.25	15.43	26
N	TRT	315.40	12.40	13
	RNFL+GCL	45.10	7.56	13
	OR	104.93	6.53	13
	RPE-ELM	86.93	6.12	13
S	TRT	255.89	18.13	13
	RNFL+GCL	25.81	5.45	13
	OR	98.31	6.86	13
	RPE-ELM	82.48	4.85	13
T	TRT	223.93	12.28	12
	RNFL+GCL	66.33	8.75	12
	OR	74.67	5.93	12
	RPE-ELM	62.62	5.11	12

Variation of the total retinal thickness (TRT)

The TRT varied among the different areas showing a maximum near the pecten, followed by the equator, the nasal area, the superior area and the temporal area (Table 5). In the equator area the retina of *Buteo buteo* had a thickness of 370.2 µm with a standard deviation of 20.10 µm among individuals of this species. An example of a B-scan of *Buteo buteo* is showed in Figure 21.

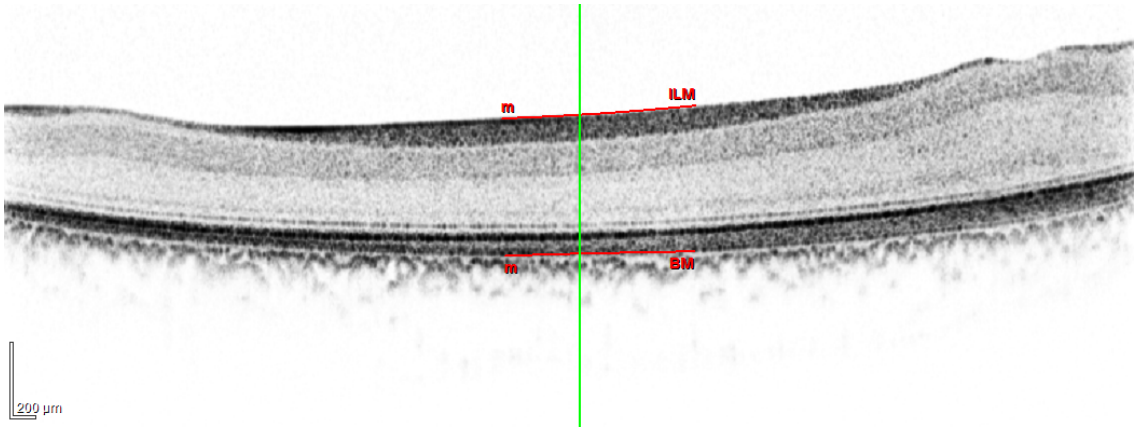

Figure 21. B-scan of the patient *Buteo buteo* identification number (i.n.) 26235, TRT, OD; E, H.

Thickness variation of the retinal nerve fiber layer and the ganglion cell layer (RNFL+GCL)

As presented in Table 5, the thickness of the combined RNFL and GCL reached its maximum in the area superior to the pecten, followed by the equator (Figure 22), the temporal area, nasal area and reached its minimum in the superior area.

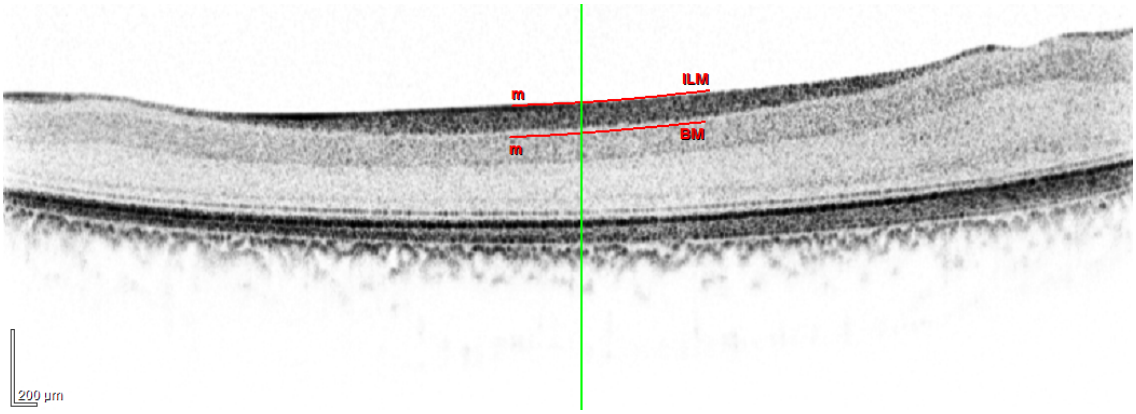

Figure 22. B-scan of the patient *Buteo buteo*, i.n. 26235, RNFL+GCL, OD, E, H.

Thickness variation of the outer retina (OR)

The OR thickness followed a different pattern compared to that observed for the TRT and RNFL+GCL. Regarding the overlapping of the standard deviation for each measurement mean, the OR thickness values observed showed no differences in all areas, except for the temporal area, where the overlapping of the standard deviation in this case was not in the interval of the standard deviation of the equator, superior and nasal areas. The Figure 23 shows an example of this measurement in the equator area.

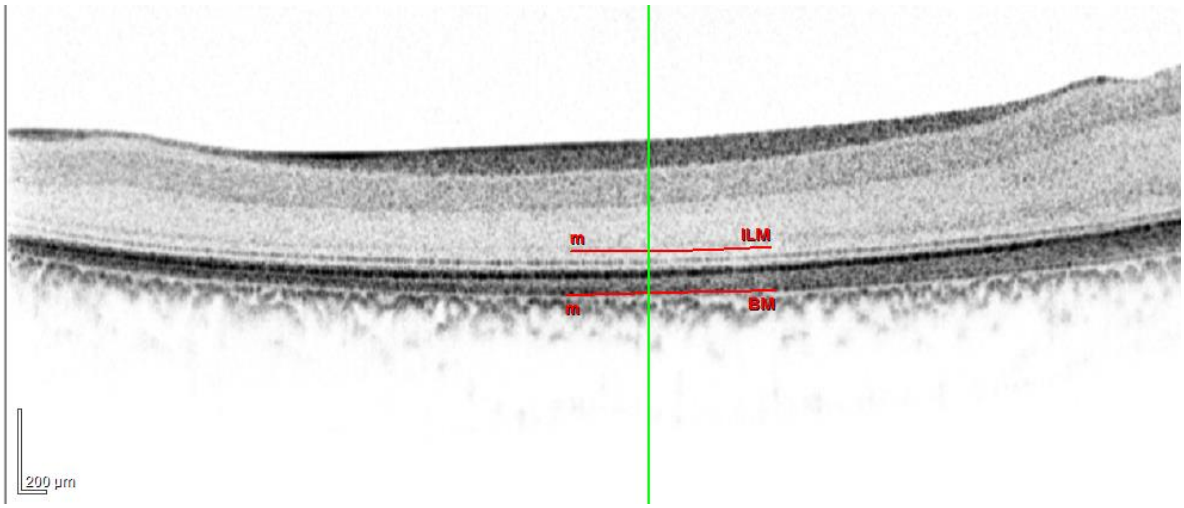

Figure 23. B-scan of the patient *Buteo buteo*, i.n. 26235, OR, OD, E; H.

Thickness variation of the layers between the retinal pigment epithelium and the external limiting membrane (RPE-ELM)

Except for the temporal area which was significant thinner, the thicknesses of RPE-ELM did not differ between the different areas of the eyes in *Buteo buteo*. (Figure 24).

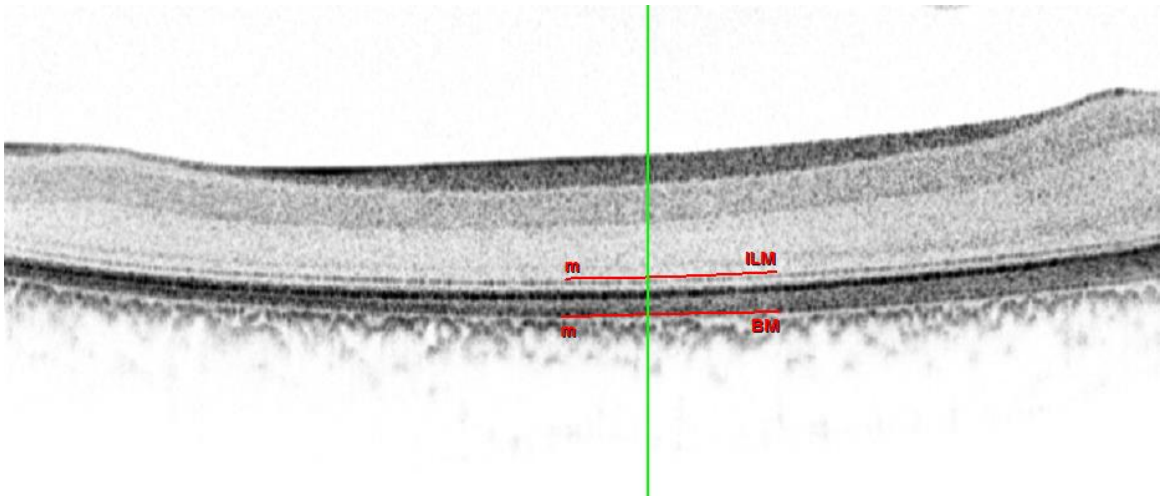

Figure 24. B-scan of the patient *Buteo buteo*, i.n. 26235, RPE-ELM, OD, E; H.

- ***Pernis apivorus***

Five individuals of the species *Pernis apivorus* underwent an OCT-examination. All of them were satisfactory imagined and therefore included in the analysis. Mean retinal thicknesses data obtained from each area except the TRT and RNFL+GCL from the area superior to the pecten are shown in Table 6. For the TRT and RNFL+GCL from the area superior to the pecten, the maximal thickness is represented instead of the mean.

Table 6: *Pernis apivorus*: Results of thickness measurements of the TRT, RNFL+GCL, OR, RPE-ELM of different ocular areas. The "x" represents the cases where no measurement could be obtained. Abbreviations used as in Table 5.

Area	Measurement	Maximal thickness (µm)	sd (µm)	Measurements per area
Ps	TRT	371.11	14.45	11
	RNFL+GCL	133.80	23.76	11
		Mean thickness (µm)		
	OR	x	x	x
	RPE-ELM	118.90	11.65	11
E	TRT	350.76	12.42	14
	RNFL+GCL	63.96	11.74	14
	OR	x	x	x
	RPE-ELM	133.14	7.07	14
N	TRT	281.93	8.06	8
	RNFL+GCL	61.57	6.77	8
	OR	x	x	x
	RPE-ELM	115.73	2.90	8
S	TRT	261.58	10.13	9
	RNFL+GCL	38.87	5.49	9
	OR	x	x	x
	RPE-ELM	121.13	4.01	9
T	TRT	282.50	6.53	10
	RNFL+GCL	60.41	6.40	9
	OR	x	x	x
	RPE-ELM	115.30	4.97	10

Variation of the total retinal thickness (TRT)

The TRT in the avian patients of the species *Pernis apivorus* was highest in the area superior to the pecten. It was higher than at the equator. The nasal, superior and temporal areas had lower TRTs than the equator area. The TRT of the superior area was lower than those of the nasal and temporal area which were similar to each other. The Figure 25 represents an example of the TRT in the equator area.

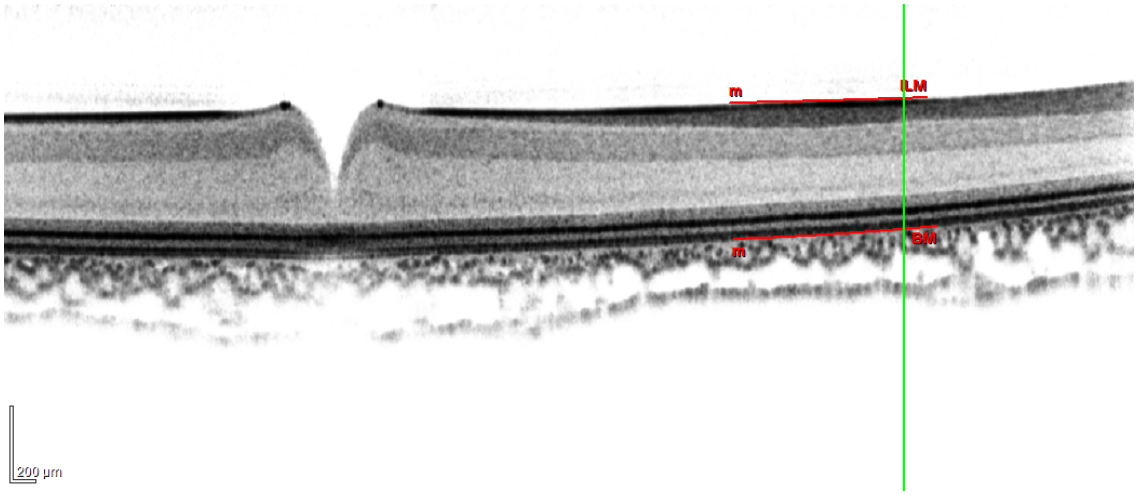

Figure 25. B-scan of the patient *Pernis apivorus* i.n. 27329, TRT, OS, E, H.

Thickness variation of the retinal nerve fiber layer and the ganglion cell layer (RNFL+GCL)

The RNFL+GCL thickness varied among the retina of the patients under examination and showed a considerable increase in the area superior to the pecten. Differences among the RNFL+GCL thickness of the equator (Figure 26), temporal and nasal areas were not detected, while the RNFL+GCL of the superior area was thinner than those mentioned before.

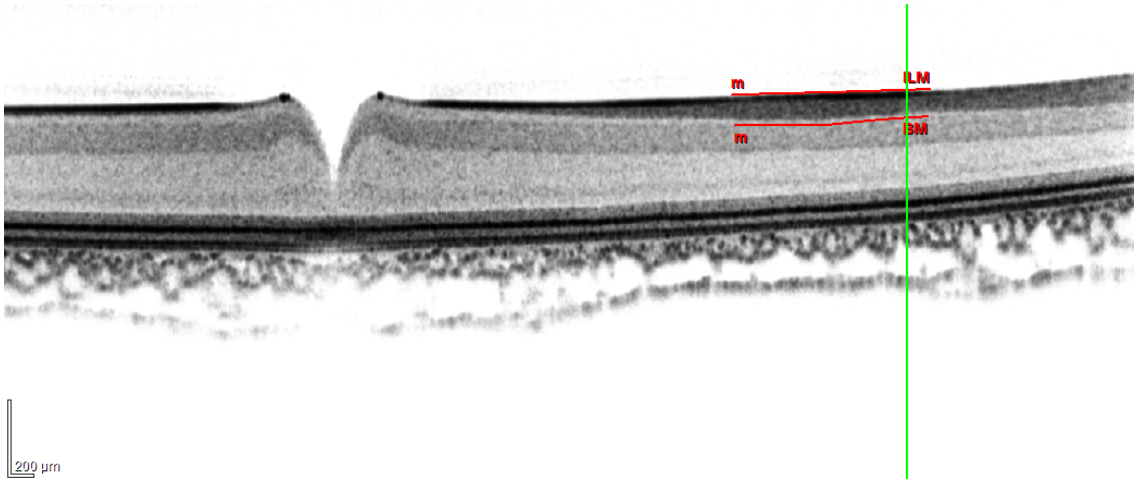

Figure 26. B-scan of the patient *Pernis apivorus* i.n. 27329, RNFL+GCL, OS, E, H.

Thickness variation of the outer retina (OR)

Since the border between the outer plexiform layer (OPL) and the outer nuclear layer (ONL) could not be distinguished in this species, no measurement of the outer retina could be taken.

Thickness variation of the layers between the retinal pigment epithelium and the external limiting membrane (RPE-ELM)

In the patients of the species *Pernis apivorus* the layers located between the RPE and the ELM were thicker in the equator area (Figure 27) than in the areas of the eccentric retina. The different areas of the eccentric retina had approximately the same thickness.

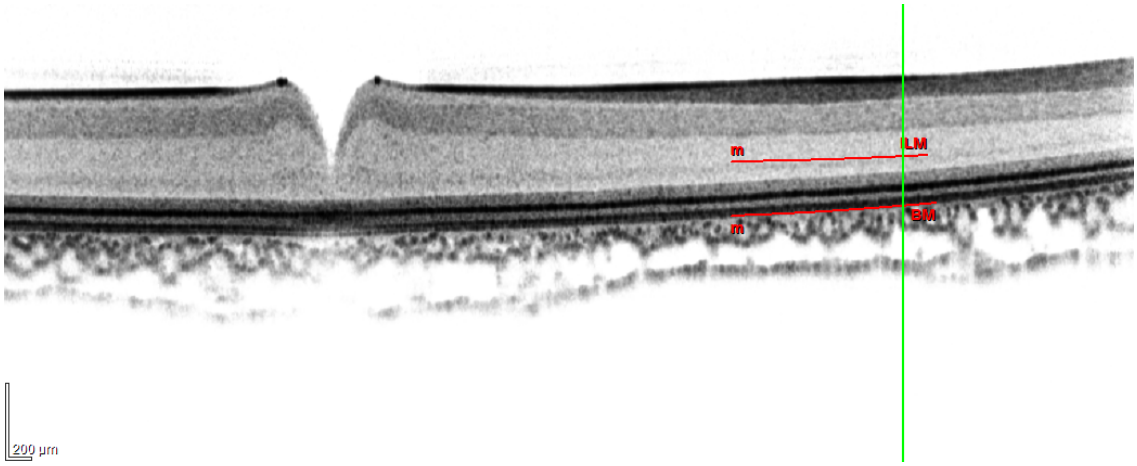

Figure 27. B-scan of the patient *Pernis apivorus* i.n. 27329, RPE-ELM, OS, E, H.

- ***Accipiter nisus***

Three of four individuals of the species *Accipiter nisus* were satisfactory imagined with the OCT-device. The thickness data are represented in Table 7.

Table 7: *Accipiter nisus*: Results of thickness measurements of TRT, RNFL+GCL, OR and RPE-ELM of different ocular areas. Abbreviations used as in Table 5.

Area	Measurement	Maximal thickness (µm)	sd (µm)	Measurements per area
Ps	TRT	384.04	11.08	6
	RNFL+GCL	230.32	19.77	6
		Mean thickness (µm)		
	OR	69.71	7.95	6
	RPE-ELM	57.05	6.40	6
E	TRT	320.95	7.10	7
	RNFL+GCL	104.86	11.25	7
	OR	84.10	3.49	7
	RPE-ELM	67.93	2.94	7
N	TRT	230.86	1.79	2
	RNFL+GCL	58.25	2.93	2
	OR	78.44	1.26	2
	RPE-ELM	67.74	1.03	2
S	TRT	220.96	6.81	2
	RNFL+GCL	39.91	2.03	2
	OR	81.05	2.21	2
	RPE-ELM	69.34	3.23	2
T	TRT	173.33	1.80	2
	RNFL+GCL	44.51	2.56	2
	OR	59.28	2.22	2
	RPE-ELM	50.04	1.69	2

Variation of the Total Retinal Thickness (TRT)

The TRT (Figure 28) reached its maximum in the area superior to the pecten being higher than in the equator area. In comparison with the equator, the TRT decreased in the eccentric retina, being lower in the nasal area, then followed by the superior area and reaching the minimum in the temporal area.

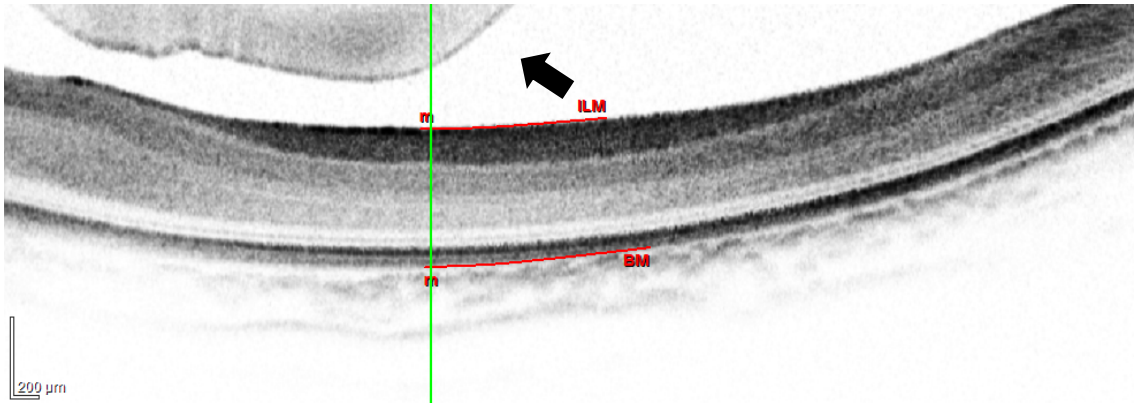

Figure 28. B-scan of the patient *Accipiter nisus*, i.n. 25089, TRT, OS, E, H. The arrow indicates the posterior vitreous face.

Thickness variation of the retinal nerve fiber layer and the ganglion cell layer (RNFL+GCL)

The RNFL+GCL reached its highest thickness in the area superior to the pecten, followed by the equator area. The thickness decreased in the nasal area, the temporal and the superior area, reaching its minimum in the last one. The Figure 29 represents an example of the RNFL+GCL in the equator area.

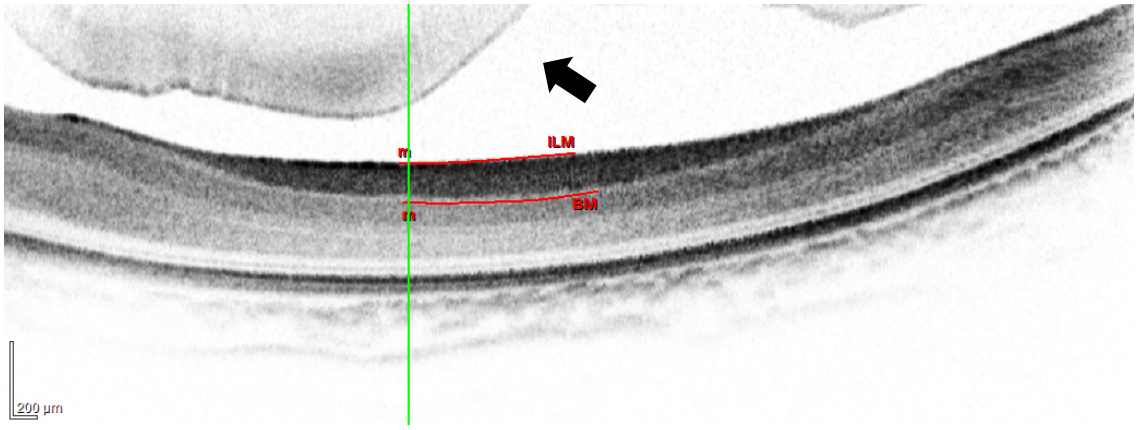

Figure 29. B-scan of the patient *Accipiter nisus*, i.n. 25089, RNFL+GCL, OS, E, H. The arrow indicates the posterior vitreous face.

Thickness variation of the outer retina (OR)

Thickness differences of the OR among the equator (Figure 30), nasal and superior areas were relatively small, but based on their interval of the standard deviation, regarded as considerable. The maximal thickness of the OR was observed in the equator area, followed by the superior area and the nasal area. The thickness was lower in the area superior to the pecten, and lowest in the temporal area, where the OR thickness reached its minimum.

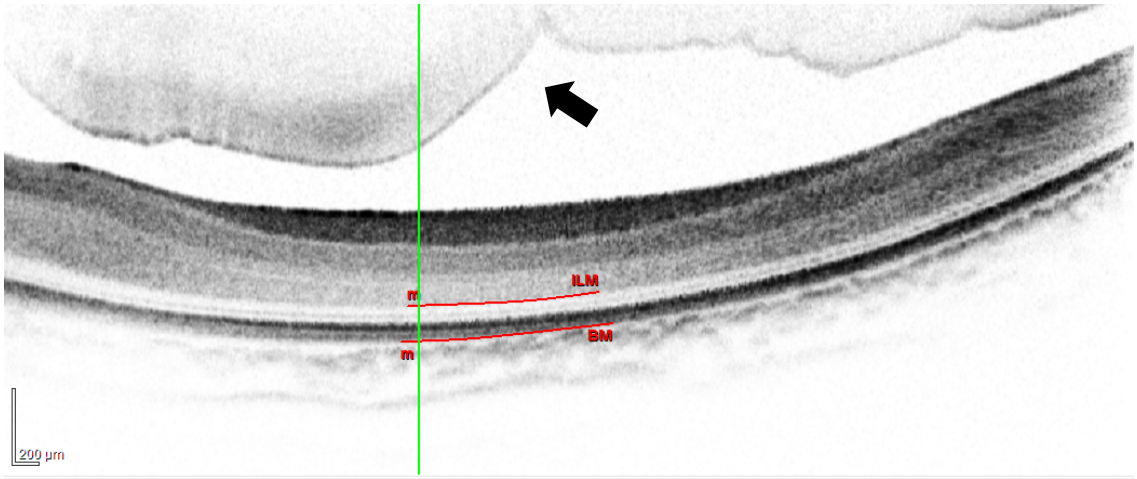

Figure 30. B-scan of the patient *Accipiter nisus*, i.n. 25089, OR, OS, E, H. The arrow indicates the posterior vitreous face.

Thickness variation of the layers between the retinal pigment epithelium and the external limiting membrane (RPE-ELM)

The RPE-ELM thickness remained the same all along the retina, except for the area superior to the pecten and the temporal area, where these layers were thinner. The Figure 31 represents an example of the RPE-ELM in the equator area.

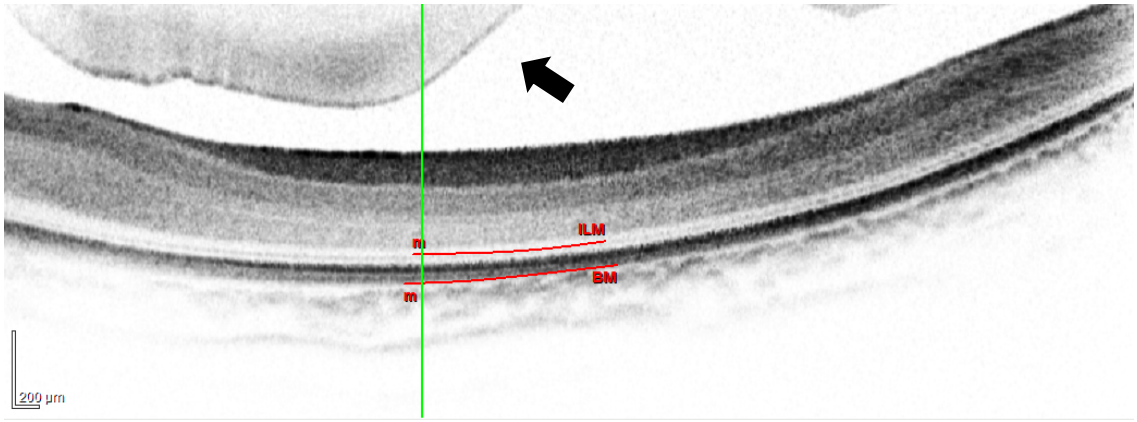

Figure 31. B-scan of the patient *Accipiter nisus*, i.n. 25089, RPE-ELM, OS, E, H. The arrow indicates the posterior vitreous face.

- ***Accipiter gentilis***

Only one individual from the species *Accipiter gentilis* was satisfactory imagined. Since the measurements belong to only one specimen, they cannot be considered as representative and this species is therefore not included in the comparisons between species. Nevertheless, these measurements can be considered as an example of retinal visualization with OCT in this species (Table 8).

Table 8: *Accipiter gentilis*: Results of thickness measurements of TRT, RNFL+GCL, OR and RPE-ELM of different ocular areas. Abbreviations used as in Table 5.

Accipiter gentilis		
OD+OS areas	OD+OS measurements	Maximal thickness (µm)
Ps	TRT	477.03
	RNFL+GCL	294.66
		Mean thickness (µm)
	OR	74.00
	RPE-ELM	63.88
E	TRT	349.11
	RNFL+GCL	99.11
	OR	87.89
	RPE-ELM	73.86
N	TRT	x
	RNFL+GCL	x
	OR	x
	RPE-ELM	x
S	TRT	x
	RNFL+GCL	x
	OR	x
	RPE-ELM	x
T	TRT	263.57
	RNFL+GCL	44.95
	OR	90.17
	RPE-ELM	75.66

4.1.1.1.2 Falconiformes

- ***Falco tinnunculus***

Three out of seven patients of the species *Falco tinnunculus* were satisfactorily imagined by OCT. The mean thickness values for the different areas are described in Table 9, except for the TRT and RNFL+GCL from the area superior to the pecten, where the maximal thickness instead of the mean is included.

Table 9: *Falco tinnunculus*: Results of thickness measurements of TRT, RNFL+GCL, OR and RPE-ELM of different ocular areas. Abbreviations used as in Table 5.

Area	Measurement	Maximal thickness (µm)	sd (µm)	Measurements per area
Ps	TRT	468.83	13.71	11
	RNFL+GCL	242.35	27.14	11
		Mean thickness (µm)		
	OR	105.15	24.36	11
	RPE-ELM	79.33	7.57	11
E	TRT	409.04	14.78	10
	RNFL+GCL	72.67	12.06	10
	OR	106.50	4.38	10
	RPE-ELM	83.87	5.05	10
N	TRT	323.14	9.71	5
	RNFL+GCL	45.70	4.87	5
	OR	103.66	5.15	5
	RPE-ELM	86.36	4.06	5
S	TRT	296.72	11.41	8
	RNFL+GCL	34.56	3.20	7
	OR	100.82	3.87	8
	RPE-ELM	84.05	3.39	8
T	TRT	249.28	9.39	6
	RNFL+GCL	85.24	9.31	6
	OR	75.10	5.98	6
	RPE-ELM	63.56	5.96	6

Variation of the Total Retinal Thickness (TRT)

The TRT within the individuals of the species *Falco tinunculus* was maximal in the area superior to the pecten, followed by the equator area (Figure 32), then the nasal and superior areas, reaching its minimum in the temporal area.

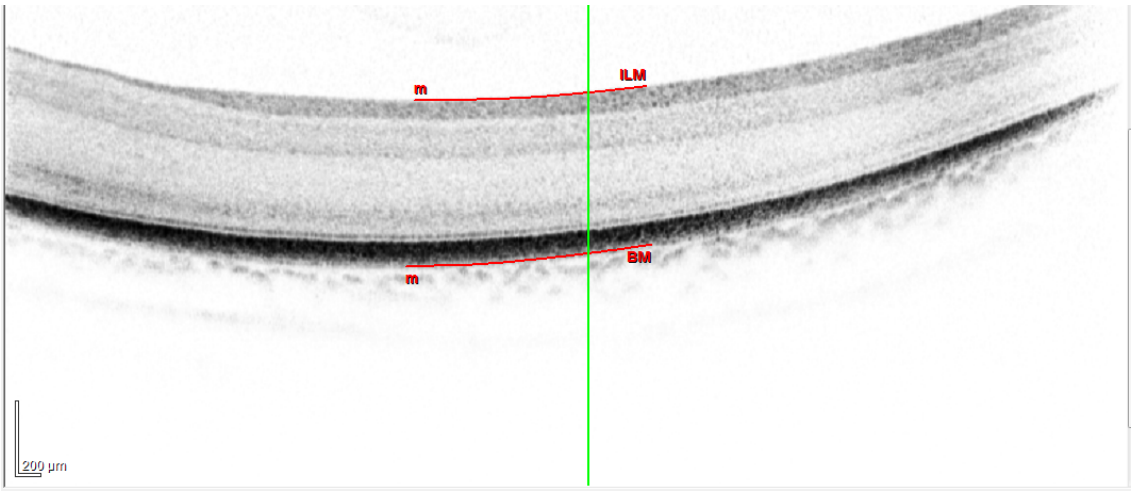

Figure 32. B-scan of the *Falco tinnunculus,* i.n. 26654, TRT, OS, E, H.

Thickness variation of the retinal nerve fiber layer and the ganglion cell layer (RNFL+GCL)

The maximal thickness of RNFL+GCL occurred in the area superior to the pecten (means were not calculated for this area). When the other areas were compared by the mean values of RNFL+GCL, the highest thickness was reached at both the temporal area and the equator area whose sd intervals overlapped. The corresponding layers of nasal and superior areas were remarkably thinner. In Figure 33 an example of the RNFL+GCL in the equator area is shown.

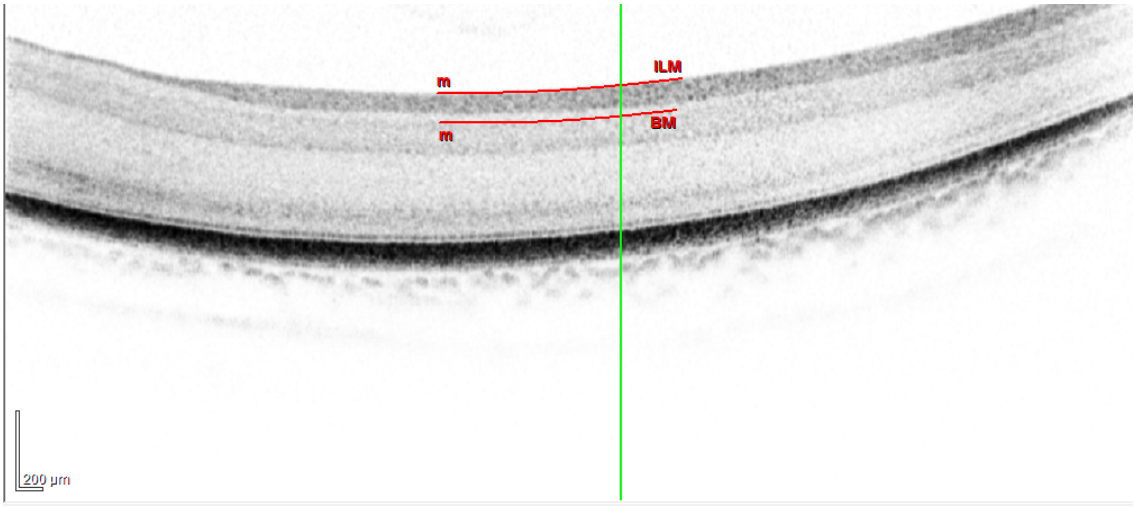

Figure 33. B-scan of the *Falco tinnunculus,* i.n. 26654, RNFL+GCL, OS, E, H.

Thickness variation of the outer retina (OR)

The OR thickness was constant in all areas investigated with the exception of the temporal area, where it was lower. In the Figure 34 an example of the RNFL+GCL in the equator area can be observed.

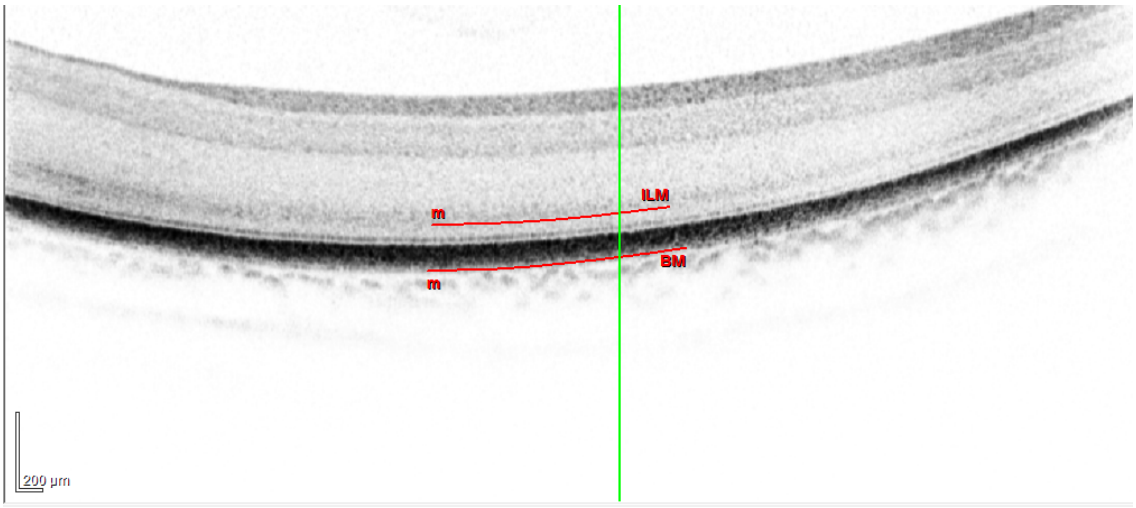

Figure 34. B-scan of the *Falco tinnunculus,* i.n. 26654, OR, OS, E, H.

Thickness variation of the layers between the retinal pigment epithelium and the external limiting membrane (RPE-ELM)

Similar to the OR thickness, the RPE-ELM retinal layers thickness remained constant over the whole retina areas. An example of the RPE-ELM in the equator area can be observed in the Figure 35. These layers were only thinner in the temporal area.

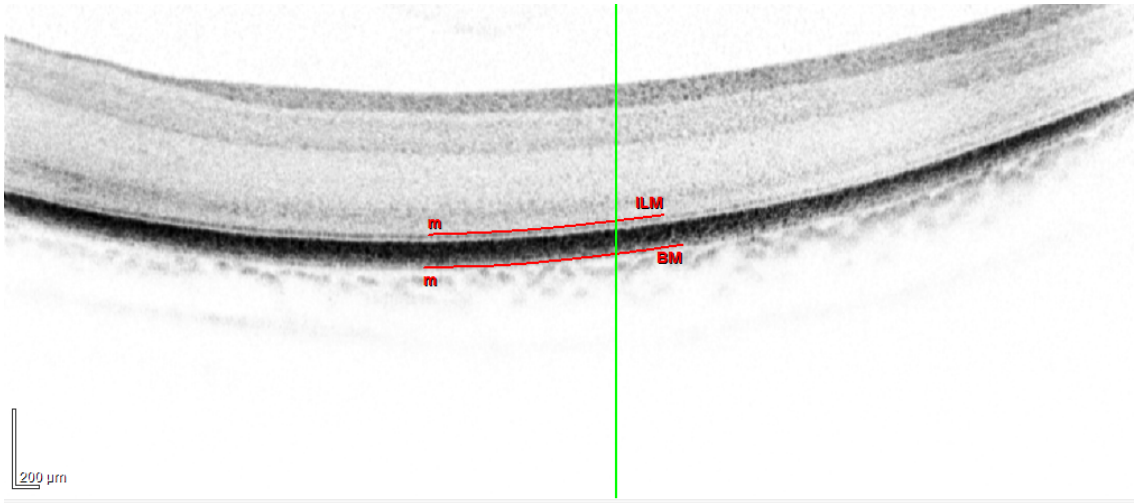

Figure 35. B-scan of the *Falco tinnunculus,* i.n. 26654, RPE-ELM, OS, E, H.

- ***Falco peregrinus***

Data obtained from three individuals of the species *Falco peregrinus* from a total of 5 patients were included and analysed (Table 10).

Table 10: *Falco peregrinus*: Results of thickness measurements TRT, RNFL+GCL, OR and RPE-ELM of different ocular areas. Abbreviations used as in Table 5.

Area	Measurement	Maximal thickness (µm)	sd (µm)	Measurements per area
Ps	TRT	395.07	39.84	6
	RNFL+GCL	210.57	49.79	6
		Mean thickness (µm)		
	OR	81.69	7.24	6
	RPE-ELM	69.46	5.28	6
E	TRT	333.26	14.80	8
	RNFL+GCL	71.42	6.90	8
	OR	98.90	6.55	8
	RPE-ELM	79.85	4.77	8
N	TRT	276.49	7.70	4
	RNFL+GCL	43.16	2.86	4
	OR	98.91	4.15	4
	RPE-ELM	80.23	3.26	4
S	TRT	245.36	7.37	4
	RNFL+GCL	31.07	2.42	4
	OR	97.97	4.10	4
	RPE-ELM	81.57	2.22	4
T	TRT	209.14	2.74	4
	RNFL+GCL	58.01	2.14	4
	OR	71.10	1.20	4
	RPE-ELM	60.30	1.65	4

Variation of the Total Retinal Thickness (TRT)

With the equator area as a reference (Figure 36), the only area with a higher TRT was the area superior to the pecten. The remaining areas had lower TRTs with the nasal area having the highest TRT among the eccentric retinal areas, and the temporal area the lowest thickness of the whole retinal areas examined.

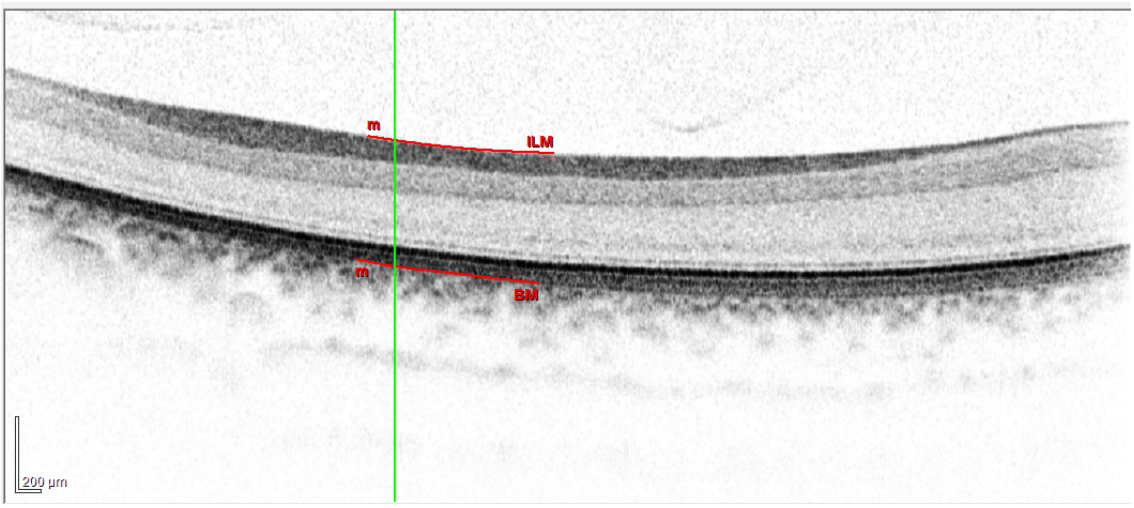

Figure 36. B-scan of the *Falco peregrinus,* i.n. 25466, TRT, OD, E, H.

Thickness variation of the retinal nerve fiber layer and the ganglion cell layer (RNFL+GCL)

The RNFL+GCL layer had a maximal thickness in the area superior to the pecten followed by the equator area, the temporal area, the nasal area, and the superior area. The Figure 37 represents an example of the RNFL+GCL in the equator area.

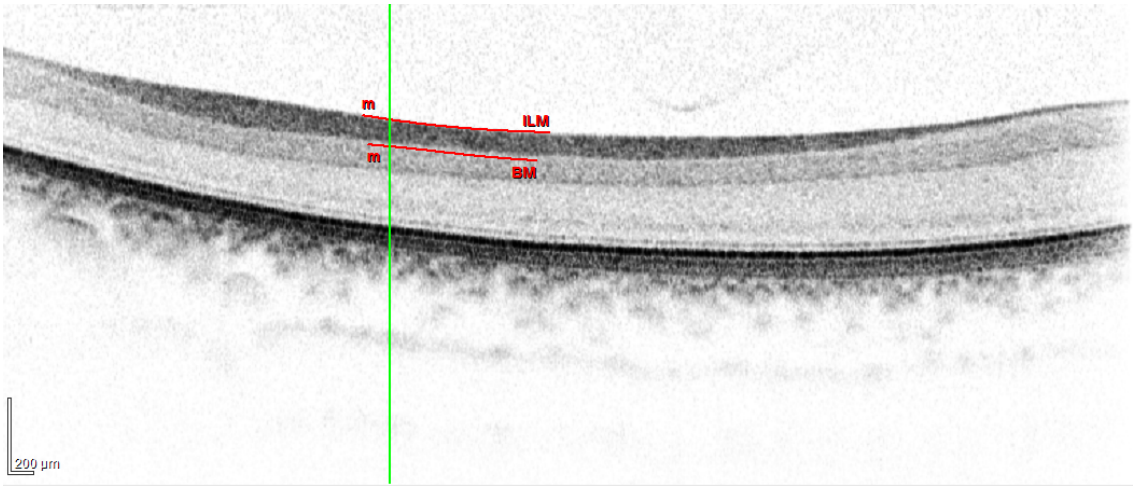

Figure 37. B-scan of the *Falco peregrinus,* i.n. 25466, RNFL+GCL, OD, E, H.

Thickness variation of the outer retina (OR)

In this species the OR was satisfactorily distinguished. Its thickness was constant along the retina, being approximately 98 µm, except for the temporal area, where a lower thickness of about 71 µm was measured. The mean of the thickness in the area superior to the pecten tended to be lower than at the equator (Figure 38) and the nasal and superior areas. Nevertheless, the standard deviation indicated that the differences were not important.

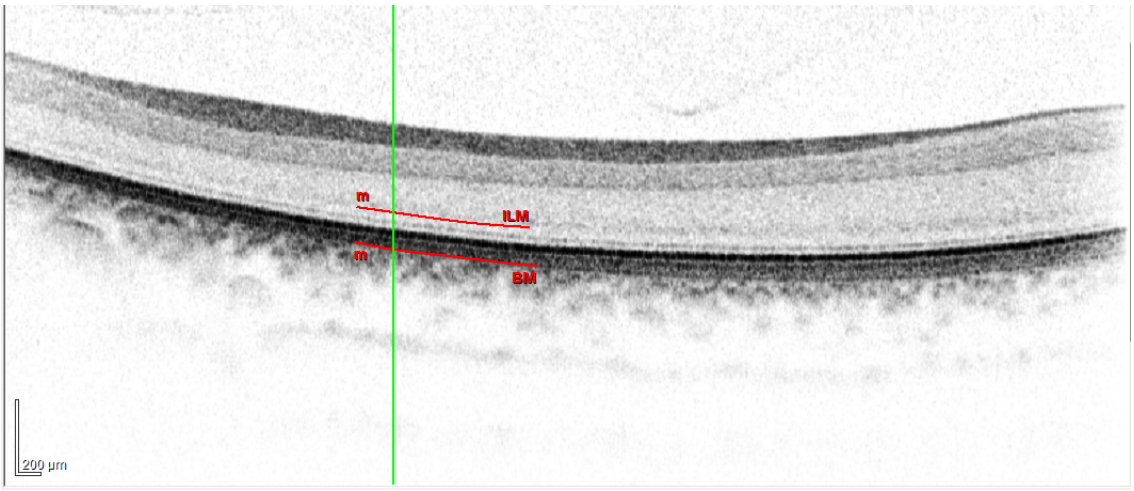

Figure 38. B-scan of the *Falco peregrinus,* i.n. 25466, OR, OD, E, H.

Thickness variation of the layers between the retinal pigment epithelium and the external limiting membrane (RPE-ELM)

The thickness of the layers between the RPE and the ELM was constant all along the retina without significant variations, with the exception of the area superior to the pecten and the temporal area. The last area had the smallest thickness. An example of the RPE-ELM in the equator area can be observed in the Figure 39.

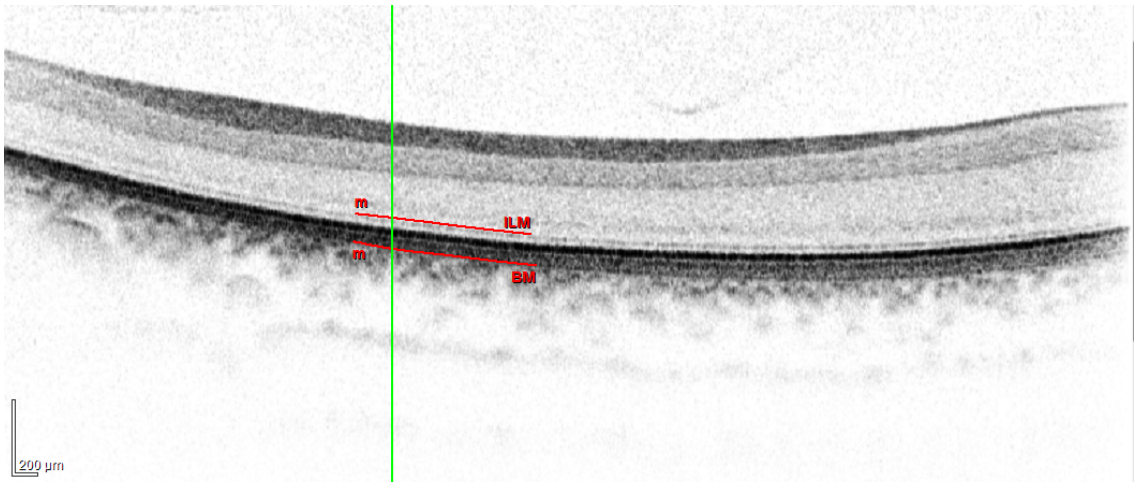

Figure 39. B-scan of the *Falco peregrinus,* i.n. 25466, RPE-ELM, OD, E, H.

- ***Circus aeruginosus***

Only one individual from the species *Circus aeruginosus* was satisfactory imagined. Since the measurements belong to only one specimen, they were not included in the comparisons between species. Nevertheless, the measurements can be considered as an example of retinal visualization with OCT in this species. The mean values are represented in table 11:

Table 11: *Circus aeruginosus*. Results of thickness measurements TRT, RNFL+GCL, OR and RPE-ELM of different ocular areas. Abbreviations used as in Table 5.

Circus aeruginosus		
OD+OS areas	OD+OS measurements	Maximal thickness (μm)
Ps	TRT	331.64
	RNFL+GCL	138.71
		Mean thickness (μm)
	OR	79.61
	RPE-ELM	64.16
E	TRT	323.53
	RNFL+GCL	51.30
	OR	90.85
	RPE-ELM	68.83
N	TRT	269.13
	RNFL+GCL	67.29
	OR	77.33
	RPE-ELM	64.55
S	TRT	204.57
	RNFL+GCL	30.49
	OR	75.33
	RPE-ELM	63.66
T	TRT	195.87
	RNFL+GCL	52.40
	OR	63.15
	RPE-ELM	54.13

4.1.1.1.3 Strigiformes

- ***Strix aluco***

Five patients of the species *Strix aluco* underwent the OCT examination. Among them, four individuals were satisfactorily imagined. The retinal thickness data are shown in Table 12.

Table 12: *Strix aluco:* Results of thickness measurements of TRT, RNFL+GCL, OR; and RPE-ELM of different ocular areas. Abbreviations used as in Table 5.

Area	Measurement	Maximal thickness (µm)	sd (µm)	Measurements per area
Ps	TRT	351.87	29.99	4
	RNFL+GCL	155.65	25.39	4
		Mean thickness (µm)		
	OR	108.56	5.83	2
	RPE-ELM	91.23	8.89	4
E	TRT	282.25	7.78	9
	RNFL+GCL	59.82	10.98	9
	OR	114.01	1.77	3
	RPE-ELM	96.07	2.83	9
N	TRT	242.53	2.61	6
	RNFL+GCL	26.00	2.23	4
	OR	119.95	1.94	4
	RPE-ELM	105.90	1.92	6
S	TRT	233.89	3.27	8
	RNFL+GCL	26.35	1.56	4
	OR	116.03	2.56	2
	RPE-ELM	103.76	3.83	6
T	TRT	243.50	7.15	7
	RNFL+GCL	28.58	2.31	5
	OR	113.45	3.65	3
	RPE-ELM	89.30	2.10	5

Variation of the Total Retinal Thickness (TRT)

The maximal TRT in these specimens was measured in the superior pecten area. TRT readings decreased constantly in the following order: equator area, nasal and temporal area (both no obvious differences) and superior area showing the lowest readings. Figure 40 represents an example of TRT in the equator area.

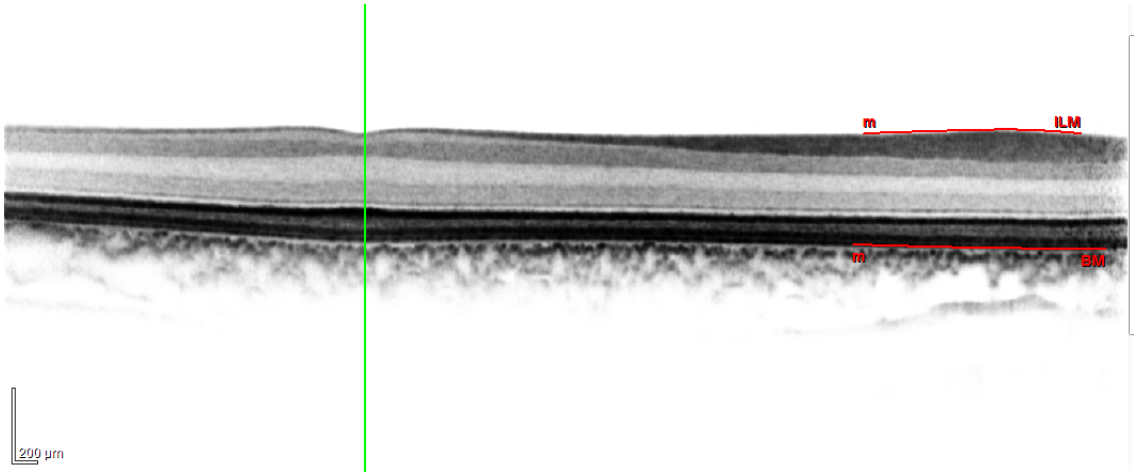

Figure 40. B-scan of the *Strix aluco*, TRT, OD, E, H.

Thickness variation of the retinal nerve fiber layer and the ganglion cell layer (RNFL+GCL)

The area superior to the pecten was the area with the maximal RNFL+GCL thickness, followed by the equator area (Figure 41). Minimum reading was found in the eccentric retinal areas with no significant-differences among them.

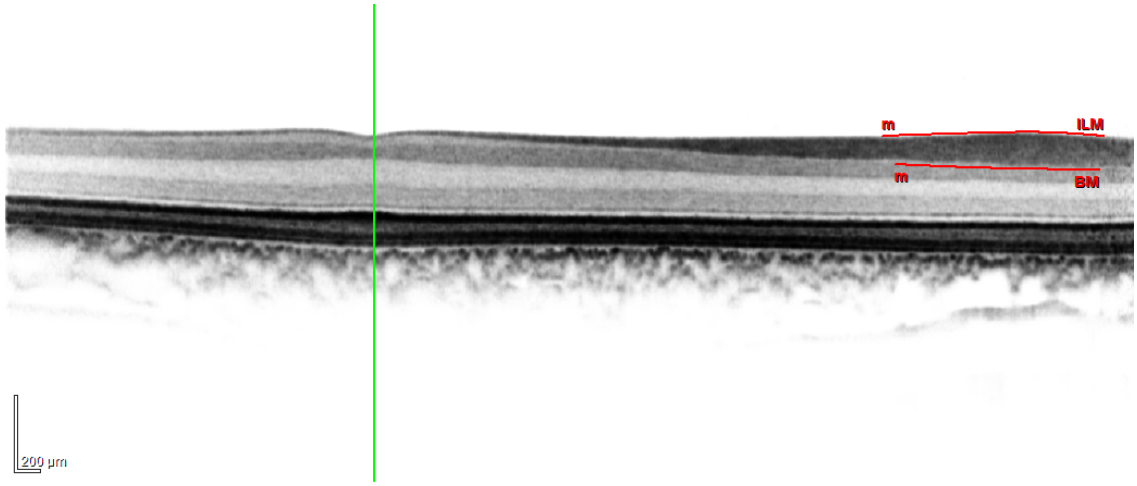

Figure 41. B-scan of the *Strix aluco*, RNFL+GCL, OD, E, H.

Thickness variation of the outer retina (OR)

The thickness of these layers remained homogenous all along the retina. Figure 42 represents an example of the OR in the equator area.

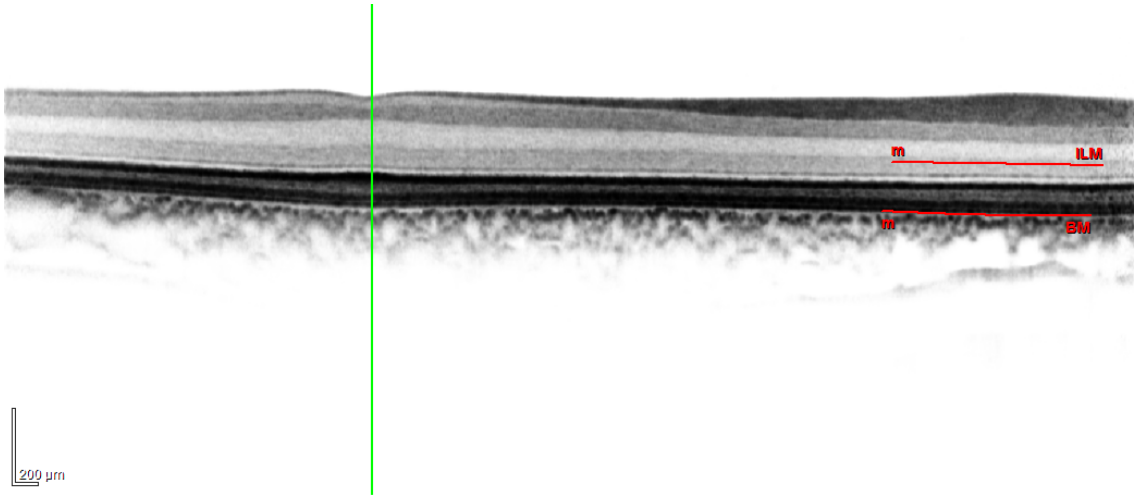

Figure 42. B-scan of the *Strix aluco*, OR, OD, E, H.

Thickness variation of the layers between the retinal pigment epithelium and the external limiting membrane (RPE-ELM)

The thickness of the layers between the RPE and ELM was almost constant all along the retina without significant variations, except for the temporal area, where it was lower according to the interval determined with the standard deviation. An example of the RPE-ELM in the equator area is shown in Figure 43.

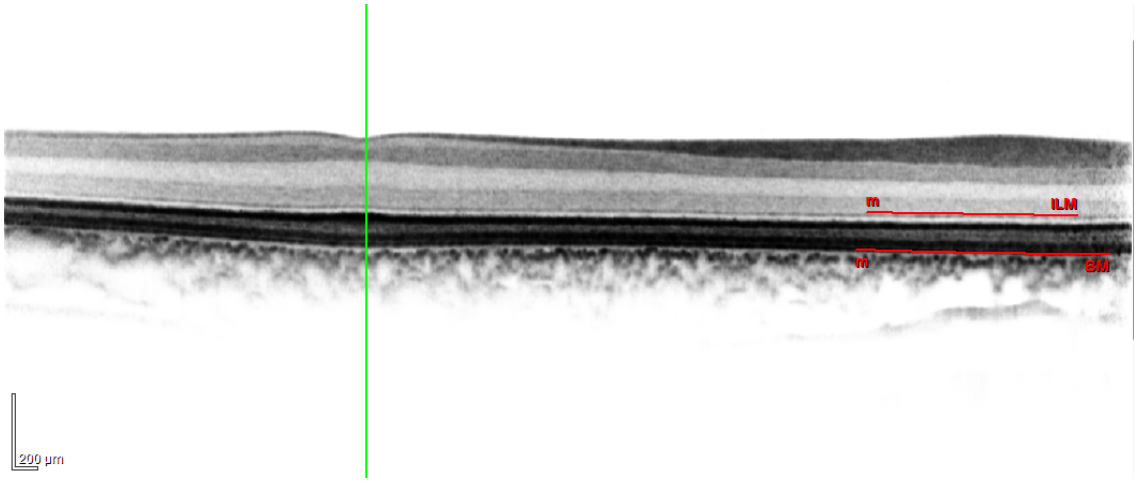

Figure 43. B-scan of the *Strix aluco*, RPE-ELM, OD, E, H.

- ***Asio otus***

Five out of seven patients of the species *Asio otus* were satisfactorily imagined. Data of the equator, nasal, superior and temporal areas are compiled in table 13.

Table 13: *Asio otus*: Results of thickness measurements of TRT, RNFL+GCL, OR and RPE-ELM of different ocular areas. The "x" represents the cases where no measurement could be obtained. Abbreviations used as in Table 5.

Area	Measurement	Maximal thickness (µm)	sd (µm)	Measurements per area
Ps	TRT	308.16	20.95	9
	RNFL+GCL	146.17	20.01	9
		Mean thickness (µm)		
	OR	x	x	x
	RPE-ELM	79.20	8.05	9
E	TRT	244.28	4.13	9
	RNFL+GCL	50.46	5.65	9
	OR	x	x	x
	RPE-ELM	87.42	3.38	9
N	TRT	197.33	4.52	8
	RNFL+GCL	26.29	4.34	7
	OR	x	x	x
	RPE-ELM	83.92	4.19	8
S	TRT	192.72	7.08	7
	RNFL+GCL	31.46	3.66	5
	OR	x	x	x
	RPE-ELM	81.72	3.17	6
T	TRT	206.81	7.92	7
	RNFL+GCL	29.13	4.42	7
	OR	x	x	x
	RPE-ELM	81.65	4.50	7

Variation of the Total Retinal Thickness (TRT)

As in the other species mentioned before, TRT was maximal in the area superior to the pecten, and higher than in the equator area (Figure 44). The equatorial total retinal thickness was higher than those of the temporal and the superior area, which did not differ from each other. In the superior area, TRT was minimal.

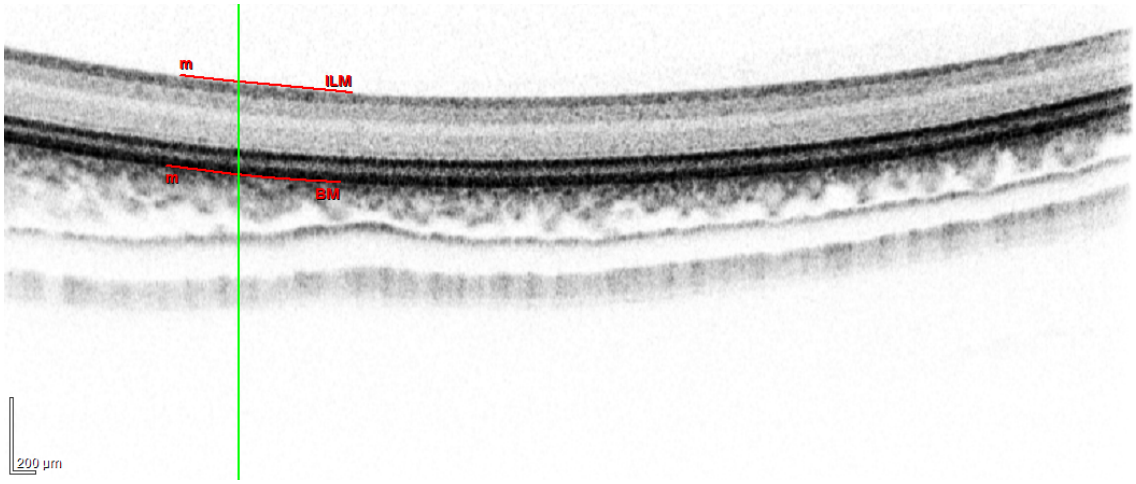

Figure 44. B-scan of the *Asio otus*, i.n. 26062, TRT; OD; E; H.

Thickness variation of the retinal nerve fiber layer and the ganglion cell layer (RNFL+GCL)

RNFL+GCL thickness was maximal in the area superior to the pecten, followed by the equator area (Figure 45). There were no differences in thickness between the nasal, superior and temporal areas where the RNFL+GCL reached the minimal thickness.

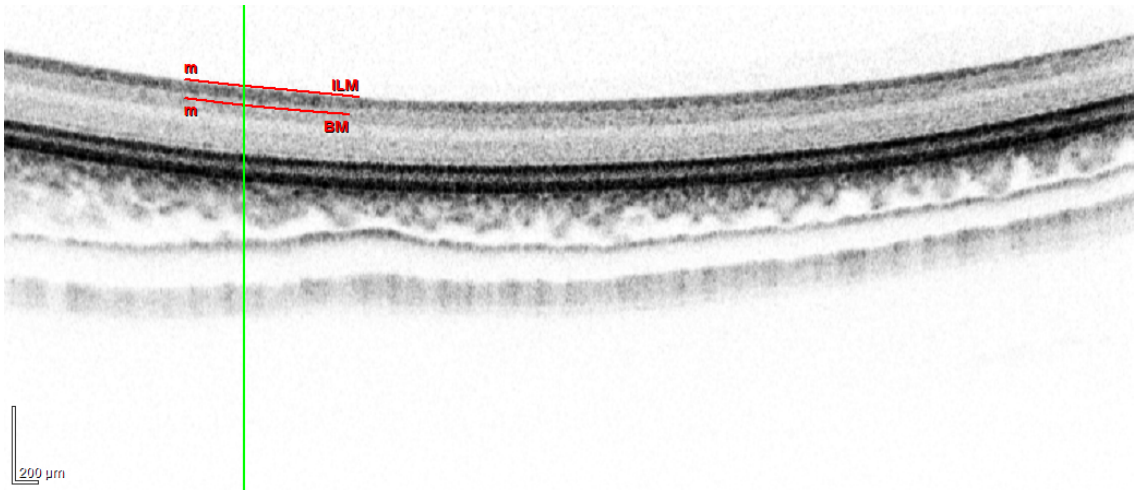

Figure 45. B-scan of the *Asio otus*, i.n. 26062, RNFL+GCL; OD; E; H.

Outer retina (OR) thickness

Since the border between OPL and ONL could not be distinguished within the pictures, measurement of the OR could not be performed.

Thickness variation of the layers between the retinal pigment epithelium and the external limiting membrane (RPE-ELM)

The layers located between the RPE and the ELM did not reveal any thickness variation along the retina areas. Figure 46 represents an example of a measurement of RPE-ELM in the equator area.

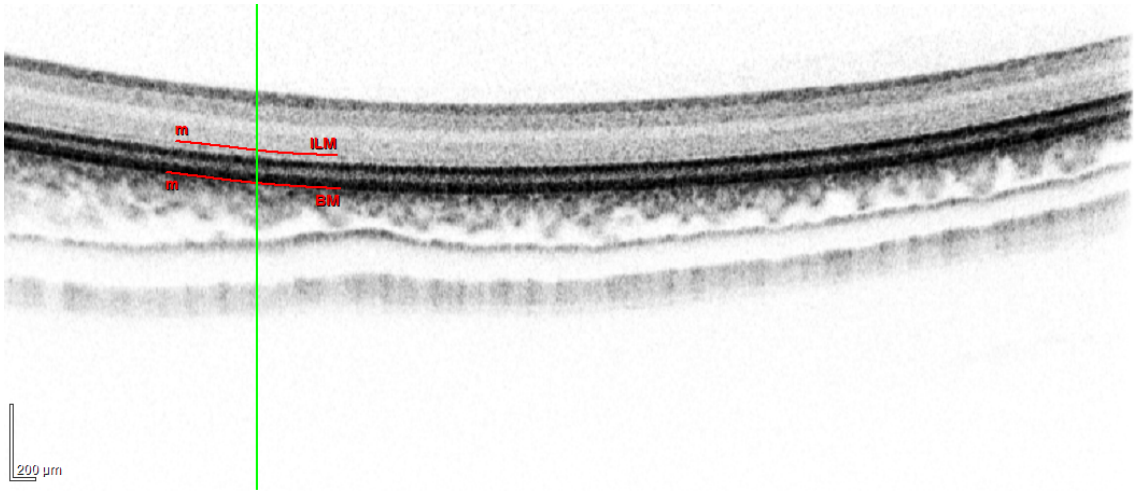

Figure 46. B-scan of the Asio otus, i.n. 26062, RPE-ELM; OD; E; H.

- ***Athene noctua***

Only one individual from the species *Athene noctua* was satisfactory imagined. Since the measurements origin from only one specimen, they were not considered in the comparisons between species. Nevertheless, the measurements can be regarded as an example of retinal visualization with OCT in this species (Table 14).

Table 14: *Athene noctua*. Results of thickness measurements of TRT, RNFL+GCL, OR and RPE-ELM of different ocular areas. The “x” represents the cases where no measurement could be obtained. Abbreviations used as in Table 5.

Athene noctua		
OD+OS areas	OD+OS measurements	Maximal thickness (µm)
Ps	TRT	346.93
	RNFL+GCL	112.48
		Mean thickness (µm)
	OR	126.75
	RPE-ELM	113.62
E	TRT	316.20
	RNFL+GCL	52.33
	OR	135.04
	RPE-ELM	120.72
N	TRT	253.34
	RNFL+GCL	41.98
	OR	116.99
	RPE-ELM	105.82
S	TRT	261.19
	RNFL+GCL	31.61
	OR	128.99
	RPE-ELM	114.94
T	TRT	261.65
	RNFL+GCL	38.80
	OR	117.16
	RPE-ELM	103.17

- ***Tyto alba***

Only one individual from the species *Tyto alba* was satisfactory imagined. Since the measurements belong to only one specimen, they cannot be considered within the comparisons between species. Nevertheless, the measurements can be seen as an example of retinal visualization with OCT in this species (Table 15).

Table 15: *Tyto alba*. Results of thickness measurements of TRT, RNFL+GCL, OR and RPE-ELM of different ocular areas. The "x" represents the cases where no measurement could be obtained. Abbreviations used as in Table 5.

Tyto alba		
OD+OS areas	OD+OS measurements	Maximal thickness (µm)
Ps	TRT	477.03
	RNFL+GCL	294.66
		Mean thickness (µm)
	OR	74.00
	RPE-ELM	63.88
E	TRT	349.11
	RNFL+GCL	99.11
	OR	87.89
	RPE-ELM	73.86
N	TRT	x
	RNFL+GCL	x
	OR	x
	RPE-ELM	x
S	TRT	x
	RNFL+GCL	x
	OR	x
	RPE-ELM	x
T	TRT	263.57
	RNFL+GCL	44.95
	OR	90.17
	RPE-ELM	75.66

- ***Aegolius funereus***

Only one individual from the species *Aegolius funereus* was satisfactory imagined. Since the measurements were obtained from only one specimen, they cannot be considered within the comparisons between species. Nevertheless, the measurements can be regarded as an example of retinal visualization with OCT in this species (Table 16).

Table 16: *Aegolius funereus*. Results of thickness measurements of TRT, RNFL+GCL, OR and RPE-ELM of different ocular areas. The "x" represents the cases where no measurement could be obtained. Abbreviations used as in Table 5.

Aegolius funereus		
OD+OS areas	OD+OS measurements	Maximal thickness (µm)
Ps	TRT	330.67
	RNFL+GCL	149.46
		Mean thickness (µm)
	OR	x
	RPE-ELM	84.24
E	TRT	236.82
	RNFL+GCL	39.46
	OR	x
	RPE-ELM	91.91
N	TRT	203.16
	RNFL+GCL	23.31
	OR	x
	RPE-ELM	93.99
S	TRT	209.08
	RNFL+GCL	25.40
	OR	x
	RPE-ELM	91.99
T	TRT	207.84
	RNFL+GCL	28.50
	OR	x
	RPE-ELM	86.09

4.1.1.2 Interspecific variations

To evaluate the interspecific variations, measurements of the selected retinal layers or groups of retinal layers were compared among species and among orders. The different sets of values (thickness mean of each selected layer and standard deviation) in each species are shown in the Tables 17, 18 and 19.

Table 17: Thickness measurements of the retinal layers from the species within Accipitriformes. Area Ps, E, N, S, T. Results of thickness measurements of TRT, RNFL+GCL, OR and RPE-ELM. The “x” represents the cases where no measurement could be obtained. Abbreviations used as in Table 5.

Accipitriformes									
		Buteo buteo		*Pernis apivorus*		*Accipiter nisus*		*Accipiter gentilis*	
Area	Retinal layers	Thickness	sd	Thickness	sd	Thickness	sd	Thickness	sd
Ps	TRT	418,83	68.61	371,11	14,45	384,04	11.08	477.03	x
	RNFL+GCL	210,43	101.65	133,80	23,76	230,32	19.77	294.66	x
	OR	89,68	16.38	x	x	69,71	7.95	74.00	x
	RPE-ELM	74,52	10.99	118,90	11.65	57,05	6.4	63.88	x
E	TRT	370,25	20.1	350,76	12,42	320,95	7,1	349.11	x
	RNFL+GCL	85,76	28.89	63,96	11,74	104,86	11,25	99.11	x
	OR	102,61	8.84	x	x	84,10	3,49	87.89	x
	RPE-ELM	83,25	15.43	133,14	7,07	67,93	2,94	73.86	x
N	TRT	315,40	12.4	281,93	8,06	230,86	1,79	x	x
	RNFL+GCL	45,10	7.56	61,57	6,77	58,25	2,93	x	x
	OR	104,93	6.53	x	x	78,44	1,26	x	x
	RPE-ELM	86,93	6.12	115,73	2,9	67,74	1,03	x	x
S	TRT	255,89	18.13	261,58	10,13	220,96	6,81	x	x
	RNFL+GCL	25,81	5.45	38,87	5,49	39,91	2,03	x	x
	OR	98,31	6.86	x	x	81,05	2,21	x	x
	RPE-ELM	82,48	4.85	121,13	4,01	69,34	3,23	x	x
T	TRT	223,93	12.28	282,50	6,53	173,33	1,8	263.57	x
	RNFL+GCL	66,33	8.75	60,41	6,4	44,51	2,56	44.95	x
	OR	74,67	5.93	x	x	59,28	2,22	90.17	x
	RPE-ELM	62,62	5.11	115,30	4,97	50,04	1,69	75.66	x

Table 18: Thickness measurements of the retinal layers from the species within Falconiformes. Area Ps, E, N, S, T. Results of thickness measurements of TRT, RNFL+GCL, OR and RPE-ELM. The “x” represents the cases where no measurement could be obtained. The “x” represents the cases where no measurement could be obtained. Abbreviations used as in Table 5.

Falconiformes							
		Falco peregrinus		*Falco tinnunculus*		*Circus aeruginosus*	
Area	Retinal layers	Thickness	sd	Thickness	sd	Thickness	sd
Ps	TRT	395,07	39.84	468,83	13.71	331.64	x
	RNFL+GCL	210,57	49.79	242,35	27.14	138.71	x
	OR	81,69	7.24	105,15	24.36	79.61	x
	RPE-ELM	69,46	5.28	79,33	7.57	64.163	x
E	TRT	333,26	14,8	409,04	14,78	323.53	x
	RNFL+GCL	71,42	6,9	72,67	12,06	51.30	x
	OR	98,90	6,55	106,50	4,38	90.85	x
	RPE-ELM	79,85	4,77	83,87	5,05	68.83	x
N	TRT	276,49	7,7	323,14	9,71	269.13	x
	RNFL+GCL	43,16	2,86	45,70	4,87	67.29	x
	OR	98,91	4,15	103,66	5,15	77.33	x
	RPE-ELM	80,23	3,26	86,36	4,06	64.55	x
S	TRT	245,36	7,37	296,72	11,41	204.57	x
	RNFL+GCL	31,07	2,42	34,56	3,2	30.49	x
	OR	97,97	4,1	100,82	3,87	75.33	x
	RPE-ELM	81,57	2,22	84,05	3,39	63.66	x
T	TRT	209,14	2,74	249,28	9,39	195.869304	x
	RNFL+GCL	58,01	2,14	85,24	9,31	52.3968117	x
	OR	71,10	1,2	75,10	5,98	63.1547311	x
	RPE-ELM	60,30	1,65	63,56	5,96	54.127156	x

Table 19: Thickness measurements of the retinal layers from the species within Strigiformes. Area Ps, E, N, S, T. Results of thickness measurements of TRT, RNFL+GCL, OR and RPE-ELM. The “x” represents the cases where no measurement could be obtained. Standard deviation (sd). The “x” represents the cases where no measurement could be obtained. Abbreviations used as in Table 5.

Strigiformes											
		Strix aluco		*Asio otus*		*Athene noctua*		*Tyto alba*		*Aegolius funereus*	
Area	Retinal layers	Thickness	sd	Thickness	sd	Thickness	sd	Thickness	sd	Thickness	sd
Ps	TRT	351,87	29.99	308,16	20.95	346.93	x	272.20	x	330.67	x
	RNFL+GCL	155,65	25.39	146,17	20.01	112.48	x	107.45	x	149.46	x
	OR	108,56	5.83	x	x	126.75	x	x	x	x	x
	RPE-ELM	91,23	8.89	79,20	8.05	113.62	x	87.69	x	84.24	x
E	TRT	282,25	7,78	244,28	4,13	316.20	x	x	x	236.81	x
	RNFL+GCL	59,82	10,98	50,46	5,65	52.33	x	x	x	39.46	x
	OR	114,01	1,77	x	x	135.04	x	x	x	x	x
	RPE-ELM	96,07	2,83	87,42	3,38	120.72	x	x	x	91.91	x
N	TRT	242,53	2,61	197,33	4,52	253.34	x	x	x	203.16	x
	RNFL+GCL	26,00	2,23	26,29	4,34	41.98	x	x	x	23.31	x
	OR	119,95	1,94	x	x	116.99	x	x	x	x	x
	RPE-ELM	105,90	1,92	83,92	4,19	105.82	x	x		93.99	
D	TRT	233,89	3,27	192,72	7,08	261.19	x	x	x	209.08	x
	RNFL+GCL	26,35	1,56	31,46	3,66	31.61	x	x	x	25.40	x
	OR	116,03	2,56	x	x	128.99	x	x	x	x	x
	RPE-ELM	103,76	3,83	81,72	3,17	114.94	x	x	x	91.99	x
T	TRT	243,50	7,15	206,81	7,92	261.65	x	x	x	207.84	x
	RNFL+GCL	28,58	2,31	29,13	4,42	38.80	x	x	x	28.50	x
	OR	113,45	3,65	x	x	117.16	x	x	x	x	x
	RPE-ELM	89,30	2,10	81,65	4,5	103.17	x	x	x	86.09	x

Taking the equator area as a reference, the values given in Table 20 can be taken as a guideline for the interpretation of OCT result when performing an OCT examination of an individual of the species mentioned in the Table 20.

Table 20: Measurements of the thickness of the outer retina (OR) and of the retinal pigment epithelium up to external limiting membrane (RPE-ELM) in the equator area (mean and standard deviation). The “x” represents the cases where no measurement could be obtained. Abbreviations used as in Table 5. Only the species with more than one individual included are considered:

Species	OR		RPE-ELM	
	mean	standard deviation	mean	standard deviation
Buteo buteo	102.61	8.84	83.25	15.43
Pernis apivorus	x	x	133.14	7.07
Accipiter nisus	84.10	3.49	67.93	2.94
Falco peregrinus	98.90	6.55	79.85	4.77
Falco tinnunculus	106.50	4.38	83.87	5.05
Strix aluco	114.01	1.77	96.07	2.83
Asio otus	x	x	87.42	3.38

Total retinal thickness (TRT)

Taking the equator area as a reference, differences in TRT among orders could be observed. The equatorial TRT was thinner in the Strigiformes than in the Accipitriformes or Falconiformes. The thickest TRT was found in the species *Falco tinnunculus*. Several common features were observed in the species included in the study. The area superior to the pecten had a higher TRT than the equator, while the eccentric retinal areas, such as superior, nasal and temporal, always had lower TRT values than the equator.

The TRT measurements obtained from the eccentric retinal areas differed not only within each species, but also among specimens from different species.

Retinal nerve fiber layer and ganglion cell layer (RNFL+GCL)

The RNFL+GCL followed a similar thickness variation pattern as that observed for TRT, the thickness being maximal in the area superior to the pecten and minimal in the areas of the eccentric retina.
The individuals of the orders Accipitriformes and Falconiformes had thicker RNFL+GCL than those of the Strigiformes. Among the two species from the order Falconiformes within this study, the RNFL+GCL did not show remarkable differences, it was slightly smaller in the *Falco peregrinus* than in the *Falco tinnunculus*.

In the order Accipitriformes, the species *Pernis apivorus* had a thinner RNFL+GCL than *Buteo buteo* or *Accipiter nisus*.

Outer retina (OR)

One common feature observed in all the species under study was, that the thickness of the OR in general remained rather constant all along the retina. This anatomical feature of constant thickness measurements differed from those observed for the TRT and RNFL+GCL, which instead showed a pattern of increasing thickness as it approaches the pecten.

In *Strix aluco* belonging to the order Strigiformes, a relatively thick OR was found compared to the values obtained for TRT. The OR was the thickest layer in the Strigiformes, thicker than those observed in species *Falco tinnunculus* or *Buteo buteo* which in contrast had high TRTs.

Retinal pigment epithelium-external limiting membrane (RPE-ELM)

Thickness variation of the RPE-ELM in the raptor retina followed a pattern similar to that found in the OR. Species belonging to Strigiformes showed relatively high thickness values for the RPE-ELM and for the OR, but low values for the TRT in comparison with the orders Accipitriformes and Falconiformes.

In the order Accipitriformes, the highest values of the RPE-ELM thickness were found in the species *Pernis apivorus* surpassing 100 µm, while they only reached approximately 80 µm and 65 µm in *Buteo buteo* and *Accipiter nisus,* respectively. The species *Pernis*

apivorus had the lowest thickness values of TRT and RNFL+GCL among the species from the order Accipitriformes under study.

4.3 Image quality and artefacts

Some of the OCT fundus pictures showed different qualities and dark regions. The phenomenon was especially evident in *Falco tinnunculus*, where it was common to obtain a fundus picture with black corners (Figure 47). The retinal layers could still be distinguished in the B-scan.

Regions with a colour degradation of the retinal layers in some B-scan were observed. These degradations are interferences in the light beam called “noises”. Therefore the retina located immediately below the material or structure producing the noise was visualized with lower quality (Figure 48).

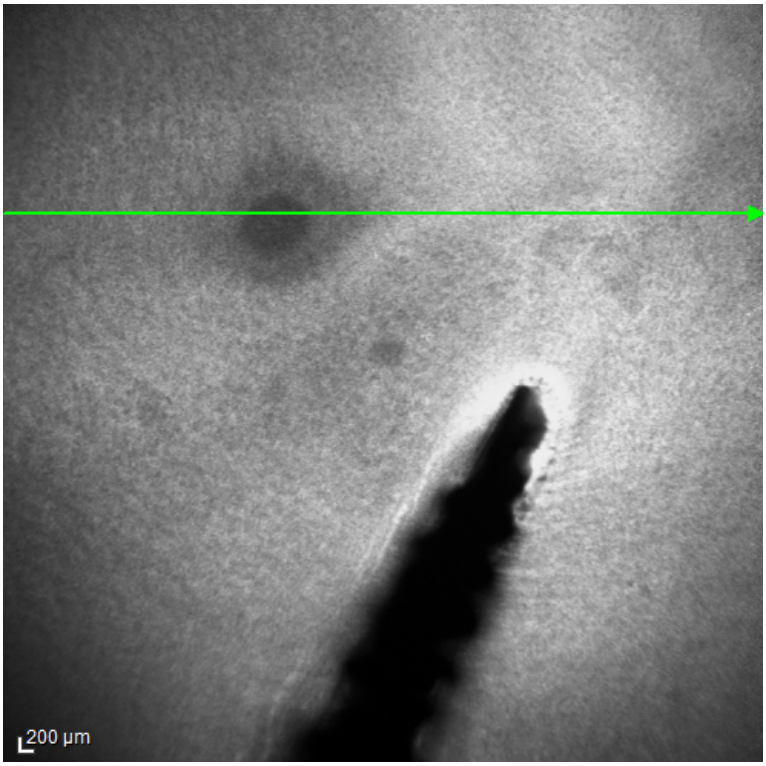

. A

B

Figure 47. A) Fundus picture from the patient *Buteo buteo* 26235 OD, E, H. The picture has a uniform lightning without dark corners. B) OCT-scan of the aforementioned fundus image. The image possesses the expected high quality.

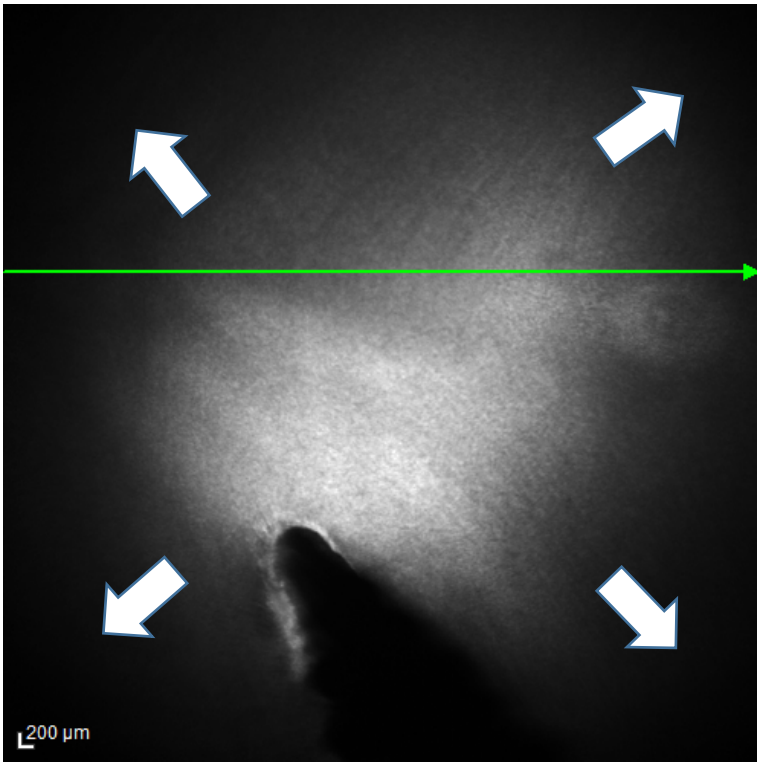

A

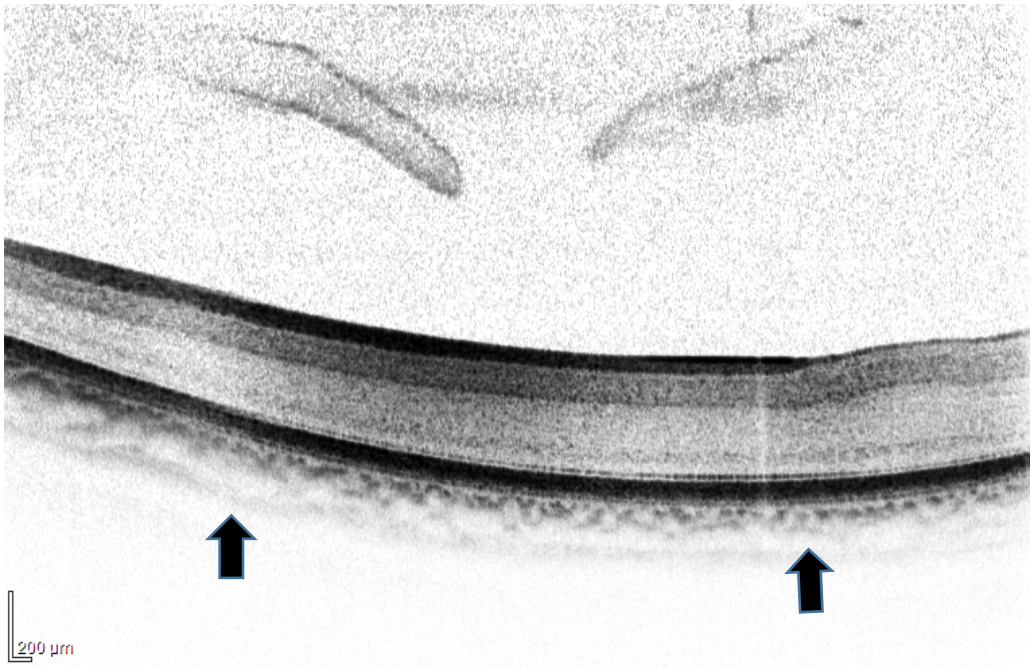

B

Figure 48. A) *Falco tinnunculus* i.n. 25494 OD, E. The white arrow shows the dark corners of the fundus image. B) OCT-scan of the aforementioned fundus in the equator area. The retinal areas marked with the black arrows show artefacts. The retinal areas on the left and on the right side of the picture have a lighter grey and lower optical resolution than the area in the center of the retinal B-scan. These lighter areas correspond with the darker areas of the fundus picture.

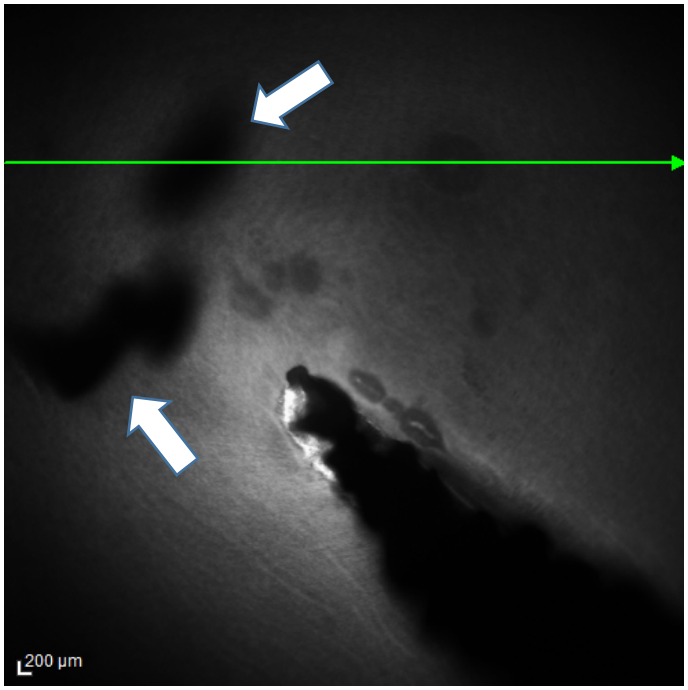

A

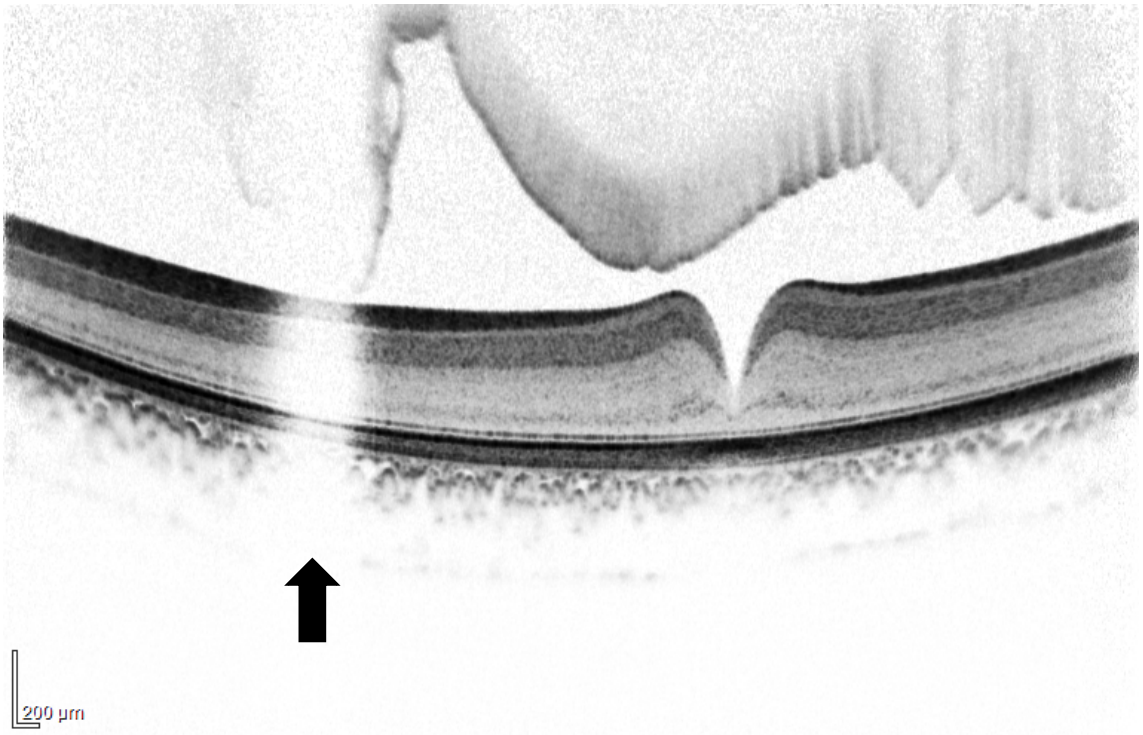

B

Figure 49. *Buteo buteo* i.n. 20419 OD, E, H. A) The arrow shows blood swimming in the posterior chamber. The green line shows the section of the B-scan. B) B-scan of the previous fundus picture. The arrow indicates the site where the bleeding causes the noise. The retina immediately below is intact.

4.4 Validation of the OCT examination with histology

Histological sections of the retina of three specimens of the species *Buteo buteo* were selected to validate the OCT results concerning this species. For two of these three specimens, patients 23200 and 25263, results of OCT examination were also available. In the three cases, the thickness measured among retinal layers were up to a 25 % lower than the thickness measured in the OCT pictures, which corresponded to the range expected due to histological shrinkage. A histological section of the equatorial retinal area of patient *Buteo buteo* 23200 illustrating the measurements is shown in Figures 50, 51, 52 and 53.

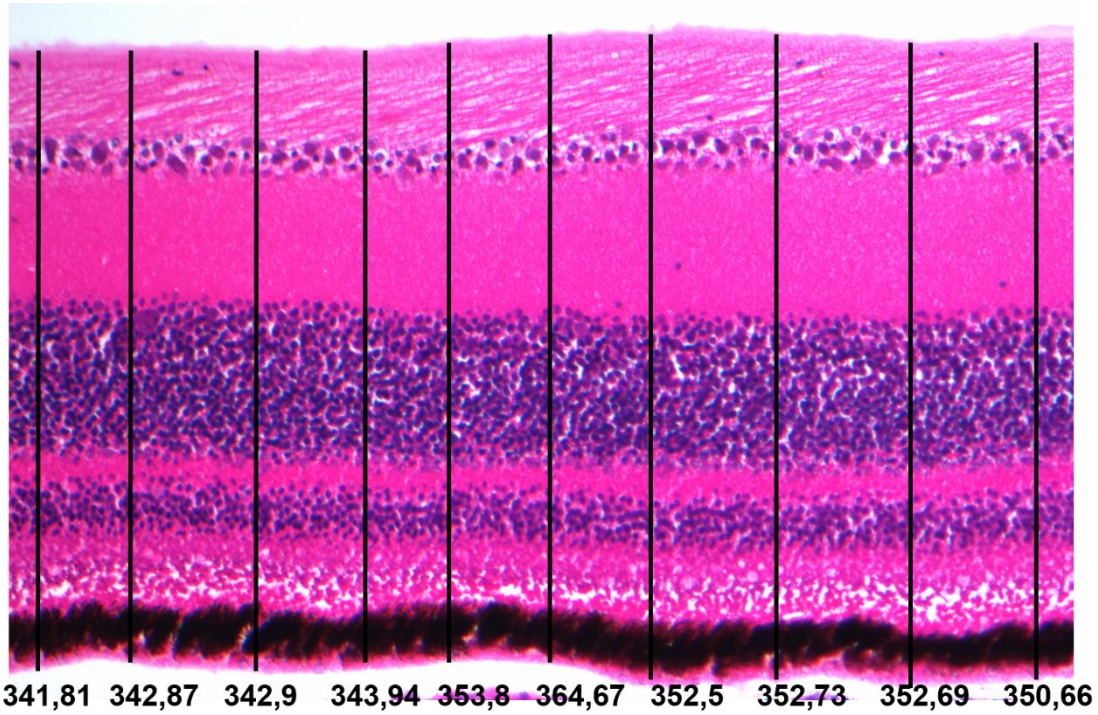

Figure 50: Histology of the equator area of the patient *Buteo buteo* 23200. OS, vertical section (V). The black lines indicate the measurements of the TRT. Each black line has a number associated, which is the thickness in micrometres. Hematoxylin & Eosin staining.

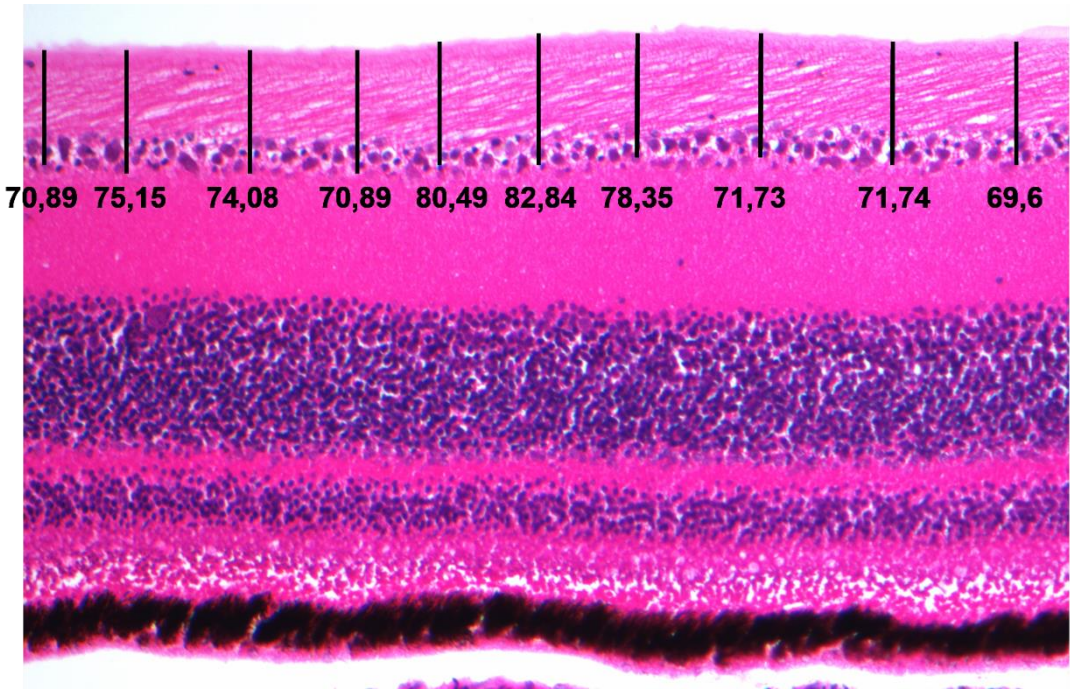

Figure 51: Histology of the equator area of the patient *Buteo buteo* 23200. OS, V. The black lines indicate the measurements of RNFL+GCL. Each black line has a number associated, which is the thickness in micrometres. Hematoxylin & Eosin.

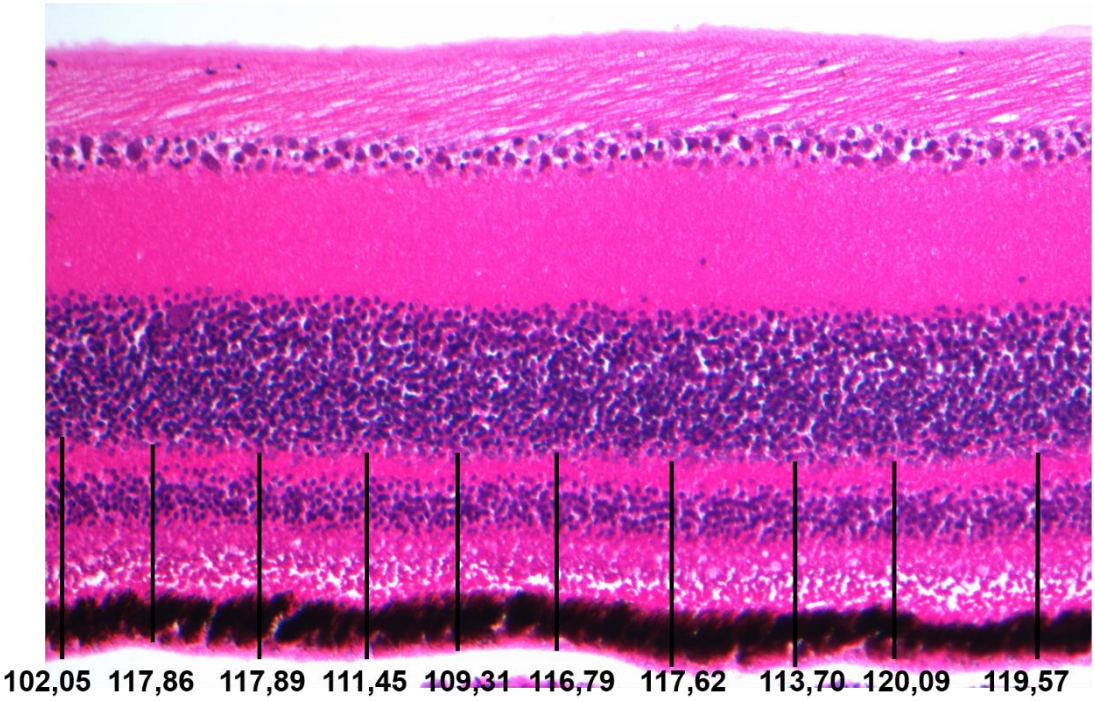

Figure 52: Histology of the equator area of the patient *Buteo buteo* 23200. OS, V. The black lines indicate the measurements of the OR. Each yellow line has a number associated, which is the thickness in micrometres. Hematoxylin & Eosin.

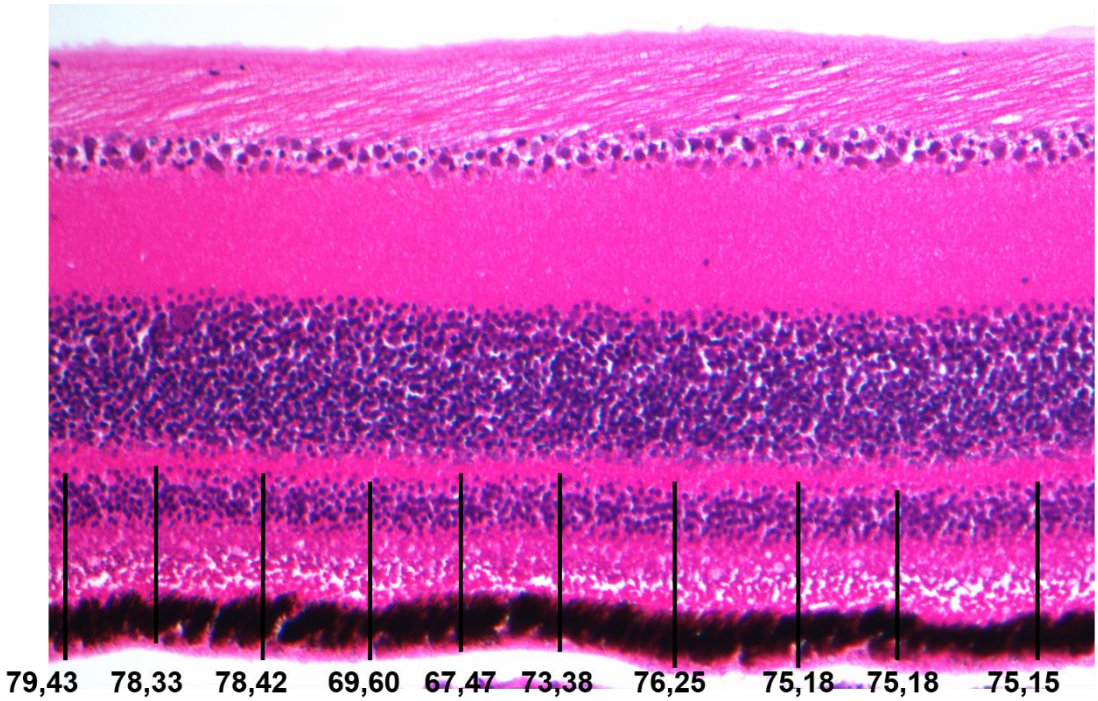

Figure 53: Histology of the equator area of the patient *Buteo buteo* 23200. OS, V. The black lines indicate the measurements of the RPE-ELM. Each black line has a number associated, which is the thickness in micrometres. Hematoxylin & Eosin.

The thickness values obtained from the measurements of the retinal layers in the histological sections of the species *Buteo buteo* shown in Table 16 were well correlated with the values received with the OCT device. The thicknesses measured in the histological sections were 15 - 25 % lower than those found in the OCT images.

The same relation was observed in the species, *Asio otus,* selected as a candidate for comparison with histology. In this species, the histological results of the eyes of three patients were used to validate their OCT examination, and for two of them OCT results were also available. The histological measurements of the species *Asio otus* are collected in Table 22.

Table 21: Thickness of the retinal layers measured in histological sections of the eyes of three patients of the species *Buteo buteo* at the equator area. i.n., (identification number)

Species	Number of measurements	Retinal layers	Mean thickness(µm)	sd
Buteo buteo i.n.				
23200	10	TRT	349.85	7.12
	10	RNFL+GCL	74.58	4.55
	10	OR	114.57	5.61
	10	RPE-ELM	75.34	3.95
24742	10	TRT	341.54	4.24
	10	RNFL+GCL	52.32	1.99
	10	OR	73.66	3.55
	10	RPE-ELM	46.62	4.37
25263	10	TRT	289.01	3.97
	10	RNFL+GCL	65.09	1.19
	10	OR	68.02	1.71
	10	RPE-ELM	42.34	1.90

Table 22: Thickness of the retinal layers measured in histological sections of the eyes of three patients of the species *Asio otus*, Equator area.

Species	Number of measurements	Retinal layers	Mean thickness (µm)	sd
Asio otus i.n.				
22570	10	TRT	188.50	4.86
	10	RNFL+GCL	31.84	3.31
	10	OR	94.08	7.05
	10	RPE-ELM	67.02	6.91
24225	10	TRT	190.86	11.08
	10	RNFL+GCL	40.47	1.26
	10	OR	82.50	6.57
	10	RPE-ELM	58.60	5.67
25239	10	TRT	183.16	4.57
	10	RNFL+GCL	32.32	2.89
	10	OR	89.70	3.53
	10	RPE-ELM	59.22	3.36

Even though the remaining retinal areas visualized with OCT were histological processed as well, they were not used for comparison with measurements performed on the B-

scans due to difficulties to relocate in the histological slide the exactly identical retinal areas investigated by OCT which was important because of spatial thickness variations. Therefore only equatorial areas were selected for evaluation. An example of the pecten superior area is shown in Figures 54 and 55.

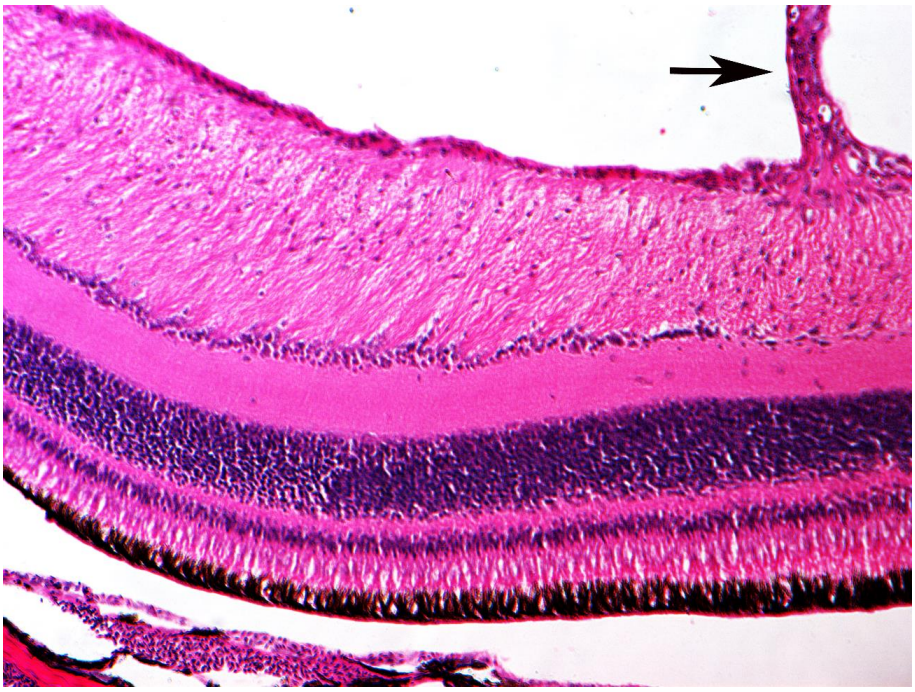

Figure 54. Histological section of the area superior to the pecten of the patient 24407 *Falco tinnunculus*. The arrow indicates the pecten. Hematoxylin & Eosin.

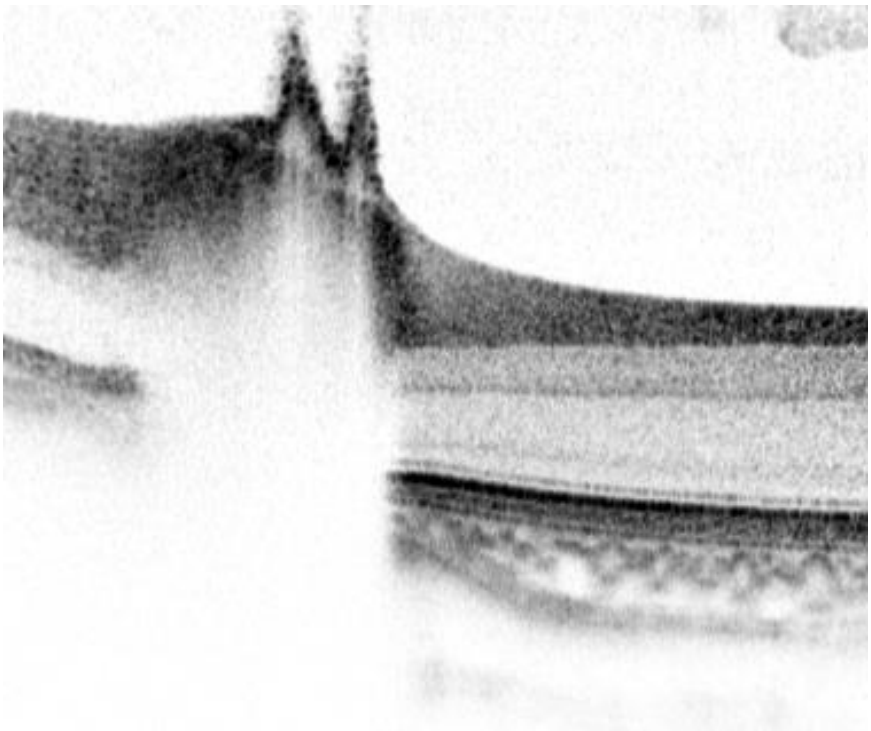

Figure 55. OCT-scan of about the same area mentioned in Figure 54, in a patient of the same species, *Falco tinnunculus* 25494.

5 DISCUSSION

5.1 OCT examination of the raptor eye

In order to answer the question, whether the OCT technique is an appropriate diagnostic method in the field of avian ophthalmology, especially in the examination of the raptor eye, 56 raptors from 13 species and three orders were included in this investigation. These birds, without exception wild raptor patients, had been taken to the Clinic for Birds, Reptiles, Amphibians and Ornamental Fish of the University Ludwig Maximilian (Munich) after being found in the wild unable to fly. They were thus suspected of suffering from trauma or other diseases and underwent ophthalmological examinations because of medical indications. During this eye investigation it was tested, whether OCT images of the avian retina could be produced improving diagnosis of disorders and reliability of prognosis for the avian patient in the future.
Since the aim of this study was to test the feasibility of OCT in a broad range of raptor species and because information on variation of the physiological morphology and thickness of retinal layers between various fundus localisation in individual birds or between various bird species did not exist at all, this study was designed as an indicative, orientating study and not to establish reference values in a statistical study, although a simple statistical analysis of the data was performed.

5.1.1 General considerations

5.1.1.1 Materials and methods

5.1.1.1.1 OCT and other tomographic techniques

Examination method

Compared to ultrasonography, OCT has several major advantages. OCT is performed without contacting the corneal surface and without the need of using a medium placed between the probe and the eye surface, which is generally used in bird ultrasonographic examination. In ultrasonography the transducer has to be placed on the surface of the tissue. In the case of the examination of the eye, there exits three modalities of examination: corneal contact, where a gel is used between the transducer and the corneal surface; trans-palpebral, or by using a standoff distance or separator

(GONZALEZ et al. 2001, WILLIAMS et al. 1995). In avian ophthalmology, the method of choice is the corneal contact method. In general, a local anaesthetic for the corneal surface has to be used before the gel is applied and the probe is brought into contact (POULSEN NAUTRUP et al. 1998 a). This method has been successfully applied already in avian ophthalmology, especially in raptors and using 3D- and 4D techniques (STROBEL 2010, DOROBEK 2013-b-c, LIEPERT 2013-a-b). In addition, the standoff distance or separator method has been demonstrated to be useful in avian ophthalmology (HUFEN & KORBEL, 2009, KORBEL et al. 2009). OCT examination does not need any local anaesthetic.

Advantages of both OCT and ultrasound are that, there is no need of chemical immobilisation of the patient compared with Computed Tomography (CT) and Magnetic Resonance Imaging (MRI) methods. In the case of CT and MRI, a close anaesthesia monitoring especially necessary for avian patients constitutes a problem because of a need to stay outside of the radiation area of CT or outside of the room for MRI. Recently CT systems based on fast-scanning multi-detectors have been developed which might allow performing a CT without the need of chemical immobilisation of the patient (GARLAND et al. 2002, PAULUS et al. 2000). Nevertheless, in case of OCT of some bird species, we observed an advantage in using light sedation by midazolam leading to a stress reduction for the patient during the OCT examination and thus providing better imaging quality. To our experience, sedation is not obligatory.

Resolution

A major advantage of OCT over other tomographic systems is a highly improved optical resolution allowing visualization of the retinal sublaminae which cannot be obtained in vivo with other methods. Thus, OCT is superior to all the tomographic techniques up to date. The OCT device from Heidelberg Engineering used in this study possessed an axial resolution of 3.9 µm, and a transversal resolution of 14 mm A-scans resulting in imaging of the retinal sublaminae in almost histological quality. In ultrasonography, the axial resolution varies depending on the probes and software used but may be as high as 0.1 – 1.5 mm (BYRNE & GREEN 2002, MANTONAVI BOTTÓS et al. 2012, POULSEN NAUTRUP et al. 1998). Recently developed micro-CT systems were reported to reach resolutions below 10 µm (PAULUS et al. 2000). However, even with these resolutions, CT and MRI methods are not able to visualize the retinal sublaminae due to the lower tissue sensitivity. It means that OCT is able to distinguish smaller anatomical tissue details than other tomographic techniques due to the physical fundament of the

OCT technique and to the tissue properties (DUONG et al. 2002, GUMPEMBERGER et al. 2006).

Tissue penetration

In this study, the OCT device used provided a scan depth in tissue of 1.9 mm. However, in some of our bird patients the retina could not be visualized by OCT because of opaque structures which did not allow passing of the light beam, and the retina could not be visualized. For instance, retinas belonging to the two adult specimens of *Bubo bubo* selected for the study could not be visualized. One of them showed a bilateral complete formed cataract. The second patient showed bilateral corneal lesion. Other example was a lens luxation in a *Falco tinnunculus*. In these cases ultrasound, CT or MRI could have given more information about the status of the patient vitreous body and retina (DUONG et al. 2002, MANTOVANI BOTTÓS et al. 2012). In the publications of Ruggeri et al. (2012) and Rauscher et al. (2013) they described the visualization of the choroid. In this study the choroid was clearly visualized in almost all cases. Esmaeelpour et al. (2010) used OCT with a different wavelength to improve the tissue depth penetration. Thanks to this improvement they visualized the sclera in some cataract human patients. Rauscher et al. (2013) described the visualization of the two scleral layers in some bird patients. We agree that the visualization of the sclera in some patients was possible. However, cartilage and fibrous scleral layers were not distinguishable. Even with this improvement, OCT tissue depth penetration is clearly lower than in the aforementioned tomographic technics.

5.1.1.1.2 OCT device and visualization of the retina layers

Castro Lima et al. (2011) described the superiority of the Heidelberg Engineering OCT device over other contemporary SD-OCT devices. In this study the UHR-SD OCT from Heidelberg Engineering allowed the visualization of all the retinal layers with a high resolution in most bird species included. However, in all individuals of the species *Pernis apivorus* and *Asio otus*, and in the one specimen examined of the species *Aegolius funereus*, the outer plexiform layer (OPL) could not be distinguished from the inner nuclear layer (INL) and outer nuclear layer (ONL). This occurred in all the retina areas included in this investigation and in all patients of the same species. This phenomenon has been described here for the first time, and we can only speculate about the causes. To our opinion, it was not correlated with eye size but most probably related to physical, backscattering properties of the cells or tissues involved and therefore to the anatomical

architecture of the retina of the species itself. It is known that the anatomical features, for instance the cellular composition of each retinal layer, determine the kind of backscattering of the light beam, and therefore their visualization. The factors that exactly determine the backscattering are still unknown. In general, plexiform layers were described to show a higher backscattering than nuclear layers (RUGGERI et al. 2007). However, in *Pernis apivorus,* in *Asio otus*, and in *Aegolius funereus*, the outer plexiform layer (OPL) could not be distinguished from the neighbouring nuclear layers and thus the outer plexiform layer (OPL) or both nuclear layers involved in this phenomenon in these species seem to have backscattering properties differing from those of the other bird species. We cannot decide if the inner plexiform layer (IPL) was too thin to produce a more intense backscattering than the outer nuclear layer (ONL) and inner nuclear layer (INL). Comparative histology of the retina of these three species is not available to argue for or against this possibility. Since the ONL could be observed in several species, it also did not seem to be related with technical factors of the device used in this case. Ruggeri et al. (2010) hypothesized that the thin layer exterior to the RNFL is related to the GCL. In some data sets they were not able to visualize this hypothesized GCL as a separate layer in the broad-winged hawk, *Buteo platypterus*. The thickness of this layer changed depending on the retinal region examined. However, they only examined one patient, and therefore if happened to be a feature of only one individual or a specific feature cannot be confirmed. Furthermore, they used a modified optical head of an OCT 2 system from Carl Zeiss Meditec. Since they used another OCT device, the results are difficult to compare with those from our study. In contrast with the research of Ruggeri et al (2010), we were able to visualize the GCL in all the B-scans obtained. However, since we measured the RNFL thickness together with the GCL, we cannot judge the possible changes in thickness of this last one.

It is noteworthy that in several cases (18 eyes of a total of 68 eyes) conventional indirect ophthalmoscopical examination using 30, 78 and 90 dioptre lenses resulted in evaluation of the eye as “healthy” while OCT examinations revealed pathological lesions including materials or structures swimming in the posterior chamber such as blood. Although diagnosis of disorders was not aim of this study, this indicated a high potential of OCT for avian ophthalmology. Rauscher et al. (2013) observed similar discrepancies in their investigations, but using direct ophthalmoscopy instead of indirect ophthalmoscopy. Direct ophthalmoscopy allows only to examine a small area of the fundus, while the indirect ophthalmoscopy enables a larger field of view. Therefore, it is more probably to miss retinal alterations using a direct ophthalmoscope (WILLIAMS 1994).

It was expected that the OCT device would be able to visualize the retina of patients with incipient or incomplete cataract, or with mild bleeding located both in the anterior or posterior chamber. In this study, the visualization of the retina in cataract patients was unsuccessful. Similarly, the retina could not be assessed in patients with hyphema, a bleeding in the anterior chamber, which was severe in all cases included in this investigation, and therefore hindering the light beam to pass through the pupil up to the retina.

Cases with a mild bleeding or fibrin in the posterior chamber were satisfactory imaged. Retinal imaging in cases with severe bleeding was unsuccessful. The blood or fibrin swimming into the posterior chamber created interferences in the light beam, resulting in a lower quality of the picture of the retina located immediately below the blood or fibrin deposit (Figure 49).

5.1.1.1.3 Retinal layers measurement procedure

Several retinal diseases produce changes in thickness of different retinal layers. For example, in glaucomatous eyes and myopia cases in human medicine, a thinning in RNFL has been described with OCT (MEDEIROS et al. 2005, RAUSCHER et al. 2009). Progressive retinal atrophy (PRA) in dogs and cats produces alterations in ONL and photoreceptor's layers which leads to thickness changes in the affected layers (PARSHALL et al. 1991, RAB et al. 2005). The study of the thickness changes in the normal retina of the avian eye can provide the normal appearance of the different layers. This is an invaluable tool in avian ophthalmology to perform an adequate diagnose of retinal diseases in vivo.

The decision to measure the TRT in the raptor eye was made in order to observe the presence of changes in its thickness depending on the retinal localization within an individual, between patients of the same species and patients of different raptors species. The software EYEX® from Heidelberg Engineering possesses a tool, where the measurement of this thickness is automatically made. However, this automatic definition of the TRT has to be corrected manually by the clinician, since the program in some cases located the measurement segmentation in the wrong layer or in structures swimming in the vitreous. The software allowed a comfortable correction of these measurement segmentation once the B-scan has been taken, and without the need to make the correction while the OCT examination procedure was taking place.

Different reasons were determinant in the decision of measuring the RNFL+GCL thicknesses. In studies such as that from Ruggeri et al. (2010) in raptors, they described several thickness changes in the visualized OCT layers, related with some retinal layers,

like The RNFL or GCL, We observed, that the variations in TRT in the species under study is due to the variations of the RNFL+GCL thickness. This fact is confirmed, since is the only group of layers showing a thickness variation. Secondly, the examination of the RNFL has been thoroughly made in human and animal medicine because its importance in the evaluation of retinal disease like glaucoma (MEDEIROS et al. 2005, RAUSCHER et al. 2009).

It has been shown for retinal diseases in human beings that lesions located in the OR and the RPE-ELM layer have special importance regarding the significance and prognosis. In macular degeneration, tearing of the RPE has been described to be connected with a poor prognosis (AUGUSTIN 2012; YÜKSELL et al. 2013). In addition, it has been demonstrated that the IS/OS and RPE integrity was closely connected with the visual acuity. For example, in cases of acute inflammation of the RPE, the observation of the visual acuity progression in combination with the OCT examination gave information to assess the prognosis of RPE disease (AHLERS et al. 2010; KIM et al. 2011). The defects in the IS/OS visualized with OCT were shown to represent a valuable prognosis indicator after macular hole surgery, which was especially important in the field of human ophthalmology (OH et al. 2010).
Pathologies located in the outer retina have been shown to indicate alteration related with the photoreceptors. The alterations located in the RPE-ELM group of layers have special significance related with the prognosis of the visual capacity. The same lesion has a better prognosis when the integrity of the retinal pigment epithelium, the inner/outer segment junction (IS/OS) and the external limiting membrane is complete. The prognosis is even better when the lesion is adjacent to these layers and is located internal to the external limiting membrane and do not interrupt the aforementioned layers. For example, it is used in cases of macular hole, after macular hole surgery, or in presence of drusenoid retinal alterations and macular degeneration (OH et al. 2010, YI et al. 2009).
The future establishment of specific measurements for these layers will facilitate the judgement of the patient retinal condition (Table 20).

5.1.1.1.4 OCT examination conditions and tolerance

In general, birds are patients with a low stress and manipulation tolerance. In our investigation, a good acceptance of the examination procedure by the patient was a priority. Therefore, the status of each patient was considered and in some individual cases sedation or anaesthesia was used to minimize a potential stress during the OCT examination.

In bird species expected to show stress related reactions we decided to use sedation with midazolam (2 mg/kg BW, intramuscularly or intranasally) before the OCT examination started. Midazolam was already shown to induce good sedation in several bird species (AJADI et al. 2009; MANS et al. 2012; PAUL-MURPHY & FIALKOWSKI 2001; VESAL & ESKANDRANI 2006). In this investigation, use of midazolam proved to be beneficial. The patients under midazolam sedation required shorter OCT examination times and a larger amount of good quality images was obtained. The eyes of almost all the patients undergoing the OCT procedure with midazolam sedation were successfully depicted. Therefore, we conclude that the application of midazolam was very useful in order to reduce the stress of the patient in case of the non-painful and short OCT examination procedure. One third (33 %) of the patients went through the OCT examination under sedation with midazolam. In a high percentage of these patients, 89 %, the retina was successfully visualized.

General anaesthesia obviously led to the highest stress reduction during OCT procedure. However, because of higher risks of side effects especially in trauma patients, general anaesthesia was only performed in cases where other indications besides eye examination existed. Most time, these were patients having a high probability of being euthanized due to humanitarian reasons. Slightly more than half of the patients examined under general anaesthesia were successfully imaged. Failures were mostly caused by pathological finding hindering any appropriate “physiological” B-scan to be used in this study. About 25 % of the patients were examined by OCT under general inhalation anaesthesia, and the eyes of 57 % of those birds fulfilled the criteria to be included in this investigation. It is important to note that general anaesthesia was performed in patients with a high probability to be euthanized due to severe trauma and humanitarian reasons. Since B-scans of physiological retinal conditions were used to measure the thickness of the retinal layers, in the majority of these cases the OCT analyses were not included because of pathological findings.

The decision to use anaesthesia or sedation was always based on the results of the clinical examination of the individual patients and was made by the responsible clinician About 42 % of the patients were examined without any anaesthesia or sedation. Among them, a 74 % were successfully visualized (data not shown). Nevertheless, the amount of images obtained in each specimen is low, and in our opinion, the examination time was remarkable longer.

Regarding this fact, we generally recommend the use of sedatives, for example midazolam, to carry out the OCT examination in raptors. The decision, however, must also include aspects of the individual patients. Rauscher et al. (2013) performed the OCT examination of raptors entirely under general anaesthesia, and on the contrary, Ruggeri et al. (2010) did with the patients totally awake and alert. Based on our experiences with a limited number of patients, differing OCT examination tolerances among the species included in this study were observed. Individuals of the species *Buteo buteo, Pernis apivorus, Accipiter nisus, Strix aluco*, and *Asio otus* tolerated the examination procedure better showing less defence movements like head shaking in comparison with individuals of the species *Falco tinnunculus, Falco peregrinus* or *Accipiter gentilis*. Pictures of good quality were more easily and faster obtained from birds of the first-mentioned species. We assume that in the case of the species *Falco tinnunculus* this was due to the small size of the eye, and in the species *Falco peregrinus* and *Accipiter gentilis* due to the nervousness shown by the patient resulting in frequent eye movements. Therefore, in these last two species, in several cases the examination had to be interrupted.

5.2 Intraspecific variations

When the results of thickness measurements of the retina were compared among birds of the same species, two main features were evident. First, there were only minimal differences among individuals with regard to a defined fundus location. These differences were not considered as being relevant. However, a statistical analysis including a higher number of birds would be necessary to confirm this statement.
Second, there were major thickness differences among fundus regions in many retinal layers which were detected in all individuals of the same species in the same way. The thickness of the total retina was maximal at the region cranial to the pecten and decreased to the peripheral regions. This pattern was observed in all individuals of each species included. When measurements of a certain fundus region of the retina were analysed, no significant intra-species variation was detected.

Interestingly, the thickness variation of the total retina could mainly be attributed to thickness changes of the retinal nerve fiber layer and the ganglion cell layer (RNFL+GCL). The ganglion cell layer, however, because of its very low thickness, contributed to the total RNFL+GCL thickness only to very small extent, and, therefore, the changes in total retinal thickness could primarily be attributed to the retinal nerve fiber layer. The thickness of this layer strongly varied depending on the retinal location

leading to the TRT changes. It increased approximating the ONH and decreased in the eccentric retina.

In all the species investigated, the OR and RPE-ELM group of layers maintained their size in a very constant way along the whole retina. They thus did not affect TRT and did not contribute to the TRT variation. It is important to remember that the most eccentric retina is very close to the Ora serrata. Near the Ora serrata there is a decrease in the thickness of all retinal layers. This justified why some result of the eccentric retina were slightly lower than in other eccentric areas. Once the OCT-scan was taken in an eccentric retinal region, and no reference landmarks were available, it was difficult to know how close to the Ora serrata the B-scan was taken. Thus, some of the OCT sections were performed within the selected eccentric area, but closer to the Ora serrata than other sections, which produces this minor thickness discrepancy.

As a consequence, it is necessary to have information on the exact localisation of the OCT section in the fundus in order to identify pathological changes or to follow up changes in the retina over time. In mammalian eyes with their vascular retinal structures, the pattern of retinal blood vessels can be used to identify the retinal location and recover it in further retinal examinations to visualize the evolution of retinal pathologies. The retina in birds, however, is an avascular structure, which was confirmed using OCT by Ruggeri et al. (2010) and in this investigation. Consequently, other structures to be used as landmarks are needed. The pecten or the foveae are useful only in cases, when the area under investigation includes these structures. The eye equator, being characterized by its position between the swallow and deep fovea in the area superior to the pecten, and which is the level where the choroidal blood vessels parting from the optical nerve head region are diverging, can be used as a subjective orientation within the fundus in some nocturnal bird species. Otherwise, until now, no landmark was available. Based on the results of our study, we conclude that the RNFL thickness might be used as a landmark to localise and define points of interest at the retina.

Ruggeri et al. (2010) already successfully used the thickness of the RNFL to aggregate OCT pictures of three different central retinal regions (the deep and the shallow fovea regions and the region of the optical nerve head) to deduce a RNFL thickness map. However, this map was based on retinal OCT measurements of a single individual of a single species, a broad-winged hawk (*Buteo platypterus*), only, and included the three selected regions only. In our investigation presented here, we could demonstrate that in all the bird species and individuals included, the retinal nerve fiber layer (RNFL) was continuously changing its thickness from a maximum close to the optical nerve head to the very peripheral retinal areas. In contrast, the other retinal layers stayed very constant

in thickness and morphology over all retinal areas investigated making them unsuitable as landmarks.

We propose to produce a RNFL thickness map, OCT sections from the whole range of all retina areas should be made for each avian species. This map has to be built with single series of OCT captures, and the individual OCT pictures have to be composed to a total retinal map using the corresponding software. In our case, the HEYEX® software provided only the possibility to create a fundus map combining several fundus captures. However, this function in combination with the OCT function (the B-scan mode) was not available.

In comparison with the retinal nerve fiber layer, the thicknesses obtained for the outer retina (OR) and for the layers between the retinal pigment epithelium and the external limiting membrane (RPE-ELM) remained rather homogeneous in all the fundus regions included. Due to this homogeneity, standard thicknesses for these two groups of retinal layers can be established independent of the retinal area, and the values obtained in this study can be taken as a preliminary species-specific guideline. However, because of low bird numbers within each species, further investigations are necessary to establish species-specific reference values. Nevertheless, for individual patients, because of the high consistency of the thickness of these aforementioned OR and RPE-ELM groups of layers, circumscribed thickness discrepancies might be considered as a pathologic finding, independent of their localisation.

5.3 Interspecific variations

Regarding the thicknesses of the layers measured in the equator area, variations were observed between the species included in this study. The species could be ordered according the thickness of the different layers from the highest to the lowest absolute values as follows:

- **Total retinal thickness (TRT):**
  Falco tinnunculus, Buteo buteo, Pernis apivorus, Falco peregrinus, Accipiter nisus, Strix aluco and *Asio otus.*

- **Retinal nerve fiber layer+ganglion cell layer (RNFL+GCL):**
  Accipiter nisus, Buteo buteo, Falco tinnunculus, Falco peregrinus, Pernis apivorus Strix aluco and *Asio otus.*

- **Outer retina (OR):**
  Strix aluco, Falco tinnunculus, Buteo buteo, Falco peregrinus and *Accipiter nisus,* (No values for the species *Asio otus* and *Pernis apivorus*)

- **Retinal pigment epithelium to external limiting membrane (RPE-ELM):**
  Pernis apivorus, Strix aluco, Asio otus, Falco tinnunculus, Buteo buteo, Falco peregrinus and *Accipiter nisus.*

Differences among orders were also observed. The two nocturnal raptor species belonging to the Strigiformes had remarkably lower total retinal thicknesses than the diurnal species from the orders Accipitriformes and Falconiformes (Table 9). The differences were mainly caused by the RNFL+GCL. In the Strigiformes the thickness of these two layers was remarkable lower compared to the other two orders while the OR and RPE-ELM layers were at least as thick as in the Falconiformes and Accipitriformes. Individuals of the species *Strix aluco* possessed the highest OR thickness of all the species under study. Since the photoreceptors are located in this layer, it might be concluded that there are structural differences between nocturnal and diurnal raptors. Unfortunately, in the other species of the Strigiformes studied here, measurements of the OR could not be obtained due to the inability to distinguish the internal border of this group of layers, as described in the section “results”. Therefore, we cannot conclude yet whether this feature characterizes nocturnal birds.

An interesting thickness pattern was observed in the species *Pernis apivorus*. Although a member of the Accipitriformes order, its retinal layers thickness patterns seemed to be similar to those observed in the two nocturnal species. *Pernis apivorus* showed lower RNFL+GCL measures and a thicker RPE-ELM than the other diurnal species, and the OR thickness could not be determined, all these being features found in the Strigiformes order. *Pernis apivorus* had the lowest total retinal thickness of all the species of the orders Accipitriformes and Falconiformes included in this investigation. As mentioned before, the lowest total retina thicknesses were observed in the Strigiformes.

Interestingly, the thickness of the retinal layers did not depend on the size of the raptor or the eye size. The highest TRT was observed in *Falco tinnunculus* which was the smallest species possessing the smallest eye size among the species under study. This characteristic was also confirmed by histology and could thus not be attributed to artefacts caused by the OCT examination of birds of this species.

5.4 Image quality and artefacts

Although the quality of the images of avian retina was generally very high, it varied among species and among retinal areas. We hypothesize that this variation is at least partly due to the fact that the OCT device and its software were originally developed for the visualization of the human eye, and consequently some problems arose because of differing bird eye sizes and retinal curves. The OCT device used in this study allowed to make settings for several eye sizes, but the range is of course always adapted to parameters of a human eye which are bigger than those of the birds included here. We observed that the quality of the image also depended on the pupillary diameter as well. Small diameters did not allow the light beam to reach periphery retinal areas as easily as big pupil diameters, and this additionally impaired the picture quality of small eyes. These factors were especially evident in *Falco tinnunculus*, which was the species under study with the smallest eye size and pupillary diameter (Fig. 53). We assume that the difficulties were mainly caused by the higher retinal concavity impairing the picture resolution, but still allowing the retinal layers to be distinguished. In our opinion, a correction and adaptation of the software might solve this problem.
Sometimes, pathological structures such as blood or fibrin swimming in the posterior chamber created interference with the light beam causing the so called “noise”, and therefore the retina located immediately below the blood or fibrin deposit was visualized with lower quality (Fig. 54). Patients showing these kind of alterations were only included in the study when the retina itself was not affected by any pathologies. We confirmed the

ability of the UHR-SD-OCT device from Heidelberg Engineering® in these cases, where the examination of the retinal integrity was difficult to perform.

5.5 Validation of the OCT examination with histology

Since the histology is the gold standard for the identification of retinal layers and diagnosis of retinal pathologies, the results obtained with the OCT were validated using this technique as the reference method in order to establish the OCT technique as an adequate diagnostic method in avian ophthalmology.

5.5.1 Evaluation of the histological processing of the samples

From 40 eyes of 20 animals that were carefully enucleated, 30 were included in the histological processing. 12 eyes were successfully cut into histological sections. Unfortunately, only 6 eyes could be considered with enough quality to perform the histological validation of the OCT results. 3 of these eyes belonged to the species *Buteo buteo*, and 3 to *Asio otus*.

Processing of eyes for histology is generally regarded as difficult and prone to many artefacts affecting the quality of the histological sections (ABBOTT et al. 2009), especially for bird eyes having bony scleral rings, existing problems are largely unsolved so far as we experienced in this investigation as well.

The folding of the tissues during the cutting process was a problem during the whole histological processing. In order to minimize occurrence of this artefact it was decided to cut paraffin blocks in sections of 10 µm instead of, 3 and 4 µm because the retinal layers should remain as stable and intact as possible, and the differentiation of single cells was not among the aims of this study. We confirmed that 10 µm sections were more adequate to maintain the normal architecture of the retinal layers, which was important for the subsequent measurement of the distances among layers.

One of the most important problems in this investigation was the difficulty to exactly relocate the exact place in the retina from which the OCT image had been obtained. Because landmarks to be used for this purpose are lacking in the avian eye, comparison was based on results obtained between OCT pictures and histological sections originating at least from the same retinal areas. However, since the total retinal thickness

varied depending on the localisation in the eye, we cannot exclude discrepancies in thicknesses related to minor deviations of the location. This was especially true for the very eccentric retinal areas and the retinal area cranial to the pecten, where small differences in location resulted in rather distinct thickness differences. Only minor discrepancies in the location point of OCT picture and the histological slide would therefore lead to marked thickness differences rendering any validation impossible. Consequently, validation of OCT using histology was based on the equatorial areas showing low retinal thickness variation over distance.

The total observed shrinkage of the retina was about 20 %, which was of the same magnitude as described for other tissues. Up to 25 % shrinkage had to be expected (ROMEIS 1989).

Histology enabled to recognize all the retinal layers. In some cases, the internal limiting membrane was not present, probably due to artefacts during the processing.

In the two species that underwent a successfully histological processing *(Buteo buteo and Asio otus*), all the retinal groups of layers were recognized and measured. This fact is remarkably important in the case of the species *Asio otus*. On the contrary with histology, no OR could be measured with OCT in this species.

5.6 Conclusions

OCT is an optical method for imaging retinal structures and the diagnosis of eye diseases which is performed in a non-contact, in vivo, and non-invasive way, with a resolution at almost cellular levels. Recent developments in the technique led to a fast, 3D and high resolution imaging of different eye structures even allowing visualization of blood perfusion and blood flow in ocular tissues (MOAYED et al. 2012).

During this study, we confirmed that OCT represents a very useful tool in ophthalmological investigation of raptors. It allowed the examination of the different layers of the retina in a quality close to histological section which had been possible before only after euthanizing the animal followed by histology. We agree with Ruggeri et al. (2007) that OCT will therefore essentially improve our understanding of pathogenesis of retinal diseases, and tracking of onset, progression and therapy. Since it can be repeatedly performed in the same individuals during longitudinal studies, OCT technology will, in ophthalmological research, strongly reduce the number of animals needed to obtain statistically valid results.

We were able to visualize the physiologic retinal architecture in several species of raptors, confirming that OCT can be used in a broad range of species.
Thicknesses of the groups of retinal layers under study varied depending on the location within the retina in patients of the same species. On the contrary, thicknesses of the same location remained almost the same between patients of the same species.
Thicknesses of the same retinal location varied remarkably between individuals of different species and orders.
Constant to all species was the variation in thickness of TRT and RNFL. These two group of layers showed the highest thickness values in the area near the pecten, and the lowest in the eccentric retinal areas. A common feature to all species under study was that the thicknesses of OR and RPE-ELM groups of layers remained constant.

We validated this technique with histology. The results of this study will serve as a basis for the establishing of reference values for retinal thicknesses and physiological retina appearance in healthy raptor eyes and for future identification of pathological processes without the need to euthanize the patient.

We were able to show that this non-invasive and non-contact examination technique can be applied in most raptors without general anaesthesia. No contact media needed to be employed, such as ultrasonography gel or contact lenses in ultrasonography. OCT was thus shown to represent a well-tolerated technique with low stress, which is a determining factor especially in avian medicine due to a low stress tolerance of many avian species (VAL VELTHOVEN et al. 2007).
As shown for rodents already (SRINVASAN et al. 2006), quantitative thickness measurements of several layers of the intact retina of raptors could be performed, even in very peripheral areas of the retina, and processing artefacts that appear during histology could be avoided using OCT.

The SD-OCT device used in this investigation in a commercially available version, the Spectralis® HRA+OCT Plus (Heidelberg Engineering, Heidelberg, Germany) provided high investigation speed and picture quality, 3D retinal imaging and eye tracking through the combination with the cSLO, adequate reference for the B-scan building, superior to SD-OCT devices (VAL VELTHOVEN et al. 2007). Nevertheless, for some birds, even a faster scanning speed, would be desirable.

We observed that the quality of the OCT retinal image was lower in patients with smaller eyes, but still successful in *Falco tinnunculus*, the smallest bird species included here.

There are also investigations where pathological findings in smaller avian species were observed with OCT such as *Turdus merula* and *Apus apus*, They only performed histological processing of one bird, a specimen of the species *Buteo buteo* (RAUSCHER et al. 2013). OCT technology has been successfully applied in animals with small eye size like rodents, although image quality and depth resolution were not sufficient to resolve all subretinal layers (RUGGERI et al. 2007, SRINVASAN et al. 2006). Future developments like additional optical lenses might solve this problem.

To our opinion, OCT technology certainly cannot completely replace histology because of physical or chemical properties of the tissues investigated. Visualization of layers in OCT depends on differing backscattering properties of the structures involved, which might deviate from differing dying properties visualized in histology. The Bruch's membrane, for example, can only be visualized using histology but not by OCT, at least with the light sources used at present (DREXLER & FUJIMOTO 2008). Both techniques might therefore be used complementarily. In conclusion, in order to distinguish single retinal cells, histology is necessary and in any case superior to OCT, since with OCT up to date only retinal layers with different backscattering properties can be visualized.

5.7 OCT future and expectations

This study corroborates the usefulness of OCT in avian ophthalmology, especially in the examination of the raptor eye. OCT not only provides uncountable new possibilities to perform in vivo investigations, but will also improve the quality of the clinical examination of the avian patient providing a better assessment of prognosis and treatment.
OCT is a technique still not commonly used in avian ophthalmology, and therefore there are still a large research field to fulfil. The establishment of reference values of the physiological retina and retinal sublaminae represents a first step to assure a proper evaluation of retinal pathologies in the avian eye. In the investigation presented here, we established a method to collect thickness measures of the retinal sublaminae and described the extent of variation to be expected among retinal areas and different raptor species. However, these first measurements have to be confirmed with a higher number of individuals per species to establish standard reference values for the different retinal layers.

In this investigation, we focussed on the retina located in the posterior eye chamber. Nevertheless, Lesions affecting the anterior chamber of the eye also occur in avian patients, even if they are not as common as those found in the posterior chamber of the

avian eye (KORBEL et al. 2001). Investigations using OCT to establish the normal and abnormal appearance of structures belonging to the anterior chamber should therefore also be performed.

There is no literature about the pathologies of the vitreous and macular vitreous detachment in the raptor eye. We observed in several patients a clear detachment of the vitreous without any traction and detachment of the retinal layers (Fig 28, 29, 31 and 31). If this traction modifies the thickness of the different retinal layers is still unknown.

There is also a need to compare OCT with other tomographic techniques such as ultrasound for usefulness in avian ophthalmology. The same patient should be investigated in parallel with these techniques in order to visualize the same physiological or pathological findings. Based on this comparison the clinician will be able to decide which method is more adequate in each future single case.

6 SUMMARY

Optical coherence tomography (OCT) is a new technique which has recently been established for routine human ophthalmology, focusing on its potential to visualize retinal structures in vivo and non-invasive, without eye contact, in a quality close to histological sections. This technique therefore permits to detect ocular disorders at almost (interpolated) histological resolution and, to be pointed out, longitudinal investigations on the course of disease or therapy. In veterinary medicine, especially in avian ophthalmology, until now, OCT has been applied only very scarcely.

The main purpose of the present study was to evaluate OCT technique as an adequate imaging method at the avian retina. The study focused on the visualization of the physiological retinal architecture in raptors. Secondly, the application of OCT was evaluated in a broad range of raptor species in order to get first indications of interspecific variations in retinal structure revealed by OCT. Finally, the results of OCT eye examination were validated using histology.

In order to test the potential of OCT to visualize the physiological retinal architecture in raptors, 56 diurnal and nocturnal wild raptors belonging to 3 orders and 12 species, underwent OCT examination. All these birds were patients of the Clinic for Birds, Reptiles, Amphibians and Ornamental Fish of the University Ludwig Maximilian (Munich) and were brought to the clinic mainly with a history of trauma. The OCT examination was performed on eyes and retinal regions considered healthy based on a previous ophthalmoscopical examination. The eyes of the patients euthanized due to humanitarian reasons were destined to histology in order to validate the technique.

A Spectralis® HRA+OCT Plus (Heidelberg Engineering, Heidelberg, Germany) was used to image and evaluate the retina of the patients. The processing of the pictures was made with the software Spectralis Software Heidelberg Eye Explorer® (HEYEX) version 5.4 (October 2011, Heidelberg Engineering, Heidelberg, Germany). Depending on the expected stress tolerance, the OCT examination was performed with the patient awake, under sedation with Midazolam (2 mg/kg BW) or under general anaesthesia with isoflurane inhalation anaesthesia.

The areas of the fundus considered were the superior portion of the Pecten oculi including a part of the optical nerve head (ONH), the most sagittal area of the retinal equator, the most sagittal area of the superiorly visualized fundus, the most temporal

equatorial fundus area and the most nasal equatorial fundus area. Thickness measurements of retinal layers in the different retinal areas were performed in order to record potential thickness variations. Measurements included first, the total retinal thickness, from the retinal pigment epithelium up to the internal limiting membrane; second, the retinal nerve fiber layer and ganglion cell layer; third, the outer retina, which included the layers between the retinal pigment epithelium up to the innermost border of the outer nuclear layer; and fourth, the layers between the retinal pigment epithelium and the external limiting membrane.
The histological processing of the eyes followed a conventional method to obtain histological sections of the retina in birds, using the Davison's solution as fixation solution, and haematoxylin & eosin staining.

The physiological architecture of the raptor retina imaged could be visualized with reproduceable results, and at a resolution not available to date. Regarding the intraspecific variations, the total retinal thickness (TRT) and the retinal nerve fiber layer and anglion cell layer (RNFL+GCL) were maximal at the region cranial to the pecten and decreased to the peripheral regions in all the species. On the contrary, the outer retina (OR) and the layers between the retinal pigment epithelium and external limiting membrane (RPE-ELM) maintained their size along the whole retina. Between species, the thickness of the different retinal measurements varied. The TRT was higher in diurnal species than in nocturnal species. By contrast, OR and RPE-ELM showed higher measurements in the nocturnal species than in the diurnal species.
In the species *Pernis apivorus*, *Asio otus*, and *Aegolius funereus*, the outer nuclear layer (ONL) could not be distinguished.

In summary, the optical coherence examination of the raptor retina may be considered as an invaluable tool in the avian ophthalmology. This study provides a basis to perform a more accurate interpretation of pathological findings observed with OCT in the retina of birds of prey.

7 ZUSAMMENFASSUNG

Die Optische Kohärenztomografie (OCT) ist eine neue Technik, die vor kurzem in der Humanophthalmologie etabliert wurde und sich durch ihr Potential auszeichnet, Retinastrukturen in vivo und nicht-invasiv (ohne Augenkontakt) in einer Qualität vergleichbar mit der von Histologieschnitten darzustellen. Diese Technik ermöglicht es, minimale pathologische Veränderungen bei fast histologischer Auflösung darzustellen, sowie longitudinale Untersuchungen im Verlauf der Erkrankung oder Therapie durchzuführen. In der Tiermedizin, vor allem in der Vogel-Ophthalmologie, wurde bis jetzt OCT nur sehr selten angewendet.

Das Hauptziel dieser Studie war es daher, die Eignung der OCT-Technik als eine Darstellungsmethode in der Vogel-Ophthalmologie zu evaluieren. Um dieses Ziel zu erreichen, fokussierte diese Studie auf die Darstellung der physiologischen Retinastrukturen von Greifvögeln. Des Weiteren wurde die Anwendung von OCT bei vielen verschiedenen Greifvogelarten evaluiert, um erste Hinweise auf Unterschiede zwischen unterschiedlichen Arten und auf innerartliche Unterschiede der Retinastruktur zu gewinnen. Die Ergebnisse der OCT-Augenuntersuchungen wurden mittels histologischer Untersuchungen validiert.

Um die Möglichkeiten der Darstellung der physiologischen Retinastrukturen von Greifvögeln mittels OCT zu überprüfen, wurden 56 wilde Tag- und Nachtgreifvögel drei verschiedener Familien und 12 verschiedener Arten untersucht. Alle einbezogenen Vögel waren Patienten der Klinik für Vögel, Reptilien, Amphibien und Zierfische der Ludwig-Maximilians-Universität München und wurden meist mit Verdacht auf Trauma vorgestellt. Die OCT-Untersuchungen wurden an Augen und Retinaregionen durchgeführt, welche nach einer vorherigen ophthalmologischen Untersuchung als gesund erachtet wurden. Bei Vögeln, die aufgrund ethischer und Tierschutzgründen euthanasiert werden mussten, wurden die Augen zur Validierung der OCT-Technik histologisch untersucht.

Zur Darstellung der Retina wurde in der vorliegenden Untersuchung das Modell Spectralis® HRA+OCT Plus (Heidelberg Engineering, Heidelberg, Germany) verwendet. Die Bearbeitung der Fotos wurde mit der Spectralis Software Heidelberg Eye Explorer® (HEYEX) version 5.4 (October 2011, Heidelberg Engineering, Heidelberg, Germany) durchgeführt. Abhängig von der zu erwartenden Stresstoleranz des Patienten erfolgte

die OCT Untersuchung im wachen Zustand oder es wurde vor Beginn der Untersuchung eine Sedation mit Midazolam (2 mg/kg KM) oder eine Inhalationsnarkose durchgeführt.

Bei der Untersuchung des Fundus wurden fünf unterschiedliche Areale einbezogen, und zwar eine Region unmittelbar superior des Pecten oculi einschließlich eines Teils des Ansatzes des Sehnervenkopfes, die sagitalste Region des retinalen Äquators und des Fundus superior sowie die am weitesten temporal und nasal gelegenen Bereiche des Äquators. Dickemessungen der Retinaschichten in unterschiedlichen Retinaabschnitten wurden durchgeführt, um potentielle Dickeunterschiede darzustellen. Die Messungen beinhalteten erstens die gesamte Retina-Dicke (TRT) von dem retinalen Pigmentepithel bis zur Membrana limitans interna, zweitens die Nervenfaserschicht und Ganglienzellschicht (RNFL+GCL), drittens die äußere Retina (OR), mit den Schichten zwischen dem retinalen Pigmentepithel und der innersten Grenze der äußeren Körnerschicht, und viertens die Schichten zwischen dem retinalen Pigmentepithel und der äußeren Grenzmembran (RPE-ELM).

Die histologischen Schnitte der Augen wurden nach einem Standardprotokoll mittels Davison's Lösung als Fixation und Haematoxylin & Eosin Färbung angefertigt.

Mittels OCT-Technik konnte die physiologische Struktur der Greifvogelretina mit einer Auflösung, die nicht von anderen tomographischen Techniken erreicht wird, reproduzierbar dargestellt werden. Die TRT und die RNFL+GCL war bei allen Spezies in der Region superior des Pectens maximal und verminderte sich zu den peripheren Regionen hin. Im Gegensatz dazu blieben die OR und die RPE-ELM von gleicher Dicke. Zwischen den einzelnen Spezies variierten die gemessenen Werte. Die gesamte Retinadicke (TRT) war bei Taggreifvögeln höher als bei Nachtgreifvögeln. Die Werte für OR und RPE-ELM hingegen waren bei Nachtgreifvögeln höer als bei Taggreifvögeln. Bei *Pernis apivorus*, *Asio otus* und *Aegolius funereus* konnte die äußere Körnerschicht nicht differenziert werden.

Die OCT-Untersuchung der Greifvogel-Retina kann zusammenfassend als eine wertvolle Methode in der Vogelophthalmologie beurteilt werden. Diese Studie bietet die Grundlage für die Interpretation von OCT-Ergebnissen hinsichtlich pathologischer Veränderungen der Retina von Greifvögeln, sowie die Basis für eine in vivo Kontrolle von Krankheitsverläufen der Retina und die Beurteilung von Behandlungserfolgen über die Zeit.

8 RESUMEN

La tomografía de coherencia óptica (OCT) es una técnica recientemente establecida en oftalmología humana de rutina, centrándose en la visualización de las estructuras de la retina en vivo, de forma no invasiva, sin contacto con el paciente y en una calidad cercana a la histología. Por ello esta técnica permite detectar desordenes oculares mínimos y de forma longitudinal, con lo que se puede seguir el curso de la enfermedad y la evolución de la terapia. En medicina veterinaria, especialmente en oftalmología aviar, esta técnica se ha aplicado de forma escasa.

El objetivo principal del presente estudio fue evaluar la técnica de la OCT como método adecuado en oftalmología aviar. Para alcanzar este propósito el estudio se centró en la visualización de la arquitectura fisiológica de la retina en rapaces. Para ello se evaluó la aplicación de la OCT en un gran rango de especies de rapaces para obtener los primeros indicios de variaciones intraespecíficas en la estructura de la retina reveladas con la OCT. Para finalizar, los resultados se validarían utilizando histología.

Como materiales y métodos para evaluar el potencial de la OCT se examinaron 56 aves rapaces, diurnas y nocturnas, de 3 órdenes y 12 especies. Los pacientes fueron en todos los casos de la Clínica de Aves, Reptiles, Anfibios y Peces Ornamentales de la Universidad Ludwig-Maximilian de Munich, prácticamente todos ellos a causa de un traumatismo. La OCT se llevó a cabo en los ojos y en las zonas de la retina consideradas sanas tras un previo examen oftalmoscópico. Los ojos de las aves que debieron eutanasiarse por razones de bienestar animal se destinaron a la validación de la técnica por medio de histología.

El aparato utilizado para visualizar la retina de los pacientes fue el Spectralis® HRA+OCT Plus (Heidelberg Engineering, Heidelberg, Alemania) y el procesamiento de las imágenes a través del software Spectralis Software Heidelberg Eye Explorer® (HEYEX) versión 5.4 (Octubre 2011, Heidelberg Engineering, Heidelberg, Alemania). Dependiendo de la tolerancia demostrada por el paciente, la OCT se realizó con el paciente despierto, en sedación con midazolam (2 mg/Kg. MC) o bajo anestesia inhalatoria general.

Las áreas del fondo de ojo consideradas en el estudio fueron la porción superior del Pecten oculi, incluyendo una parte de la cabeza del nervio óptico, las zonas más sagitales del ecuador y de la zona más superior visualizada y las zonas ecuatoriales más temporales y nasales visualizadas. En cada sección de cada área se llevaron a

cabo medidas del grosor de las capas de la retina tales como el grosor de la retina total (TRT), la capa de fibras nerviosas de la retina junto con la capa de células ganglionares (RNFL+GCL), la retina externa (OR), y por último las capas comprendidas entre el epitelio pigmentario retiniano y la membrana limitante externa (RPE-ELM).
Posteriormente los ojos a disposición de los pacientes eutanasiados se sometieron al procesado histológico utilizando como solución fijadora la solución de Davidson, y una tinción convencional de hematoxilina & eosina.
La arquitectura fisiológica de la retina se visualizó de manera fiable con la técnica de la OCT, alcanzando resoluciones no posibles de alcanzar mediante otras técnicas topográficas. Entre las variaciones intraespecíficas observadas, se obtuvo como resultado que el TRT y el RNFL+GCL alcanzan valores máximos en el área craneal al pecten, y mínimos en las zonas de la retina excéntrica en todas las especies del estudio. Por el contrario, la OR y el RPE-ELM se mantuvieron constantes en grosor a lo largo de toda la retina. Se observaron grandes variaciones interespecíficas, entre los diferentes órdenes, y entre especies diurnas y nocturnas. El TRT es mayor en las especies diurnas que en las nocturnas. En cambio la OR y el RPE-ELM revelaron medidas más grandes en las especies nocturnas que en las diurnas. Una peculiaridad observada fue que en ciertas especies como *Pernis apivorus*, *Asio otus*, y *Aegolius funereus*, no se pudo observar la capa nuclear externa.

Para finalizar, la tomografía ce coherencia óptica en cuanto al examen de la retina de las aves rapaces puede considerarse como una herramienta de incalculable valor en la oftalmología aviar. Este estudio proporciona la base para llevar a cabo una interpretación más exacta y adecuada de los hallazgos patológicos observados con la técnica de OCT en la retina de las aves rapaces.

9 CITATION INDEX

1. ABBOTT, C. J., MCBRIEN, N. A., GRÜNERT, U., & PIANTA, M. J. (2009). Relationship of the Optical Coherence Tomography Signal to Underlying retinal Histology in the Tree Shrew (Tupaia belangeri). *Investigative Ophthalmology & Visual Science 50*(1), 414 – 423.

2. ADLER, D. C., KO, T. H., FUJIMOTO, J. G. (2004). Speckle reduction in optical coherence tomography images by use of a spatially adaptive wavelet filter. *Optics Letters 29*, 2878 - 2880.

3. AHLERS, C., GÖTZINGER, E., PIRCHER, M., GOLBAZ, I., PRAGER, F., SCHÜTZE, C., BAUMANN, B., HITZENBERGER, C. K., SCHMIDT-ERFURTH, U. (2010). Imaging of the Retinal Pigment Epithelium in Age- Related Macular Degeneration Using Polarization- Sensitive Optical Coherence Tomography. *Investigative Ophthalmology & Visual Science 51*(4), 2149 – 2156.

4. AJADI, R. A., KASALI, O. B., MAKINDE A. F., ADELEYE, A. I., OYEWUSI J. A., AKINTUNDE O. G. (2009) Effects of Midazolam on Ketamine-Xylazine Anesthesia in Guinea Fowl (Numida meleagris galeata). *Journal of Avian Medicine and Surgery 23*(3), 199 – 204.

5. AMERI, H., CHADER, G. J., KIM, J. G., SADDA, S. R., RAO, N. A., HUMAYUN, M. S. (2007). The effects of intravitreous bevacizumab on retinal neovascular membrane and normal capillaries in rabbits. *Investigative Ophthalmology & Visual Science 48*, 5708 – 5715.

6. AUGUSTIN, A. J. (2012). Tomography Imaging and Quantitative Assessment for Monitoring Dry Age-related Macular Degeneration. *European Ophthalmic Review* 1 - 8.

7. AZMANIS, P., KOCH, C., FRANKE, M., RAUSCHER, F. G., HÜBEL, J., THIELEBEIN, J., KRAUTWALD-JUNGHANNS, M. E. (2012). Der Einsatz der optischen Kohärenztomographie (OCT) als diagnostisches Verfahren in der Ornitho-ophthalmologie.pp 38 – 42. In *Proceedings 17*. DVG-Tagung über Vogelkrankheiten, München

8. BAI, Y., XU, J., BRAHIMI, F., ZHUO, Y., SARUNIC, M. V., SARAGOVI, H. U. (2010). An Agonistic TrkB mAb Causes Sustained TrkB Activation, Delays RGC Death, and Protects the Retinal Structure in Optic Nerve Axotomy and in Glaucoma. *Investigative Ophthalmology & Visual Science 51*(9), 4722 – 4731.

9. BEZERRA, H., COSTA, M. A., GUAGLIUMI, G., ROLLINS, A. M., SIMON, D., I. (2009). Intracoronary Optical Coherence Tomography: A Comprehensive Review. *Journal of the American College Cardiovascular Interventions 2*, 1035 – 1046.

10. BOPPART, S.A., BREZINSKI, M. E., BOUMA, B.E., TEARNEY, G. J., FUJIMOTO, J. G. (1996). Investigation of developing embryonic morphology using optical coherence tomography. *Developmental Biology 177*, 54 – 63.

11. BYRNE, S. F. & GREEN, R. L. (2002). Physics and Instrumentation. In Ultrasound of the Eye and Orbit. 2 edn. Eds S. F. BYRNE, R. L. GREEN. St. Louis, Mosby. pp 1 – 12.

12. CASTRO LIMA, V., RODRIGUES, E. B., NUNES, P. R., SALLUM, J. F., FARAH, M. E., MEYER, C. H. (2011). Simultaneous Confocal Scanning Laser Ophthalmoscopy Combined with High-Resolution Spectral-Domain Optical Coherence Tomography: A Review. *Journal of Ophthalmology Vol. 2011*, 1 - 6.

13. COHIMBRA, J. P., NOLAN, P. M., COLLIN, S. P., HART, N. S. (2012). Retinal Ganglion Cell Topography and Spatial Resolving Power in Penguins. *Brain Behavior and Evolution 80*, 254 - 268.

14. CONG, L., SUN, D., ZHANG, Z., JIAO, W., RIZZOLO, W., PENG, S. (2008). A novel rabbit model for studying RPE transplantation. *Investigative Ophthalmology & Visual Science 49*, 4115 - 4125.

15. DOBRE, G.M., PODOLEANU, A.G., ROSEN, R.B., (2005). Simultaneous optical coherence tomography—indocyanine Green dye fluorescence imaging system for investigations of the eye's fundus. *Optics Letters 30*, 58 – 60.

16. DOROBEK, K., (2013) a. Fixation. Vorbereitung der Augen. Pathologisch-anatomische Untersuchung des Auges. Dreidimensionale Sonographie am

Vogelauge- das vordere Augensegment (pp. 54 - 55). München, Ludwig-Maximilians-Universität München.

17. DOROBEK, K., (2013) b. Einleitung. Inaugural-Dissertation. Dreidimensionale Sonographie am Vogelauge- das vordere Augensegment (pp. 6). München, Ludwig-Maximilians-Universität München.

18. DOROBEK, K., (2013) c. Die Sonographische Untersuchung. Untersuchungsmethoden. Material und Methoden. Inaugural – Dissertation. Dreidimensionale Sonographie am Vogelauge- das vordere Augensegment (pp. 73-74). München, Ludwig-Maximilians-Universität München.

19. DOUKAS, J., MAHESH, S., UMEDA, N., KACHI, S., AKIYAMA, H., YOKOI, K., CAO, J., CHEN, Z., DELLAMARY, L., TAM, B., RACANELLI-LAYTON, A., HOOD, J., MARTIN, M., NORONHA, G., SOLL, R., CAMPOCHIARO, P. A. (2008). Topical Administration of a Multi-Targeted Kinase Inhibitor Suppresses Choroidal Neovascularization and Retinal Edema. *Journal of Cellular Physiology 216*, 29 – 37.

20. DREXLER, W., & FUJIMOTO, J. G. (2008). State-of-the-art retinal optical coherence tomography. *Progress in retinal and Eye Research 27*, 45 - 88.

21. DREXLER, W., MORGNER, U., GHANTA, R. K., KÄRTNER, F. X., SCHUMAN, J. S., FUJIMOTO, J. G. (2001). Ultrahigh-resolution ophthalmic optical coherence tomography. *Nature Medicine. 7*(4), 502 – 507.

22. DUBOIS, A., VABRE, L., BOCCARA, A., BEAUREPAIRE, E. (2002). High-Resolution Full-Field Optical Coherence Tomography with a Linnik Microscope. *Applied Optics 41*, 805 - 812.

23. DUCROS, M. G., MARSACK, J. D., RYLANDER, H. G., THOMSEN, S. L., MILNER. T. E. (2001). Primate retina imaging with polarization-sensitive optical coherence tomography. *Journal of the Optical Society of America 18*(12), 2945 – 2956.

24. DUKE, ELDER. The eye in evolution. Systems of Ophthalmology. Vol. XII DUKE ELDER System of Ophthalmology 1958. Vol. XII, pp. 357 – 427.

25. DUONG, T. Q., NGAN, S-H., UGURBIL, K., KIM S-G. (2002). Functional Magnetic Resonance Imaging of the Retina. *Investigative Ophthalmology & Visual Science 43*(4), 1176 – 1181.

26. ESMAEELPOUR, M., POVAZAY, B., HERMANN, B., HOFER, B., KAJIC, V. KAPOOR, K., SHEEN, N. J. L., NORTH, R. V., DREXLER, W. (2010). Three-Dimensional 1060-nm OCT: CHoroidal Thickness Maps in Normal Subjects and Improved Posterior Segment Visualization in Cataract Patients. *Investigative Ophthalmology & Visual Science* 51, 5260 – 5266.

27. EVANS, H. D., & MARTIN, G. R. (1993). Chapter 16: Organa Sensuum (Organa sensoria). In J. J. BAUMEL, A. S. KING, J. E. BREAZILE, H. E. EVANS, & J. C. VANDEN BERGE (Eds.), Handbook of Avian Anatomy: Nomina Anatomica Avium (pp 585 - 611). Cambridge, Massachusetts: Nuttall Ornithological Club, N° 23.

28. FERCHER, A. F. (1996). Optical coherence tomography. *Journal of Biomedical Optics 1*(2), 157 - 173.

29. FERGUSON, R. D., HAMMER, D. X., PAUNESCU, L. A., BEATON, S., SCHUMAN, J. S. (2004) Tracking optical coherence tomography. *Optics Letters 29*, 2139 - 2141.

30. FREWEIN, J., & SINOWATZ, F. (2004). Sinnesorgane. In R. NICKEL, A. SCHUMMER & E. SEIFERLE (Eds.), Lehrbuch der Anatomie der Haustiere (Vol. 5, pp. 365-386). Berlin, Hamburg: Parey.

31. FUJIMOTO, J. G., BREZINSKI, M. E., TEARNEY, G. J., BOPPART, S. A., BOUMA, B., HEE, M. R., SOUTHERN, J. F., SWANSON, E. A. (1995). Optical biopsy and imaging using optical coherence tomography. *Nature Medicine 1*(9), 970 - 972.

32. GABRIELE, M. L., WOLLSTEIN, G., ISHIKAWA, H., KAGEMANN, L., XU, J., FOLIO, L. S., SCHUMAN, J. S. (2011) Optical Coherence Tomography: History, Current Status, and Laboratory Work. *Investigative Ophthalmology & Visual Science 52*(5), 2425 - 2436.

33. GARLAND, M. R., LAWLER, L. P., WHITAKER, B. R., WALKER, I. D. F., CORL, F. M., FISCHMAN, E. K. (2002). Modern CT Applications in Veterinary Medicine. *RadioGraphics 22*, 55 - 62.

34. GEKELER, F., GMEINER, H., VÖLKER, M., SACHS, H., MESSIAS, A., EULE, C., BARTZ-SCHMIDT, K. U., ZRENNER, E., SHINODA, K. (2007). Assessment of the posterior segment of the cat eye by optical coherence tomography (OCT). *Veterinary Ophthalmology 3*, 173 – 178.

35. GLOESMANN, M., HERMANN, B., SCHUBERT, C., SATTMANN, H., AHNELT, P. K., DREXLER, W. (2003). Histologic correlation of pig retina radial stratification with ultrahigh-resolution optical coherence tomography. *Investigative Ophthalmology & Visual Science 44*, 1696 - 1703.

36. GONZALEZ, E. M., RODRIGUEZ, A. & GARCIA, I. (2001) Review of ocular ultrasonography. *Veterinary Radiology & Ultrasound 42*, 485 – 495.

37. GUMPENBERGER, M., KOLM, G. (2006). Ultrasonographic and computed tomographic examinations of the avian eye: physiologic appearance, pathologic findings, and comparative biometric measurement. *Veterinary Radiology & Ultrasound 47*(5), 492 - 502.

38. HAOUCHINE, B., MASSIN, P., GAUDRIC, A. (2001). Foveal Pseudocyst as the First Step in Macular Hole Formation. A prospective Study by Optical Coherence Tomography. *Ophthalmology 108*, 15 – 22.

39. HAYES, B. P., MARTIN, G. R., BROOKE, M. L. (1991) Novel area subserving binocular vision in the retinae of Procellariiform seabirds. *Brain Behavior and Evolution 37*, 79 – 84.

40. HUANG, Y., CIDECIYAN A. V., PAPASTERGIOU, G. I., BANIN, E., SEMPLE-ROWLAND, S L., MILAM, A. H., & JACOBSON S. G. (1998). Relation of Optical Coherence Tomography to Microanatomy in Normal and rd Chickens. *Investigative Ophthalmology & Visual Science 39*(12), 2405 - 2416.

41. HUANG, D., SWANSON, E. A., LIN, C. P., SCHUMAN, J. S., STINSON, W. G., CHANG, W., HEE, M. R., FLOTTE, T., GREGORY, K., PULIAFITO, C. A. (1991). Optical coherence tomography. *Science 22*, 254 (5035), 1178 – 1181.

42. HUFEN, HEIKE & KORBEL, RÜDIGER (2009) Investigations in the appliance of immersion shells in avian ocular ultrasonography. In Proceedings of the 11th European AAV Conference. Ed EAAV.

43. HUBER, G., BECK, S. C., GRIMM, C., SAHABOGLU-TEKGOZ, A., PAQUET-DURAN, F., WENZEL, A., HUMPRHIES, P., REDMOND, T. M., SEELIGER, M. W., FISCHER, M. D. (2009). Spectral Domain Optical Coherence Tomography in Mouse Models of Retinal Degeneration. *Investigative Ophthalmology & Visual Science 50*, 5888 – 5895.

44. ISHIKAWA, H., KIM, J., FRIBERG, T. R., WOLLSTEIN, G., KAGEMANN, L., GABRIELLE, M. L., TOWNSEND, K. A., SUNG, K. R., DUKER, J. S., FUJIMOTO, J. G., SCHUMAN, J. S. (2009). Three-Dimensional Optical Coherence Tomography (3D-OCT) Image Enhancement with Segmentation Free Contour Modelling C-Mode. *Investigative Ophthalmology & Visual Science 50*(3), 1344 – 1349.

45. JIAO, S., KNIGHTON, R., HUANG, X., GREGORI, G., PULIAFITO, C. A. (2005). Simultaneous acquisition of sectional and fundus ophthalmic images with spectral-domain optical coherence tomography. *Optics Express 13*(2), 444 – 452.

46. JOHNSON, M. W., VAN NEWKIRK, M. R., MEYER, K. A. (2001). Perifoveal vitreous detachment is the primary pathogenic event in idiopathic macular hole formation. *Archives of Ophthalmology 119*, 215 – 222.

47. KAGEMANN, L., ISHIKAWA, H., ZOU, J. ET. AL. (2008). Repeated, noninvasive, high resolution spectral domain optical coherence tomography imaging of zebrafish embryos. *Molecular Vision 14*, 2157 – 2170.

48. KAGEMANN, L., WOLLSTEIN, G., ISHIKAWA, H., BILONICK, R. A., BRENNEN, P. M., FOLIO, L. S., GABRIELLE, M. L., SCHUMAN, J. S. (2010). Identification and Assessment of Schlemm´s Canal by Spectral-Domain Optical Coherence Tomography. *Investigative Ophthalmology & Visual Science 51*, 4054 -4059.

49. KERN, T. J., & COLITZ, C. M. H. (2013). Section IV: Special Ophthalmology. In K. N. GELATT, B. C. GILGER & T. J. KERN (Eds), Veterinary Ophthalmology, Fifth Edition, Vol II, (pp 1750 - 1819) John Wiley & Sons, Inc.

50. KIAMA, S. G., MAINA, J. N., BHATTACHARJEE, J., WEYRAUCH, K. D. (2001). Functional morphology of the pecten oculi in the nocturnal spotted eagle owl (Bubo bubo africanus), and the diurnal black kite (Milvus migrans) and domestic fowl (Gallus gallus var. domesticus): a comparative study. *Journal of Zoology, London 254*, 521 - 528.

51. KIM, J. W., JANG, S. Y., PARK, T. K., OHN, Y. H. (2011). Short-Term Clinical Observation of Acute Retinal Pigment Epitheliitis Using Spectral-Domain Optical Coherence Tomography. *Korean Journal of Ophthalmology 25*(3), 222 - 224.

52. KIM, J. S., ISHIKAWA, H., GABRIELLE, M. L., WOLLSTEIN, G., BILONICK, R. A., KAGEMANN, L., FUJIMOTO, J. G., SCHUMAN, J. S. (2010). Retinal Nerve Fiber Layer Thickness Measurement Comparability between Time Domain Optical Coherence Tomography (OCT) and Spectral Domain OCT. *Investigative Ophthalmology & Visual Science 51*(2), 896 – 902.

53. KIM, E. T., KIM, C., LEE, S. W., SEO, J. M., CHUNG, H., KIM, S. J. (2009). Feasibility of microelectrode array (MEA) based on silicone-polyimide hybrid for retina prosthesis. *Investigative Ophthalmology & Visual Science 50*, 4337 – 4341.

54. KOBAYASHI, Y., OKURA. H., KUME, T., YAMADA, R., KOBAYASHI, Y., FUKUHARA, K., KOYAMA, T., NEZUO, S., NEISHI, Y., HAYASHIDA, A., KAWAMOTO, T., YOSHIDA, K. (2014). Impact of Target Coronary Calcification on Stent Expansion. *Circulation Journal, Official Journal of the Japanese Circulation Society*. www.j-circ.or.jp

55. KORBEL, R. (1991). Zum derzeitigen Stand der Ornithoophthalmologie. *Tierärztliche Praxis 19*, 497 – 507.

56. KORBEL, R. (1994). Augenheilkunde bei Vögeln: Ätiologie und Klinik von Augenkrankheiten, Luftsack-Perfusionsanästhesie, ophthalmologische

Photographie und Bildatlas der Augenerkrankungen bei Vögeln. In Vet. Habil. München, pp. 49.

57. KORBEL, R. (1999). Erkrankungen des Augenhintergrundes beim Vogel – Untersuchungstechniken und Befunde. *Tierärztliche Monatsschrift 86*, 395 – 410.

58. KORBEL, R., BARWIG, S., RINDER, M. (2012). Vergleichende Untersuchungen zur Ophthalmoskopie, digitalen Scanning Ophthalmoskopie (SDO) und optischen Kohärenztomographie (OCT) unter besonderer Berücksichtigung Bornavirus-assoziierter ophthalmologischer Befunde am Vogelauge. *Tagungsband der 17. DVG-Tagung über Vogelkrankheiten, München, 1.-3. März*, 43-46.

59. KORBEL., R, DOROBEK, K., LIEPERT, A., HUFEN, H VELASCO GALLEGO, M. L. SCHULZE, C., RINDER, M., BRANDSTÄTTER, P., POHL, R. (2013) a. Comparative aspects of ophthalmological imaging techniques in pet birds, poultry, reptiles and fish using optical coherence tomography (OCT), fundus photography, scanning digital ophthalmoscopy (SDO) and 2D & 3D ultrasonography. *Proceedings of the 8th Joint Scientific Symposium of the Veterinary Faculties of T.C. Istanbul Üniversitesi and Ludwig-Maximilians-Universität München, München, 9.-12. April*, 26.

60. KORBEL, R., REESE, S., & KÖNIG, H. E. (2001). Propädeutik. Klinischer Untersuchungsgang- Ophthalmologische Untersuchung. In H. E. KÖNIG & H-E LIEBICH (Eds), Anatomie und Propädeutic des Geflügels. Stuttgart: Schattauer Verlagsgesellschaft, pp 243 – 249.

61. KORBEL, R., VELASCO GALLEGO, M. L., SCHULZE, C., RINDER, M. (2013) b. Avian bornavirus infections in parrots: characterization of ophthalmological lesions using optical coherence tomography (OCT). *1th International Conference on Avian, Herpetological and Exotic Mammal Medicine. Wiesbaden, April 20-26*, 357-358.

62. VELASCO GALLEGO, M. L., SCHULZE, C., RINDER, M. KORBEL, R. (2014). Vergleichende Untersuchungen an Greifvogelaugen mittels Optischer Kohärenztomografie (OCT) und Histologie. *1. Jahrestagung der DVG-Fachgruppe „Zier-, Zoo- und Wildvögel, Reptilien und Amphibien“, München, 6.-8. März,* 27-29.
*Tierärztl Prax 2014;42 (K):*A38.

63. KORBEL, R., WIESNER, H., HECTOR, J. (1997). Ophthalmoskopie bei Zoo – und Wildvögeln – Untersuchungstechniken und Befunde. *Verh. Ber. Erkrg. Zootiere 38*, 103 -110.

64. KORBEL, RÜDIGER, HUFEN, HEIKE, SCHWEIKL, MONIKA & STROBEL, BIRTE KATJA (2009) Ocular Ultrasonography in Birds. In 30th Annual Association of Avian Veterinarians Conference & Expo. Ed AAV. Milwaukee, Wisconsin, pp. 95 – 97.

65. KUSUHARA, S., TERAOKA ESCAN, M. F., FUJII, S., NAKANISHI, Y., TAMURA, Y., NAGAI, A., YAMAMOTO, H., TSUKAHARA, Y., NEGI, A. (2004). Prediction of Postoperative Visual Outcome Based on Hole Configuration by Optical Coherence Tomography in Eyes With Idiopathic Macular Holes. *Ophthalmology 138*, 709 – 716.

66. LATENDRESSE, J. R., WARBRITTION, A. R., JONASSEN, H., CREASY, D. M. (2002). Fixation of Testes and Eyes Using a Modified Davidson's Fluid: Comparison with Bouin's Fluid and Conventional Davidson's Fluid. *TOXICOLOGIC PATHOLOGY 30*(4), 524 – 533.

67. LIEPERT, A., (2013) a. Einleitung. Inaugural –Dissertation (pp. 1). Dreidimensionale Sonographie des Vogelauges - das hintere Augensegment. München, Ludwig-Maximilians-Universität München.

68. LIEPERT, A., (2013) b. Dreidimensionale Datengewinnung.Die Sonographische Untersuchung. Untersuchungspethodik. Material und Methoden. Inaugural – Dissertation (pp. 75 - 79). Dreidimensionale Sonographie des Vogelauges - das hintere Augensegment. München, Ludwig-Maximilians-Universität München.

69. LUMBROSO, B. RISPOLI, M. (2009). Guide to Interperting Spectral Domain Optical Coherence Tomography. I.N.C. Innovation-News-Communication, Roma

70. MANS, C., SANCHEZ-MIGALLON GUZMAN, D., LAHNER L. L., PAUL-MURPHY, J., SLADKY, K. (2012). Sedation and Physiologic Response to Manual Restraint After Intranasal Administration of Midazolam in Hispaniolan Amazon

Parrots (Amazona ventralis). *Journal of Avian medicine and Surgery 26*(3), 130 – 139.

71. MANTOVANI BOTTÓS, J., LUCAS TORRES, V. L., ALMEIDA KANECADAN, L. A., GONZÁLEZ MARTÍNEZ A. A., BUENO MORAES, N. S., MAIA, M., ALLEMANN, N. (2012). Macular hole: 10 and 20 – MHz ultrasound and spectral-domain optical coherence tomography. *Arquivos Brasileiros de Oftalmologia 75* (6), 415 – 409.

72. MARKWELL, E. L., FEIGL, B., ZELE, A. J. (2010) Intrinsically photosensitive melanopsin retinal ganglion cell contributions to the pupillary light reflex and circadian rhythm. *Clinical and Experimental Optometry 93*, 137 – 149.

73. MARTIN, GRAHAM R. (1985) Eye. In Form and Function in Birds. Eds A. S. KING, J. & MCLELLAND. London, Academic Press. pp 311 – 373.

74. MEDEIROS, F. A., ZANGWILL, L. M., BOWD, C., VESSANI, R. M., SUSAMNNA, R., WEINREB, R. N. (2005). Evaluation of Retinal Nerve Fiber Layer, Optic Nerve Head, and Macular Thickness Measurements for Glaucoma Detection Using Optical Coherence Tomography. *American Journal of Ophthalmology 139*, 44 – 55.

75. MOAYED, A. A., CHOH, V., HARIRI, S., LUI, C., WONG, A., & BIZHEVA, K. (2012). Stimulus-Specific pupil Dynamics measured in Birds (Gallus gallus domesticus) In Vivo with Untrahigh Resolution Optical Coherence Tomography. *Investigative Ophthalmology & Visual Science 53*(11), 6863 - 6869.

76. MOAYED, A. A., HARIRI, S., CHOH, V., BIZHEVA, K. (2012). Correlation of visually evoked intrinsic optical signals and electroretinagrams recorded from chicken retina with a combined functional optical coherence tomography and electroretinography system. *Journal of biomedical Optics 17*(1), 016011 – 016015.

77. MOAYED, A. A., HARIRI, S., SONG, E. S., CHOH, V., BIZHEVA, K. (2011). In vivo volumetric imaging of chicken retina with ultrahigh-resolution spectral domain optical coherence tomography. *Biomedical Optics Express 2*(5), 1268 – 1274.

78. MUMFORD, S. L. (2004). Histology for Finfish (pp 1 – 12). NWFHS Laboratory Procedures Manual, Chapter 13- Second Edition, 2004

79. MURPHY, C. J. (1984). Raptor Ophthalmology. Proceedings AAV Conference, 43 – 56.

80. NAGATA, A., HIGASHIDE, T., OHKUBO, S., TAKEDA, H., SUGIYAMA, K. (2009). In vivo quantitative evaluation of the rat retinal nerve fiber layer with optical coherence tomography. *Investigative Ophthalmology & Visual Science 50*, 2809 – 2815.

81. OFRI, R. (2008). Retina. In D. J. MAGGS, P. E. MILLER & R. OFRI (Eds.), Slatter´s Fundamentals of Veterinary Ophthalmology (4 ed., pp 285 - 317). St. Louis: Saunders Elsevier.

82. OH, J., SMIDDY, W. E., FLYNN H. W., GREGORI, G., LUJAN, B. (2010). Photoreceptor Inner/Outer Segment Defect Imaging by Spectral Domain OCT and Visual Prognosis after Macular Hole Surgery. *Investigative Ophthalmology & Visual Science 51*(3), 1651 – 1658.

83. OSTRIN, L. A., LIU, Y., CHOH, V., & WILDSOET, C. F. (2011). The Rol of the Iris in Chick Accommodation. *Investigative Ophthalmology & Visual Science 52*(7), 4710 – 4716.

84. PARSHALL, C. J., WYMAN, M., NITROY, S., ACLAND, G., AGIRRE, G. (1991). Photoreceptor Dysplasia: An Inherited Progressive Retinal Atrophy of Miniature Schnauzer Dogs. *Progress in Veterinary & Comparative Ophthalmology 1*(3), 187 – 203.

85. PAUL-MURPHY, J., FIALKOWSKI, J. (2001). Injectable Anesthesia and Analgesia of Birds. Recent Advances in Veterinary Anesthesia and Analgesia: Companion Animals, R. D. Gleed and J. W. Ludders (Eds.). International Veterinary Information Service, Ithaca, New York, USA.

86. PAULUS, M. J., GLEASON, S. S., KENNEL, S. J., HUNSICKER, P. R., JOHNSON, D. K. (2000). High Resolution X-ray Computed Tomography: An Emerging Tool for Small Animal Cancer Research. *Neoplasia 2*(1 and 2), 62 -70.

87. PILGE, H., HUBER-VAN DER VELDEN, K., HERTEN, M., KURYIDEM, S., KRAUSPE, R., BITTERSOHL, B., ZILKENS C. (2014). Comparison of hip joint cartilage degeneration assessed by histology and ex vivo optical coherence tomography. *Orthopedic Reviews, 6*(5342), 90 – 93.

88. POULSEN NAUTRUP, C., HEIDER, H. J. & EGGERS, S. (1998) a. Auge. Kopf. In Atlas und Lehrbuch der Ultraschalldiagnostik von Hund und Katze. 2 edn. Eds C. POULSEN NAUTRUP, R. TOBIAS. Hannover, Schlütersche GmbH. pp 92 – 108.

89. POULSEN NAUTRUP, C. (1998) Auflösungsvermögen. Technische Grundlagen. In Atlas und Lehrbuch der Ultraschalldiagnostik von Hund und Katze. 2 edn. Eds C. POULSEN NAUTRUP, R. TOBIAS. Hannover, Schlütersche GmbH. pp 31 – 59.

90. RAH, H. C., MAGGS, D. J., BLANKENSHIP, T. N., NARFSTROM, K., LYONS, L. A. (2005). Early-Onset, Autosomal Recessive, Progressive Retinal Atrophy in Persian Cats. *Investigative Ophthalmology & Visual Science 46*(5), 1742 – 1747.

91. RADHAKRISHNAN, S., ROLLINS, A. M., ROTH, J. E., YAZDANFAR, S., WESTPHAL V., BARDENSTEIN, D. S., IZATT, J. A. (2001). Real-Time Optical Coherence Tomography of the Anterior Segment at 1310 nm. *Archives of Ophthalmology 119*(8), 1179 – 1185.

92. RAUSCHER, F. G., AZMANIS, P., KÖRBER, N., KOCH, C., HÜBEL, J., VETTERLEIN, W., WERNER, B., THIELEBEIN, J., DAWCZYNSKY, J., WIEDEMANN, P., REICHENBACH, A., FRANCKE, M., KRAUTWALD-JUNGHANNS, M. E. (2013). Optical coherence tomography as a diagnostic tool for retinal pathologies in avian ophthalmology. *Investigative Ophthalmology & Visual Science 54*(13), 8259 – 8269.

93. RAUSCHER, F. M., SEKHON, N., FEUER, W. J., BUDENZ, D. L. (2009). Myopia Affects Retinal Nerve Fiber Layer Measurements as Determined by Optical Coherence Tomography. *J. Glaucoma 18*(7), 501 – 505.

94. RAVELHOFER, K. (1996). Pathologisch – anatomische Untersuchungen an Augen verschiedener Vogelspezies. München.

95. REESE, S., KORBEL, R., & LIEBICH, H.G. (2009). Sehorgan (Organum visus). In H. E. KÖNIG, R.KORBEL & H.G. LIEBICH (Eds.), Anatomie der Vögel – Klinische Aspekte und Propädeutik. Zier-, Greif-, Zoo-, Wildvögel und Wirtschafsgeflügel (2 ed., pp. 229 - 276). Stuttgart: Schattauer

96. ROMEIS, B (1989). Mikroskopische Technik, 17., neubearbeitete Auflage, Herausgegeben von P. Böck, Urban & Schwarzenberg, München - Wien – Balitmore.

97. RUGGERI, M., MAJOR, J. C., MCKEOWN, J. C., KNIGHTON, R. W., PULIAFITO, C. A., & JIAO, S. (2010). Retinal Structure of Birds of Prey Revealed by Ultra-High Resolution Spectral-Domain Optical Coherence Tomography. *Investigative Ophthalmology & Visual Science 51*(11), 5789 – 5795.

98. RUGGERI, M., WEHBE, H., SHULIANG, J., GREGORI, G., JOCKOVICH, M. E., HACKAM, A., DUAN, Y., & PULIAFITO C. A. (2007). In Vivo Three-Dimensional High-Resolution Imaging of Rodent Retina with Spectral-Domain Optical Coherence Tomography. *Investigative Ophthalmology & Visual Science 48*(4), 1808 - 1814.

99. SANDER, B., LARSEN, M., THRANE, L., HOUGAARD, J.L., JORGENSEN, T.M., (2005). Enhanced optical coherence tomography imaging by multiple scan averaging. *British Journal of Ophthalmology 89*, 207 – 212.

100. SAUNDERS, L. Z., & RUBIN, L. F. (1975). Postmortem technique. In L. Z. SAUNDERS & L. F. RUBIN (Eds.), Ophthalmic Pathology of Animals. An Atlas and Reference Book (pp. 244 - 253). Basel, München, Paris, London, New York, Sydney: Karger.

101. SCHMIDT-ERFURTH, U., LEITGEB, R. A., MICHELS, S., POVAZAY, B., SACU, S., HERMANN, B., AHLERS, C., SATTMANN, H., SCHOLDA, C., FERCHER, A. F., DREXLER, W. (2005). Ultrahigh-Resolution Optical Coherence Tomography of Macular Diseases. *Investigative Ophthalmology & Visual Science 46*(9), 3393 - 3402.

102. SCHMITT, J. M. (1999). Optical Coherence Tomography (OCT): A Review. IEEE *Journal of Selected Topics in Quantum Electronics, 5*(4), 1205 – 1215.

103. SCHMITT, J. M., XIANG, S. H., YUNG, K. M. (1999). Speckle in Optical Coherence Tomography. *Journal of Biomedical Optics 4*(1), 95 – 105.

104. SEIDEL, B. (1988). Augenkrankheiten der Vögel. In V SCHMIDT (Ed.), Augenkrankheiten der Haustiere (Vol. 2, pp. 237-261). Stuttgart: Enke.

105. SILMAN, A. J. (1973). Avian Vision. In Avian biology 2: pp. 349 - 387 Farner, D. S., King, J. R. & Parker, K. C. (Eds). New York: Academic Press.

106. SLONAKER, JAMES ROLLIN (1918) A physiological study of the anatomy of the eye and its accessory parts of the English sparrow (passer domesticus). *Journal of Morphology 31*, 351 – 459.

107. SRINVASAN, V. J., KO, T. H., WOJTKOWSKI, M., CARVALHO, M., CLERMONT, A., BURSELL, S. E., SONG, Q. H., LEM, J., DUKER, J. S., SCHUMAN J. S., & FUJIMOTO, J. (2006) Noninvasive Volumetric Imaging and Morphometric of the rodent retina with High-Speed, Ultrahigh-Resolution Optical Coherente Tomography. *Investigative Ophthalmology & Visual Science 47*(12), 5522 – 5528.

108. STROBEL, B. K. (2010). Einleitung. Inaugural-Dissertation (pp. 5-6). Okulare Sonographie des gesunden und erkrankten Auges bei Wildgreifvögeln. München, Ludwig-Maximilians-Universität München.

109. STROUTHIDIS, N.G., YANG, H, FORTUNE, B, DOWNS, J. C., BURGOYNE, C. F. (2009) a. Detection of optic nerve head neural canal opening within histomorphometric and spectral domain optical coherence tomography data sets. *Invest Ophthalmol Vis Sci., 50*, 214 – 223.

110. STROUTHIDIS, N. G., YANG, H., REYNAUD, J. F., GRIMM, J., GARDINER, S. K., FORTUNE, B., BURGOYNE, C. F. (2009) b. Comparison of

Clinical and Spectral Domain Optical Coherence Tomography Optic Disc Margin Anatomy. *Invest. Ophthalmol. Vis Sci., 50*(10), 4709 – 4718.

111. TIEDEMANN, D. F. (1810). Von den Sehorganen der Vögel. In D. F. TIEDEMANN (Ed.), Anatomie und Naturgeschichte der Vögel-Band 1 (pp. 48 - 88). Heidelberg: Mohr und Zimmer.

112. TUNSTALL, M. (1771). Ornithologia Britannica: seu Avium omnium Britannicarum tam terrestrium, quam aquaticarum catalogus, sermone Latino, Anglico et Gallico redditus: cui subjuctur appendix avec alennigenas, in Angliam raro advenientes, complectens. London, J. Dixwell.

113. TUCKER, V. A. (2000). The deep fovea, sideways vision and spiral flight paths in raptors. *The Journal of Experimental Biology 203*, 3745 – 3754.

114. ULLRICH, S., HARITOGLOU, C., GASS, C., SCHAUMBERGER, M., ULBIG, M. W., KAMPIK, A. (2002). Macular hole size as a prognostic factor in macular hole surgery. *British Journal of Ophthalmology 86*, 390 – 393.

115. VAN VELTHOVEN, M. E., DE VOS, K., VERBRAAK, F. D., POOL, C. W., DE SMET, M. D. (2005). Overlay of conventional angiographic and en-face OCT images enhances their interpretation. *Biomed Central Ophthalmoogy 5*, 12.

116. VAN VELTHOVEN, M. E. J., FABER, J. D., VERBRAAK, F. D., VAN LEEUWEN, T. G., & DE SMET, M. D. (2007). Recent developments in optical coherence tomography for imaging the retina. *Progress in retina and Eye Research 26*, 57 – 77.

117. VAN VELTHOVEN, E. J., SMET, M. D., SCHLINGEMANN, R. O., MAGNANI, M., VERBRAAK, F. D. (2006). Added value of OCT in evaluating the presence of leakage in patients with age-related macular degeneration treated with PDTM. *Graefe's Archive of Clinical and Experimental Ophthalmology 244*, 1119 – 1123.

118. VESAL N., ESKANDARI M. H. (2006). Sedative effects of midazolam and xylazine with or without ketamine and detomidine alone following intranasal

administration in Ring-necked Parakeets. *Journal of the American Veterinary Medical Association 228*(3), 383 – 388.

119. VIZZERI, G., BALASUBRAMANIAN, M., BOWD, C., WEINREB, R. N., MEDEIROS, F. A., ZANGWILL, L. M. (2009). Spectral domain-optical coherence tomography to detect localized nerve fiber layer defects in glaucomatous eyes. *Optics Express 17*(5), 4004 – 4018.

120. WANG, Y., FAWZI, A., TAN, O., GIL-FLAMER, J., HUANG, D. (2009). Retinal blood flow detection in diabetic patients by Doppler Fourier domain optical coherence tomography. *Optics Express 17*(5), 4061 – 4073.

121. WERTHER, K., HUFEN, H., STROBEL, B. K., STEIN, K., & KORBEL, R. (2011). Effects of Formalin Fixation on Avian Eye. Proceedings EAAV Madrid, 440 – 442.

122. WILLIAMS, D. (1994). Section Four: Internal Medicine. Ophthalmology. In B: W: RITCHIE, G. J. HARRISON & L. R. HARRISON (Eds.), Avian Medicine: Principles and Application (pp. 637 - 695). Lake Worth, Florida: Wingers Publishing.

123. WILLIAMS, J., WILKIE, D. A. & GRÄNITZ, U. (1995) Ultraschalluntersuchungen in der Veterinärophthalmologie. *Tierärztliche Praxis 23*, 111 – 115.

124. WOOD, C. S. (1917). Chapter VI. Ophthalmoscopy of the Fundus in Living Birds. The Fundus Oculi Of Birds. Chicago, The Lakeside Press, 33 – 48.

125. YANG, H., Q. I. J., HARDIN, C., GARDINER S. K., STROUTHIDIS, N. G., FORTUNE, B., & BURGOYNE C. F. (2012). Spectral-Domain Optical Coherence Tomography Enhanced Depth Imaging of the Normal and Glaucomatous Nonhuman Primate Optic Nerve Head. *Investigative Ophthalmology & Visual Science 53*(1), 394 – 405.

126. YANNUZI, L.A., OBER, M.D., SLAKTER, J.S., SPAIDE, R.F., FISHER, Y.L., FLOWER, R.W., ROSEN, R., (2004). Ophthalmic fundus imaging: today and beyond. *American Journal of Ophthalmology 137*, 511 – 524.

127. YI, K., MUJAT, M., PARK, B. H., SUN, W., MILLER, J. W., SEDDON, J. M., YOUNG, L. H., DE BOER, J. F., CHEN, T. C. (2009). Spectral domain optical coherence tomography for quantitative evaluation of drusen and associated structural changes in non-neovasular age-related macular degeneration. *British Journal of Ophthalmology 93,* 176 – 181.

128. YÜKSEL, H., TÜRKCÜL, F. M., SAHIN, A., ED SAHIN, M., CINAR, Y., CINGÜL, A. K., ARIL, S., ÇAÇA, I. (2013). One year results of anti-VEGF treatment in pigment epithelial detachment secondary to macular degeneration. *Arquivos Brasileiros de Oftalmologia 76*(4), 209 – 211.

10 IMAGE INDEX

11 TABLE INDEX

12 APPENDIX

Appendix 1. Program designed with the software Mathematica 8.0 (Wolfram Research, Hanborough, United Kingdom).

Fitting;

```
sol=FindFit[resta2,{a+b*(x-x0)+c*(x-x0)^2+d*(x-x0)^3+e*(x-x0)^4+f*(x-x0)^5+h*(x-x0)^6},{a,b,c,d,e,f,h,x0},{x}];
a1=a/.sol[[1]];
b1=b/.sol[[2]];
c1=c/.sol[[3]];
d1=d/.sol[[4]];
e1=e/.sol[[5]];
f1=f/.sol[[6]];
h1=h/.sol[[7]];
x01=x0/.sol[[8]];
GFT=Table[a1+b1*(x-x01)+c1*(x-x01)^2+d1*(x-x01)^3+e1*(x-x01)^4+f1*(x-x01)^5+h1*(x-x01)^6,{x,0,L1}];
GF=ListPlot[GFT,DataRange→{0,final-
inicio},PlotStyle→Red,AxesStyle→Thick,PlotLabel→Style["",Black,35],LabelStyle
→Directive[Black,25],GridLines→Automatic,Joined→True,FrameLabel→{"Distan
ce (mm)", "Thickness (μm)","" ,""
},Frame→True,RotateLabel→True,PlotRange→{0,600}]
TotalPlot=Show[G,GF]
rutaarchivoplotfit=StringJoin[rutageneral, rutaarchivo, "_plotfit.jpg"];
Export[rutaarchivoplotfit,TotalPlot,
"Graphics",ImageResolution→500,ImageSize→{1000,1000}];
```

Statistics;

```
Media=Mean[resta2];
Desviacion=StandardDeviation[resta2];
Mediana=Median[resta2];
Maximo=Max[resta2];
Varianza=Variance[resta2];
{"Media",Media,"Desviacionstandard",Desviacion,"Mediana",Mediana,"Maximo",
Maximo,"Varianza",Varianza}
sol2=NonlinearModelFit[resta2,{a+b*(x-x0)+c*(x-x0)^2+d*(x-x0)^3+e*(x-x0)^4+f*(x-x0)^5+h*(x-x0)^6},{a,b,c,d,e,f,h,x0},{x},AccuracyGoal→4];
eq=sol2["BestFit"];
Rsq=sol2["RSquared"];
{"Rcuadrado",Rsq}
res=sol2["FitResiduals"];
Pt=sol2["ParameterTable"]
resP=ListPlot[res,DataRange-
>{0,L1},PlotStyle→PointSize[0.012],PlotLabel→Style["",Black,35],LabelStyle→Directive[Black,25],GridLines→Automatic,FrameLabel→{"Distance (10^-2mm)",
"Residuals (μm)","" ,"" },Frame→True,RotateLabel→True,PlotRange→Automatic]
Parametros={"Media",Media,"Desviacionstandard",Desviacion,"Mediana",Median
a,"Maximo",Maximo,"Varianza",Varianza,"Coeficientes",eq,"Rcuadrado",Rsq,"Re
siduales",res};
rutaarchivoresiduals=StringJoin[rutageneral, rutaarchivo, "_residuals.jpg"];
Export[rutaarchivoresiduals,resP,
"Graphics",ImageResolution→500,ImageSize→{1000,1000}];
```

Parameters;

```
rutaarchivoparametros=StringJoin[rutageneral, rutaarchivo, "_parametros.txt"];
Export[rutaarchivoparametros,Parametros, "Table"];
rutaarchivotable=StringJoin[rutageneral, rutaarchivo, "_table.jpg"];
Export[rutaarchivotable,Pt,

"Graphics",ImageResolution→500,ImageSize→{1000,1000}];
```

13 ACKNOWLEDGEMENTS

First and foremost, it gives me great pleasure in acknowledging the assistance of Mr. Prof. Dr. Korbel. I cannot find words to express his work directing this dissertation.
I feel totally indebted with Ms. Priv.-Doz. Dr. Monika Rinder. Her compromise with me as her doctorate student has been determined of a great responsibility sense. Even in the worse moments she has always shown patience and understanding. The good quality of her indications and corrections is more than any doctorate can expect. Because of her guidance I was able to finish this dissertation.
If someone can understand the complications and rewards during the development of this dissertation is Ms. Céline Schulze, my partner, colleague and moreover my friend. I would like to express my gratitude for listening my opinions and problems. Your effort and enthusiasm during this doctorate was contagious, being my most important motivation source.
I considered an honor to have worked during these two years with the team of the Clinic for Birds, Reptiles, Amphibians and Ornamental Fish of the University Ludwig Maximilian (Munich). They have taught me much more than the German language and avian medicine. Especially I would like to thank Mr. Dr. Franz Kronthaler and Ms. Dr. Heike Hufen, both specialists in avian medicine, whose great knowledge helped us all, and Ms Andrea Liepert, Kristina Doroben and Anna Smitz, all of them already doctor in veterinary medicine, who were always there to answer any question.
My deepest gratitude lies on Ms. Martina Rzepka. She was always there to share her broad knowledge about the patients. Her care about each patient and about each co-worker is from the best kind of person and integrity as human being.

I would like to thank the invaluable guidance and support of the Neuroanatomy Department of the University Ludwig Maximilian (Munich), especially Ms. Beate Aschauer, Ms Astrid Baltruschat, and Ms Dr. Maren Kiessling.

Por último, quiero dedicar esta tesis doctoral a mi querida familia, en especial a mis padres, Marcial y Esperanza, y a mi hermano Santiago. A pesar de la distancia siempre han estado ahí para apoyarme en los momentos complicados. Mi agradecimiento va mucho más allá de lo que es posible transmitir con palabras. Sobre todo, la distancia se hace difícil de llevar. El haber concluido este doctorado no habría sido posible sin su paciencia y sus ánimos. Y para finalizar, a mi novio Edu. En este caso, realmente no tengo palabas para describir lo agradecida que me siento. Su ayuda ha sido más que

incalculable, y su paciencia ha demostrado no tener límites. Ha demostrado que el amor lo puede superar todo.